Best
Available
Copy

AD-A015 567

LASER WINDOW STUDIES

C. B. Willingham, et al

Raytheon Company

Prepared for:

Army Missile Command
Advanced Research Projects Agency

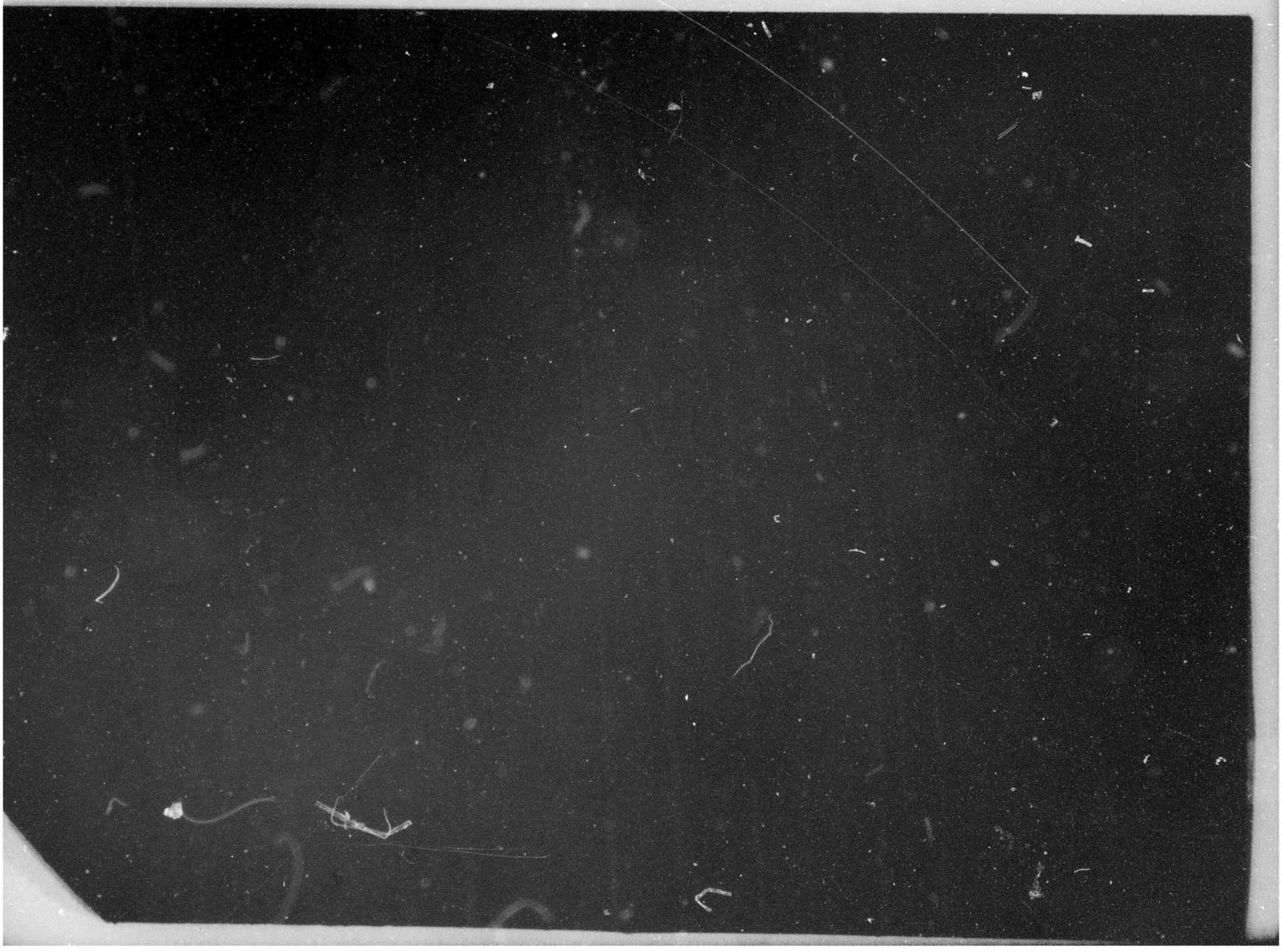
August 1975

DISTRIBUTED BY:

NTIS

National Technical Information Service
U. S. DEPARTMENT OF COMMERCE

Reproduced by
NATIONAL TECHNICAL
INFORMATION SERVICE
US Department of Commerce
Springfield, VA. 22151



Unclassified

SECURITY CLASSIFICATION OF THIS PAGE (When Data Entered)

REPORT DOCUMENTATION PAGE		READ INSTRUCTIONS BEFORE COMPLETING FORM
1 REPORT NUMBER	2 GOVT ACCESSION NO.	3 RECIPIENT'S CATALOG NUMBER
4 TITLE (and Subtitle) LASER WINDOW STUDIES		5 TYPE OF REPORT & PERIOD COVERED Final Technical 5/20/74 - 8/15/75 6 PERFORMING ORG. REPORT NUMBER S-1900
7 AUTHOR(s) C.B. Willingham H. Statz D. Burt F. Horrigan		8 CONTRACT OR GRANT NUMBER(s) DAAH01-74-C-0719
9 PERFORMING ORGANIZATION NAME AND ADDRESS Raytheon Research Division 28 Seyon Street Waltham, MA 02154		10 PROGRAM ELEMENT, PROJECT, TASK AREA & WORK UNIT NUMBERS Program Code No. 4D10 ARPA Order No. 1180
11 CONTROLLING OFFICE NAME AND ADDRESS Advanced Research Projects Agency 1400 Wilson Blvd. Arlington, VA 22209		12 REPORT DATE August 1975 13 NUMBER OF PAGES 120
14 MONITORING AGENCY NAME & ADDRESS (if different from Controlling Office) U.S. Army Missile Command Redstone Arsenal, Huntsville, Alabama 35809		15 SECURITY CLASS. (of this report) Unclassified 15a DECLASSIFICATION/DOWNGRADING SCHEDULE
16 DISTRIBUTION STATEMENT (of this Report) N/A Approved for public release; Distribution Unlimited		
17 DISTRIBUTION STATEMENT (of the abstract entered in Block 20, if different from Report)		
18 SUPPLEMENTARY NOTES		
19 KEY WORDS (Continue on reverse side if necessary and identify by block number) Infrared Optical Thin Films: Absorption Coefficient Determination, Laser Calorimetry, Attenuated Total Reflection Spectroscopy, Adhesion, Durability, Microhardness Testing. High Power Laser Windows: Diamond Abrasive Superpolishing, Cleaning Techniques, Hydrocarbon Contamination, Liquid Coolants		

20 ABSTRACT (Continue on reverse side if necessary and identify by block number)

The primary objective of this program was the development of experimental techniques for determining important optical and mechanical properties of surfaces and of coatings for infrared laser optical components. Secondary objectives included evaluation of surface fabrication and cleaning techniques for important laser window materials, a search for liquid coolants for infrared lasers, and delivery of candidate window materials to the Monitoring Agency for chemical laser testing.

DD FORM 1 JAN 73 1473 EDITION OF 1 NOV 65 IS OBSOLETE

Unclassified

SECURITY CLASSIFICATION OF THIS PAGE (When Data Entered)

Abstract (continued)

Laser calorimetry was applied to the determination of absorption coefficients of optical films and a study of commercially available examples of thorium fluoride, arsenic trisulfide, zinc sulfide and zinc selenide films was made. Absorptivities measured at 5.25 and at 10.6 micrometers were found to exceed bulk values and to vary significantly not only among suppliers but also between depositions for single vendors.

Attenuated total reflection spectroscopy was used to determine absorption behavior of the films between 2.5 micrometers and the infrared cutoff of their substrates. Exploratory development of a more sensitive technique for determining wavelength dependence of absorption and scattering began and an intense black body point source was designed and constructed.

An apparatus for determining the microhardness of thin films was designed and constructed. The device will produce indentations on the order of 1000 angstroms deep and record the load and depth automatically. Film materials were found to be harder than their corresponding bulk materials. Areas of application of microhardness testing to thin film work include separation of film from substrate properties, adhesion testing, and quantitative determination of the effects of environmental exposure to film hardness and adhesion.

Preparation and cleaning procedures were developed which produced optically-figured alkaline earth fluoride surfaces free of microscopically detectable defects and residues which absorb 5.25 micrometer radiation significantly. Evidence that the surfaces of alkaline earth fluorides are major contributions to their total absorptivity at hydrogen and deuterium fluoride laser wavelengths was produced.

Six two-inch diameter polycrystalline strontium fluoride specimens manufactured at Raytheon by fusion casting were fabricated into windows by the diamond abrasive polishing techniques developed on this program and delivered to the Monitoring Agency.

PREFACE

This report describes studies of surfaces and coatings for high-power laser windows performed at Raytheon Research Division during the period from May 20, 1974 to August 15, 1975 on Contract DAAH01-74-C-0719. During the first six months of the period, Dr. F. Horrigan acted as principal investigator for the project; for the remainder of the project, Dr. C.B. Willingham was the principal investigator. Mr. D.P. Bua performed the ATR spectroscopy and designed, built and operated the mechanical testing equipment. Dr. H. Statz acted as a consultant to the program and refined the theory for calorimetric determination of film absorption coefficients originally derived by Dr. Horrigan. Calorimetry was performed by T. Varitimos and M. Schapira; surface finishing by R. Cosgro. Others participating in the research include: J. Grenda, O. Guentert and W. Tye. This report has the internal number S-1900.

TABLE OF CONTENTS

		Page
PREFACE		3
LIST OF ILLUSTRATIONS		5
LIST OF TABLES		7
TECHNICAL REPORT SUMMARY		8
1.0	INTRODUCTION	13
2.0	THIN FILM CHARACTERIZATION	15
2.1	Optical Characterization	17
2.1.1	Laser calorimetry	17
2.1.2	Attenuated total reflection spectroscopy	42
2.1.3	Integrated optics experiments	55
2.2	Mechanical Property Characterization	59
2.2.1	Adhesion measurements	63
2.2.2	Microhardness measurements	70
3.0	SURFACE PREPARATION PROCEDURES	95
3.1	Abrasive Polishing	95
3.2	Surface Cleaning	101
4.0	DIRECTIONS FOR FUTURE WORK	107
4.1	Optical Properties	107
4.2	Mechanical Properties	108
5.0	REFERENCES	109
APPENDIX A		

LIST OF ILLUSTRATIONS

Number	Title	Page
1	Substrate and Coating Design for Vendor-Supplied Films	18
2	Flow Chart for Treatment of Vendor-Supplied Films	19
3	Calculation of Power Inside Sample	21
4	Exact and Approximate Equations for Absorption Coefficient	23
5	Calculation of Power Inside Thin Film	25
6	5.25 Micrometer Carbon Monoxide Laser Calorimeter Chamber - Schematic	29
7	10.6 μm Carbon Dioxide Laser Calorimeter	30
8	Micrographs of Vendor No. 2 As_2S_3 Films on Barium Fluoride	40
9	Internal Reflection Plate	43
10	Schematic Diagram of Harrick Scientific Horizontal Single Pass IRS Attachment	44
11	ATR Spectra of Thorium Fluoride on Zinc Selenide Substrates	46
12	ATR Spectra of Thorium Fluoride Films on Barium Fluoride	47
13	Infrared Absorption Spectrum of $ThF_4 \cdot 4\ H_2O$	48
14	ATR Spectra of Zinc Sulfide Films on Zinc Selenide	51
15	ATR Spectra of Zinc Selenide Films on Barium Fluoride	52
16	ATR Spectra of Arsenic Trisulfide Films on Barium Fluoride	53
17	ATR Spectra of Arsenic Trisulfide Films on Barium Fluoride	54
18	Thin Film Absorption Spectrometer - Schematic	57
19	High Intensity Infrared Point Source	58
20	Output Spectrum of Alumina Point Source	60

LIST OF ILLUSTRATIONS (CONT'D)

Number	Title	Page
21	Nomarski Interference Microscopy of Surface of Film Substrates	61
22	Test Fixture for Direct Pull Adhesion Tests	65
23	Apparatus for Scratch-Adhesion Testing	67
24	Scratch Test of Arsenic Trisulfide Film on Zinc Selenide	69
25	Ultramicrohardness Tester (a) Photograph (b) Cross Section of Operation	72
26	Block Diagram of Ultramicrohardness Apparatus	73
27	Voltage-Displacement Calibration of Piezoelectric Translator	75
28	Load-Position Calibration of LVDT - Beam System	76
29	Recorder Trace of Typical Microhardness Experiment	78
30	Balance Beam Microhardness Tester - Schematic	79
31	Stress-Strain Curve for Material Undergoing Work Hardening	82
32	Indentation Behavior of Potassium Chloride Surfaces	83
33	Anomalous Indentation Behavior	85
34	Indentations in As_2S_3 Films - Nomarski Microscopy	92
35	Indentations in As_2S_3 Films - Scanning Electron Microscopy	93
36	Interferograms of Polished Polycrystalline Strontium Fluoride Surfaces	96
37	Grain Boundary Removal by Diamond Abrasive Polishing	98
38	Absorption vs Length, Strontium Fluoride Specimens	102
39	Hydrocarbon Contamination of Barium Fluoride ATR Plate	104

LIST OF TABLES

Number	Title	Page
I	Vendor-Supplied Film-Substrate Pairs	16
II	Absorption Coefficient Measurements: As_2S_3 Films	34
III	Absorption Coefficient Measurements: ThF_4 Films	35
IV	Absorption Coefficient Measurements: ZnS and ZnSe Films	36
V	Calorimetry of Infrared Optical Films: Vendor No. 2	38
VI	Direct Pull Adhesion Testing: As_2S_3 Film on SrF_2	66
VII	Depth Corrections for Microhardness Indentations	86
VIII	Comparison of Ultramicrohardness and Kentron Measurements of Bulk Materials	88
IX	Comparison of Ultramicrohardness and Kentron Measurement of Film Materials	88
X	Comparison of Bulk and Film Microhardness Values	89
XI	Microhardness of Vendor-Supplied Films	90
XII	Summary of Diamond/Pitch Polishing Technique	99
XIII	Cleaning Procedures for Strontium Fluoride	101
XIV	ATR Spectroscopy: Hydrocarbon Contamination of BaF_2	106

TECHNICAL REPORT SUMMARY

A. Program Objectives

The primary objective of this program was the development of experimental techniques for determining important optical and mechanical properties of surfaces and coatings for infrared laser components. Laser window technology has matured rapidly over the past several years; although the difficulties attending the production of optimized bulk material have not been completely resolved, the time has arrived for a closer evaluation of their surfaces and coatings. Surface and coating properties either do now or soon will limit the absorptive loss, light scattering, laser damage threshold, mechanical stability, and environmental durability of laser optical components. Techniques for determining all these properties and relating them to the details of the surface or coating fabrication procedures must eventually be developed.

This project focussed primarily on determining the infrared absorptivities of important optical film materials obtained from commercial suppliers (as thin films) and the application of microhardness testing to the study of the mechanical properties of thin films. The secondary objectives included: the evaluation of surface finishing techniques for important laser window materials, the search for liquids which were sufficiently transparent at infrared laser wavelengths to be useful as laser coolants, and the delivery of characterized specimens of window materials to the Monitoring Agency for testing with chemical lasers.

B. Significant Accomplishments

Laser calorimetry was shown to be a reliable technique for determining the absorptivities of infrared optical films. A theory which permits calculation of the film absorption coefficient from calorimeter data and other film and substrate parameters was derived. Thin films of zinc sulfide, zinc selenide, thorium fluoride, and arsenic trisulfide obtained from commercial

suppliers were evaluated by laser calorimetry at 5.25 and 10.6 micrometers. The results demonstrate that the film absorptivities substantially exceed the values of their corresponding bulk materials, that very large variations in the film absorptivity occur not only from supplier-to-supplier but also from deposition-to-deposition for single suppliers, and that it is the deposition process and not any fundamental characteristic of the film materials which limits their absorptivity. The minimum detectable absorption coefficients for the films studied during this program were usually limited by the variability of the substrate absorptivities to approximately one reciprocal centimeter. The use of more uniform substrates should improve the lower limit to a few tenths of a reciprocal centimeter.

Attenuated total reflection spectroscopy was used to study the absorption behavior of the commercially-supplied films at a lower sensitivity than laser calorimetry but at all wavelengths between 2.5 micrometers and the infrared cut-off of the substrates. This technique increases the sensitivity of detection of surface absorptions over conventional transmission spectroscopy by means of multiple reflections of the probe beam from the film/substrate surface. ATR spectra could not be quantitatively correlated with the laser calorimetry results, but the thorium fluoride and zinc sulfide spectra did contain characteristic absorptions which varied in intensity from supplier-to-supplier and could be qualitatively correlated with the calorimetric results. Hydrocarbon contamination of the specimens was generally observed in the form of characteristic absorptions in the 3.4-3.5 micrometer range. We point out that these absorptions have a tail which extends to the deuterium fluoride laser wavelengths near 3.8 micrometers.

Exploratory development of a technique which would greatly increase the sensitivity of absorption and scattering measurements of thin films at all infrared wavelengths was begun. An apparatus for the measurements was designed and a high intensity black-body point source was constructed for it.

A new, highly-sensitive apparatus for measuring the microhardness of thin films was designed and constructed. The apparatus will

produce indentations on the order of a tenth micrometer deep and automatically determine the applied load and indentation depth. Operational characteristics of the apparatus were determined and three areas of application to the study of thin film mechanical properties were identified.

1. Direct microhardness measurement - Film materials were found to be approximately four times harder than their corresponding bulk materials. Planned refinements of the apparatus may permit correlation of film microhardness with deposition conditions and macroscopic durability.

2. Film adhesion - Indentation of arsenic trisulfide films frequently produced lifting of quantities film from their substrates the extent of which increased with increasing loads applied to the indenter. In some cases, these films passed the cellophane tape test commonly used for adhesion evaluation. A more thorough study of this effect might produce improved methods for determining the adhesion of marginally adherent films.

3. Environmental stability of surfaces - Fresh chemically polished surfaces of potassium chloride could be distinguished from older weathered surfaces by their indentation behavior. Degradations of film properties caused by environmental exposure should be determinable by quantitative microhardness measurements made either after the exposure or during it, with the apparatus mounted in the test chamber.

An apparatus for determining thin film adhesion by the "scratch" method was also constructed. In this technique a diamond stylus under a series of increasing loads is dragged over the film surface and the adhesion ranked by the minimum load required to remove the film. Nomarski interference microscopy was used to inspect the scratched surfaces. The method was found to be less useful for transparent optical films than for the metallic films with which it has largely been associated. Scanning electron microprobe techniques could be used to improve the usefulness substantially.

Surface finishing procedures for strontium fluoride was explored and a technique for producing scratch-free, optically-figured surfaces on polycrystalline specimens of the material was developed. This technique represents a substantial advance of the state-of-the-art of

surface finishing beyond that used to polish the vendor-supplied substrates used for the thin film studies of this program. Surface cleaning procedures which produced per surface fractional absorptions on strontium fluoride (determined at 5.25 micrometers) of $1\text{-}3 \times 10^{-5}$ were developed. Cooperative efforts carried out with Professor Harrington of the University of Alabama, Huntsville, during the course of this project have determined that surface effects are major contributors to the absorptivity of alkaline earth fluorides at the deuterium and hydrogen fluoride laser frequencies.

Six two-inch diameter specimens of polycrystalline strontium fluoride produced at the Raytheon Research Division by fusion casting were fabricated into windows by the diamond abrasive polishing technique developed during this project and delivered to the Monitoring Agency for evaluation.

Finally, a literature search for liquids which were sufficiently transparent at important infrared laser wavelengths to be useful as laser coolants was carried out. No candidate materials were identified.

C. Conclusions

The tasks of this project have addressed a broad range of subject matter within the purview of surface characterization of optical elements and significant contributions have been made in all areas.

The applicability of laser calorimetry to the study of infrared optical thin films was established and the first evaluation of the present state-of-the-art of commercial samples was completed. Correlation of film absorptivity with deposition conditions is an important research area which should be pursued vigorously. Continuing assessments of commercially-available films should be made to document processing advances.

The results of this project demonstrate that with the possible exception of thorium fluoride, the absorptivities of presently available films are determined by their fabrication procedures and not by fundamental film or material properties.

Optical evaluation experiments should be extended to include calorimetry at chemical laser wavelengths and measurements of light scattering behavior of the films. Absorption and scattering behavior should be correlated with laser damage behavior, if possible, to provide nondestructive testing procedures for optical films. In this context, the integrated optics techniques developed during this project should continue.

Microhardness testing of thin films was developed and shown to be capable of providing a new approach to the study of thin film mechanical properties. The utility of this technique extends to thin films generally. The effort should continue, the technique should be refined and used to correlate film properties with deposition conditions, determine environmental effects on film hardness and adhesion, and correlate microhardness behavior with macroscopic film durability tests.

Surface preparation procedures which simultaneously produce minimal surface absorption, maximum mechanical strength, and maximum adherence for optical coatings deposited onto them must be developed. Preparation and cleaning procedures which are capable of producing optically-figured alkaline earth fluoride surfaces which are free of microscopically detectable defects and residues which absorb 5.25 micrometer radiation significantly are now available. These should now be optimized for performance at chemical laser wavelengths. Chemical polishing, vacuum heat treatments, and perhaps ion beam polishing should be pursued.

1.0 INTRODUCTION

The extensive studies of infrared optical materials which have been conducted over the past several years have produced many notable successes. Theoretical bases for identification and characterization of potential window materials have been developed. Manufacturing methods for materials so identified are progressing rapidly at Raytheon and elsewhere. As of this writing, polycrystalline zinc selenide with absorption coefficients in the mid 10^{-4} cm^{-1} range at 10.6 micrometers is available in sizes as large as 75 centimeter squares. Alkali halide materials for use at the same wavelength are being developed. Absorption coefficients at 5.25 micrometers as low as 4×10^{-5} cm^{-1} have been measured for polycrystalline alkaline earth fluorides, and work on these and oxide materials for use at chemical laser wavelengths is continuing. In sum, the laser window materials effort has made possible the production of optical elements for use at important infrared laser wavelengths which will absorb no more than 10^{-4} of the radiation incident upon them. While much development of bulk materials remains to be done - simultaneous maximization of mechanical strength, optical transparency, laser damage resistance, and thermal shock resistance has not been reported for any material - the rapid progress which has taken place permits more attention to be given to other, related areas of concern. Among these, perhaps the most pressing is the production and characterization of low-loss, low-scatter, damage-resistant surfaces and coatings on the window materials.

The experimental work discussed in this report has largely been directed toward the optical and mechanical characterization of infrared optical thin films which were obtained from commercial vendors. Optical characterization work includes laser calorimetry, which was used to measure absorption coefficients at 5.25 and 10.6 micrometers; attenuated total reflection spectroscopy, which was used to determine the presence of absorption bonds in the films; and an attempt to use integrated optics techniques to couple light into the films for absorption and scattering measurements. Calorimetry and ATR spectroscopy have not been widely applied to optical films which until the appearance of high-power lasers, were required only to have the correct wavelength dependence of transmission or reflection.

Mechanical characterization of thin films by contrast, has received considerable attention over many years. The subject is very complex because the mechanical properties of both the thin film and its substrate and the strength of the film-substrate bond combine in an unknown way to determine the results of most traditional mechanical properties tests. As a result, mechanical testing of films consists largely of user-oriented engineering tests which cannot be used to understand the properties of the films themselves. During the course of this project, an apparatus for measuring the microhardness of thin films was designed and constructed. Preliminary results obtained with the instrument indicate that it may be used to study the environmental stability and in some cases the adhesion of thin films, as well as their microhardness. In addition to the microhardness work, some traditional mechanical evaluation of the films is reported.

Surface preparation techniques for polycrystalline strontium fluoride are explored, and a recommended procedure for the simultaneous production of a scratch-free and optically-figured surface is presented.

The techniques developed here were used for the production of six two-inch diameter cast polycrystalline strontium fluoride windows for delivery to the Monitoring Agency.

Finally, a literature search for liquids which might be useful transparent coolants for lasers operating in the 3-5 and 10.6 micrometer spectral ranges is presented as an appendix tc the report.

2.0 THIN FILM CHARACTERIZATION

A first-order characterization of most optical thin films is not difficult. Spectrometer traces will determine the extent to which the film meets its spectral performance requirements, and cellophane tape and rubber eraser tests may be used to gauge its physical durability.[1] As more than cursory information is required from the characterization tests, however, the problem becomes more complex and the data less rewarding. Ultimately, important film parameters must not only be measured, but related to the details of the deposition procedures which produce them.

Optical coatings for high-power laser elements must have minimized absorptivity and be free from light-scattering and damage-inducing inclusions. These optical properties, which are beyond the analytical capability of most commercial optical coating suppliers, must not only be produced in the original coating but must be retained after the film is exposed to its use environment. The critical mechanical properties for optical films are adhesion and durability, those required of all thin films, but again the relationship between physical and optical degradation must be determined. Both film characterization procedures must eventually operate at three levels. They must quantitatively identify important film properties, relate them to film behavior in use, and relate them to the original deposition conditions.

During this project, the first of these levels has been emphasized. Films obtained from commercial vendors have been studied and development of characterization techniques has begun. These experiments are intended to develop techniques which can be used for the eventual correlation of film properties with deposition parameters. At that stage, the optical and mechanical properties of the films must be correlated with their chemical and microstructural properties, as well as such deposition parameters as evaporant purity, deposition rate, source and substrate temperatures, deposition pressure and residual atmosphere composition.

The film-substrate combinations listed in Table I were obtained from three commercial film producers: Broomer Laboratories, Plain View,

TABLE I

VENDOR-SUPPLIED FILM-SUBSTRATE PAIRS

Substrate	Film
BaF_2	ThF_4
	As_2S_3
	ZnSe
ZnSe	ThF_4
	As_2S_3
	ZnS

New York; Optical Coating Laboratories, Inc., Santa Rosa, California; and Spectra-Physics, Inc., Mountain View, California. During the evaluation of the films, discussions of the nonproprietary aspects of the deposition processes were requested from the vendors. Broomer Labs., because of personnel changes in their coating operation could not contribute to the discussions. Since the primary focus of this project is intended to be upon the use of the analytical techniques and range of properties presently obtained from commercial sources rather than upon a direct competition among coaters, these companies will be referred to as Vendors No. 1, 2 and 3, respectively,in the remainder of the text.

The substrates were barium fluoride single crystals obtained from Harrick Scientific and chemical vapor deposited polycrystalline zinc selenide produced at the Raytheon Research Division. The substrates were fabricated into the shape given in Fig. 1 and polished by Harrick Scientific Corp., Ossining, N.Y. This substrate shape was chosen to permit both laser calorimetry and attenuated total reflection spectroscopy to be performed on the films. Harrick was chosen for the fabrication on the basis of their development of the ATR technique. The coating vendors were requested to produce two specimens of each film-substrate pair in separate runs to provide run-to-run as well as vendor-to-vendor comparisons. Substrates were to be half-coated on the larger face, as shown in Fig. 1. Vendors were to supply their own substrate cleaning procedures, evaporant materials, and "optimized" evaporation procedures. The films were to have an optical thickness of one-half wave at 5.0 micrometers. The sequence of experiments performed upon the vendor-supplied specimens is outlined in Fig. 2 and discussed in the following sections.

2.1 Optical Characterization

2.1.1 Laser calorimetry

2.1.1.1 Theory

The absorption coefficients of the films were measured directly by laser calorimetry at 5.25 and at 10.6 micrometers. Laser calorimetric techniques which measure the temperature rise in a bulk sample caused

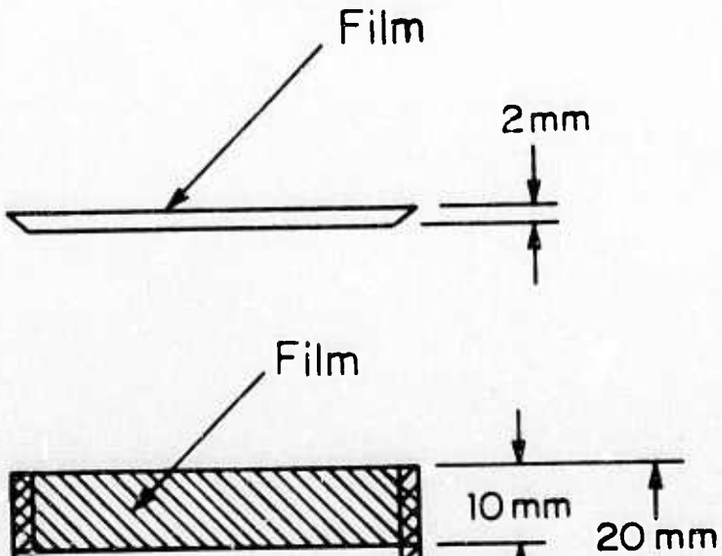


Fig. 1 Substrate and Coating Design for Vendor-Supplied Films.

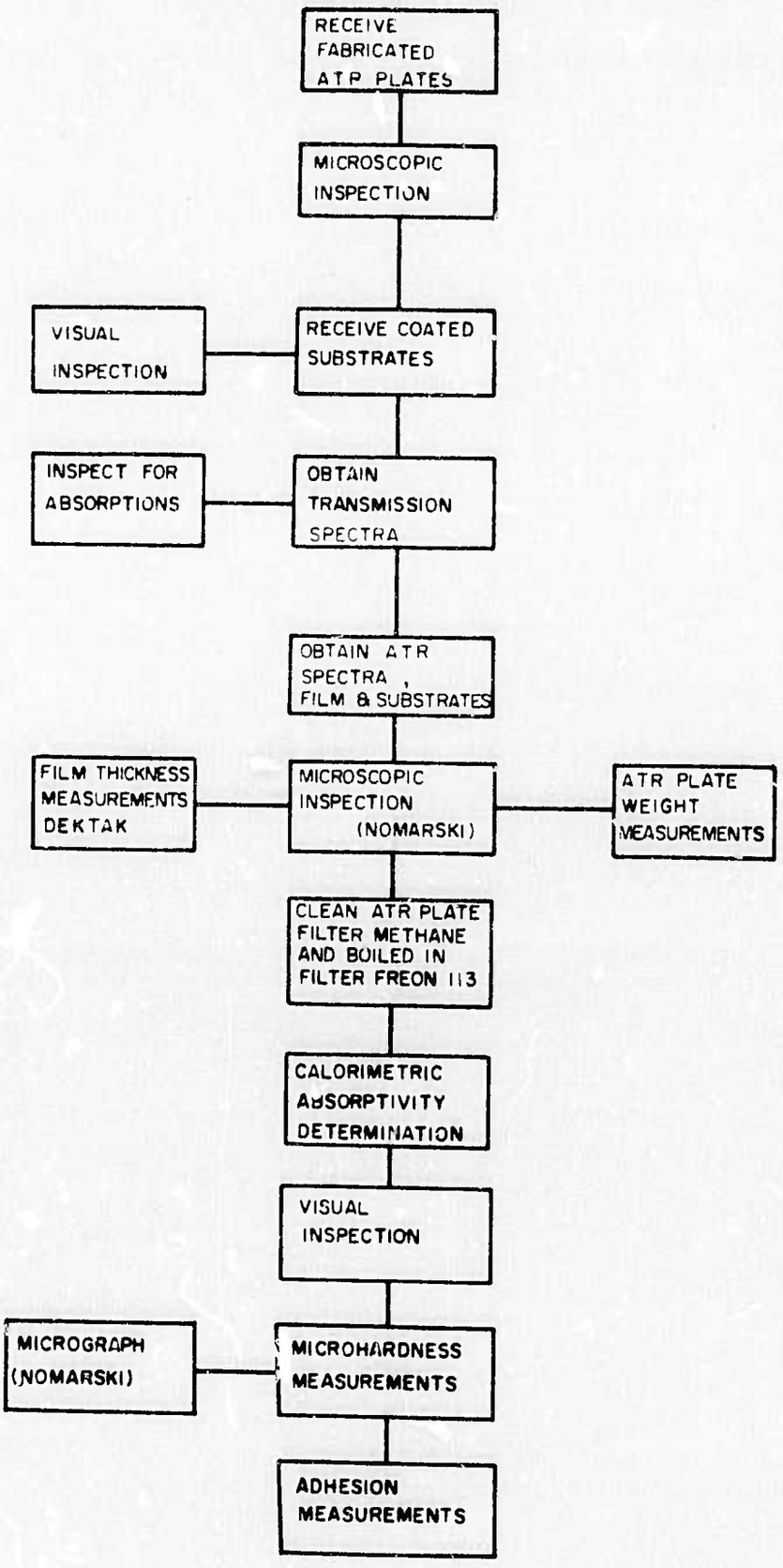


Fig. 2 Flow Chart of Treatment of Vendor-Supplied Films

by a known quantity of laser radiation, have been widely reported.[2,3] We treat here the elaborations of the technique which were used to obtain film values.

Most measurements of film absorption are made by measuring the substrate material and then the film/substrate combination; the difference is given as a percentage increase in the absorption. However, this interpretation is oversimplified since the film changes the surface reflection and thus the power incident on the substrate. What is really needed is the absolute value of the absorption coefficient of the film. To obtain this, the β (absorption coefficient) of the substrate must first be known.

The power absorbed by a substrate of thickness ℓ, and absorption coefficient β when $\beta\ell$ is small is

$$P_{absorbed} = P_{inside} (1 - e^{-\beta\ell}) \quad . \tag{1}$$

For $\beta\ell << 1$, this equation becomes

$$P_{absorbed} = \beta\ell \; P_{inside} \quad . \tag{2}$$

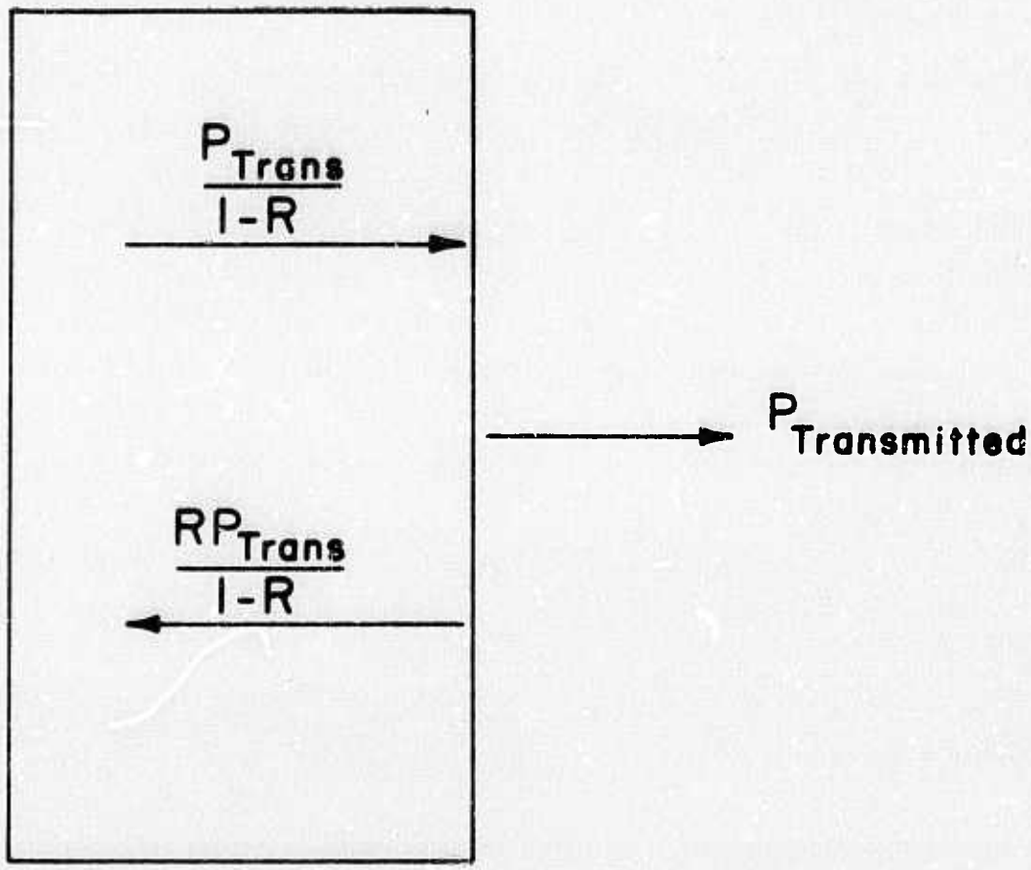
Figure 3 shows the calculation of P_{inside} (the power inside the sample). If the transmitted power and the index of refraction of the sample are known, we can determine the two components of power, i.e., a wave traveling toward the exit surface and a reflected wave, whose sum is the total power in the sample. Substituting the result from Fig. 3 into Eq. (2) gives

$$P_{absorbed} = \beta\ell \; P_{tran} \left(\frac{1+R}{1-R}\right) = \beta\ell \; P_{tran} \frac{n^2+1}{2n} \quad , \tag{3}$$

or

$$\beta = \frac{1}{\ell} \; \frac{P_{absorbed}}{P_{transmitted}} \left(\frac{2n}{1+n^2}\right) \quad . \tag{4}$$

Again, this equation for the absorption coefficient, β, assumes $\beta\ell << 1$. To determine the usefulness of this assumption, the exact equation for the absorption coefficient was calculated



$$P_{Inside} = P_{Trans} \times \frac{(1+R)}{(1-R)} \qquad R = \left(\frac{n-1}{n+1}\right)^2$$

$$P_{Inside} = P_{Trans} \times \left(\frac{n^2+1}{2n}\right)$$

Fig. 3 Calculation of Power Inside Sample.

$$\beta = \frac{1}{\ell} \ln \left\{ \frac{(2n)\left((P_{abs}/P_{tran}) + 1\right)}{(n+1)^2} \left[1 + \sqrt{1 + \left[\frac{n^2 - 1}{2n\left(\frac{P_{abs}}{P_{tran}} + 1\right)} \right]^2} \right] \right\} \quad (5)$$

This equation is plotted in Fig. 4 together with the approximate Eq. (4); for an index of refraction of 1.40 the two equations deviate about five percent for $\beta\ell = 0.1$. Thus, for $\beta\ell < 0.1$, the approximate equation can be used and for $\beta\ell$ greater than 0.1 the exact equation should be used. Both of these equations are independent of the coherence of the infrared beam and the possibility of interference fringes because the absorption coefficient is determined from the transmitted power and the reflectivity of the rear surface of the sample. The incident power can only be used to calculate the power inside the sample if the IR beam is incoherent. If it is coherent, resonance effects can change the ratio of P_{inside} to $P_{incident}$ making it difficult to do the calculation. Therefore, our experimental apparatus is set up to measure transmitted power.

Once the β_s for the substrate is known, one can calculate the (β_F) absorption coefficient of the film.

In the following, we want to derive the formulas necessary to evaluate the absorption of the surface film from calorimetric measurements. As shown in conjunction with Fig. 3, the absorbed laser power in a simple uncoated slab of material is given in terms of the absorption coefficient β_s of the substrate, the thickness of the substrate L_s, the reflection coefficient of the surface R_s by

$$P_{abs} = \beta_s L_s \frac{1 + R_s}{1 - R_s} P_{trans} \quad . \quad (6)$$

We can conveniently generalize this equation to cover the absorption both in the substrate and in the film if we orient the sample such that the film is at the exit side of the laser beam. The total film acts like a Fabry-Perot reflector of as yet unknown reflectivity R_F. Thus, Eq. (7) gives the absorption in the substrate if we replace R_s by the film reflectivity R_F

$$P_{abs}\ (\text{substrate}) = \beta_s L_s \frac{1 + R_F}{1 - R_F} P_{trans} \quad . \quad (7)$$

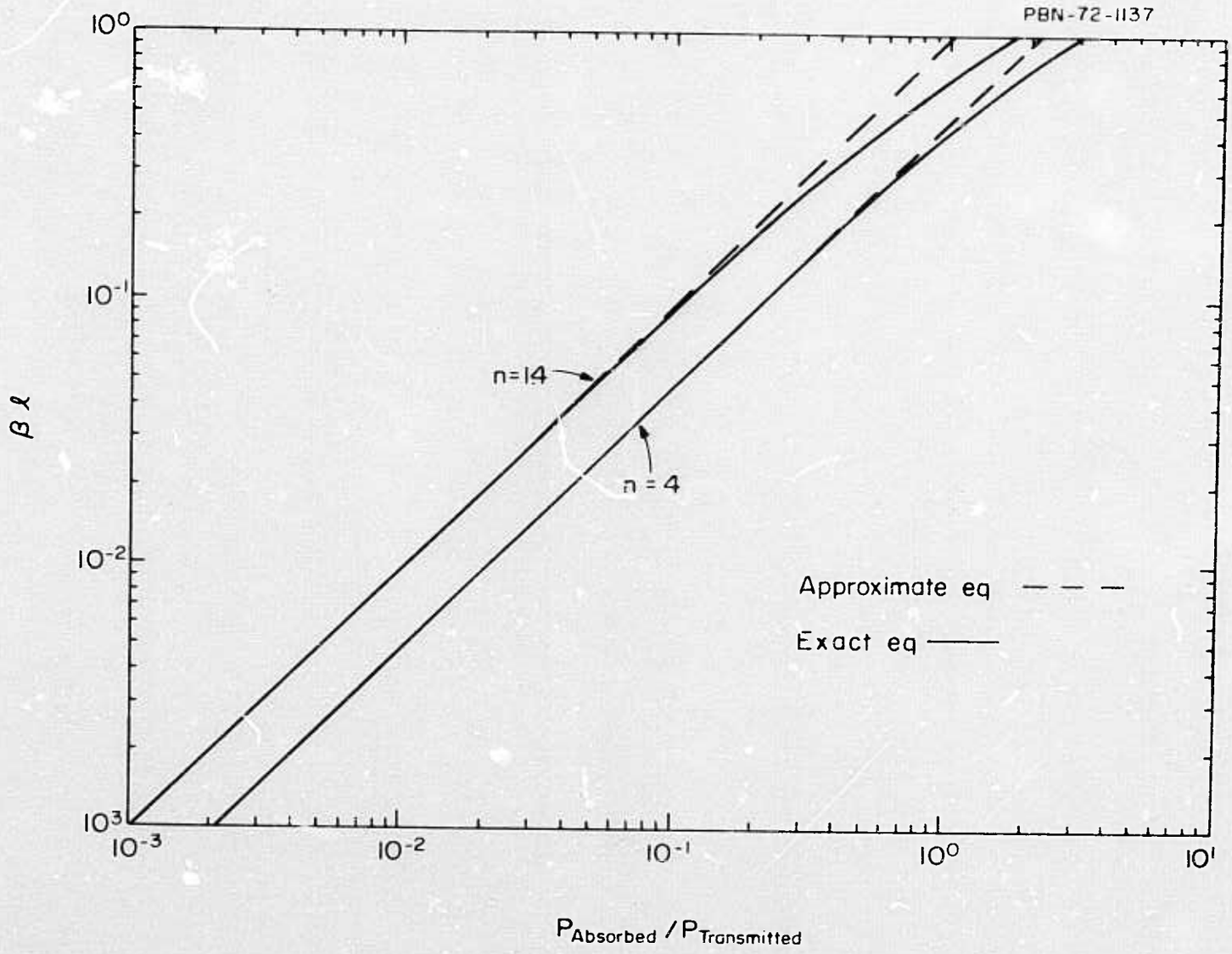


Fig. 4 Exact and Approximate Equations for Absorption Coefficient.

We must also calculate the power absorbed in the film. Since the film is relatively thin and comparable in thickness to a wavelength we must take into account the interference of light waves traveling in the film towards the film/air interface and those reflected from that interface. Referring to Fig. 5 we write for the electric field of a wave traveling to the right towards the air/film interface at x = 0.

$$E = A \exp(i\,kx) \tag{8}$$

In Eq. (8) A is some amplitude normalized such that A^2 represents intensity of the light beam and k is the propagation vector given by

$$k = \frac{n_F \omega}{C} = n_F \frac{2\pi}{\lambda_0} \tag{9}$$

where n_F is the index of refraction of the film, ω the orbital frequency of the light wave, C the velocity of light and λ_0 the free space wavelength.

By adding the wave reflected at air/film interface at x = 0 we obtain:

$$E = A \exp(i\,kx) + r\,A \exp(-\,j\,kx) \tag{10}$$

where

$$r = \left(\frac{n_F - 1}{n_F + 1}\right)^2 . \tag{11}$$

Note, the reflected wave experiences no phase change upon reflection since the reflection occurs from a transition to a less dense medium. Taking the absolute magnitude squared of the field gives

$$|E|^2 = A^2 (1 + r^2) + 2r\,A^2 \cos 2\,kx \tag{12}$$

Remembering the normalization of A the absorbed energy is simply given by:

$$\begin{aligned} P_{abs} &= \beta_F \int_{-\Delta L_F}^{0} \{ A^2(1+r)^2 + 2rA^2 \cos 2\,kx \}\, dx \\ &= \beta_F \Delta L_F\, A^2 (1 + r^2)\, \beta_F \frac{r A^2 \lambda_0}{2\pi\, n_F} \sin \frac{4\pi\, n_F}{\lambda_0} \Delta L_F . \end{aligned} \tag{13}$$

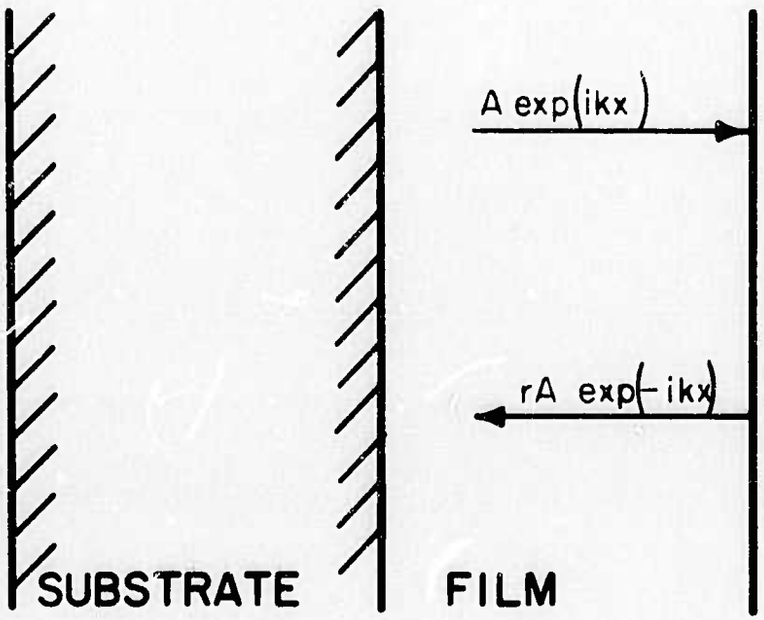


Fig. 5 Calculation of Power Inside Thin Film.

In Eq. (13) β_F is the absorption coefficient of the film. Also use has been made of Eq. (9).

Finally, we want to relate A^2 to the transmitted power P_{trans} by stating that the power incident on the film-air interface minus the power reflected from that interface is equal to the transmitted power, or

$$A^2 \left[1 - \left(\frac{n_F - 1}{n_F + 1} \right)^2 \right] = P_{trans} \tag{14}$$

Equation (14) can be solved to give

$$A^2 = P_{trans} \frac{(n_F + 1)^2}{4 n_F} \tag{15}$$

$$A^2 (1 + r^2) = P_{trans} \frac{n_F^2 + 1}{2n_F} \quad . \tag{16}$$

Inserting Eqs. (15) and (16) in Eq. (13) gives

$$P_{abs}(film) = P_{trans} \beta_F \Delta L_F \left\{ \frac{n_F^2 + 1}{2n_F} + \frac{n_F^2 - 1}{4 n_F^2} \frac{\lambda_0}{2\pi \Delta L_F} \sin \frac{4\pi n_F}{\lambda_0} \Delta L_F \right\} \tag{17}$$

The total absorption of film and substrate follows by adding Eqs. (7) and (17)

$$\frac{P_{abs}}{P_{trans}} = \beta_s L_s \frac{1 + R_F}{1 - R_F} + \beta_F \Delta L_F \left\{ \frac{n_F^2 + 1}{2n_F} + \frac{n_F^2 - 1}{4n_F^2} \frac{\lambda_0}{2\pi \Delta L_F} \sin \frac{4\pi n_F}{\lambda_0} \Delta L_F \right\}$$

$$= \overline{\beta}_s L_s \frac{1 + R_{FA}}{1 - R_{FA}} \quad . \tag{18}$$

In Eq. (18) we also defined an effective absorption coefficient $\overline{\beta}_s$ for the film and substrate in analogy with Eq. (7). By noting that

$$R_{FA} = \left(\frac{n_F - 1}{n_F + 1} \right)^2 \tag{19}$$

the last part of Eq. (18) may be written

$$\frac{P_{abs}}{P_{trans}} = \bar{\beta}_s \, L_s \, \frac{n_F^2 + 1}{2n_F} \tag{20}$$

Solving Eq. (18) for β_F in terms of β_s and $\bar{\beta}_s$ gives with the help of Eq. (19)

$$\beta_F = \frac{L_s}{\Delta L_F} \left[\bar{\beta}_s \frac{n_F^2 + 1}{n_F^2 + 1 + \frac{n_F^2 - 1}{2n_F} \frac{\lambda_0}{2\pi \Delta L_F} \sin \frac{4\pi n_F}{\lambda_0} \Delta L_F} \right. \tag{21}$$

$$\left. - \beta_s \frac{\frac{1 + R_F}{1 - R_F}}{\frac{n_F^2 + 1}{2n_F} + \frac{n_F^2 - 1}{4n_F^2} \frac{\lambda_0}{2\pi \Delta L_F} \sin \frac{4\pi n_F}{\lambda_0} \Delta L_F} \right]$$

Equation (21) is the basis for determining β_F from measurements. In essence β_s is determined by measuring the absorbed power in the uncoated substrate and using Eq. (6) with

$$R_s = \left(\frac{n_s - 1}{n_s + 1} \right)^2 . \tag{22}$$

Furthermore, $\bar{\beta}_s$ is determined from Eq. (12) with measurements carried out on the coated sample. The quantity R_F is being measured by monitoring the transmission of light through the sample. The necessary equations for this measurement are derived in the following. In Fig. 5 we show light of intensity P_o falling on the uncoated side of the substrate. The light transmitted into the substrate is $(1-R_s)P_o$. Upon the first reflection from the film, the amount of light transmitted is given by $(1-R_s)(1-R_F)P_o$. We can add up all transmitted light waves after bouncing back and forth in the substrate neglecting the phase factors (because of the large thickness to give

$$\frac{P_{trans}}{P_o} = (1-R_s)(1-R_F)(1+R_F R_s + R_F^2 R_s^2 + \dots) \tag{23}$$

$$= \frac{(1-R_s)(1-R_F)}{1-R_s R_F} .$$

By defining a transmittivity T through

$$\frac{P_{trans}}{P_o} = T \quad , \tag{24}$$

we obtain from Eqs. (14) and (15)

$$R_F = \frac{1-R_s-T}{1-R_s-TR_s} \quad . \tag{25}$$

Experimentally we measure T using an infrared spectrometer and calculate R_s from Eq. (22) to obtain R_F. Thus, all factors are in hand to determine β_F in Eq. (21).

2.1.1.2 Experimental apparatus and procedure

The calorimetry was performed in the calorimeters shown in Figs. 6 and 7. The carbon monoxide calorimeter chamber is rectangular with a one-inch thick plexiglas cover. The outside dimensions of the chamber, which is made of 1/2 in. thick aluminum, are approximately 13 × 14 × 25 in. An optical rail is mounted within the chamber and the various components, such as irises, sample mounts, and the power cone are mounted on optical carriers with adjustable x-y motions, permitting ready removal or alignment of any component. The chamber vacuum is evacuated by three 50 cfm pumps. A He-Ne alignment laser has been permanently incorporated into the system; a flip mirror allows the beam to be directed along the same axis as the measurement lasers. Preliminary sample alignment is performed using the visible laser, and the final alignment may be checked using burn spots made by the infrared lasers. The sealed CO laser uses a dry-ice and methanol cooling system and is capable of producing 20W of multimode power. The center of gravity of the intensities of the various spectral lines of the laser has been determined to be 5.25 micrometers. A grating monochromator is incorporated in the system to permit frequent wavelength checks. Reflections from the faces of the sample are directed onto a

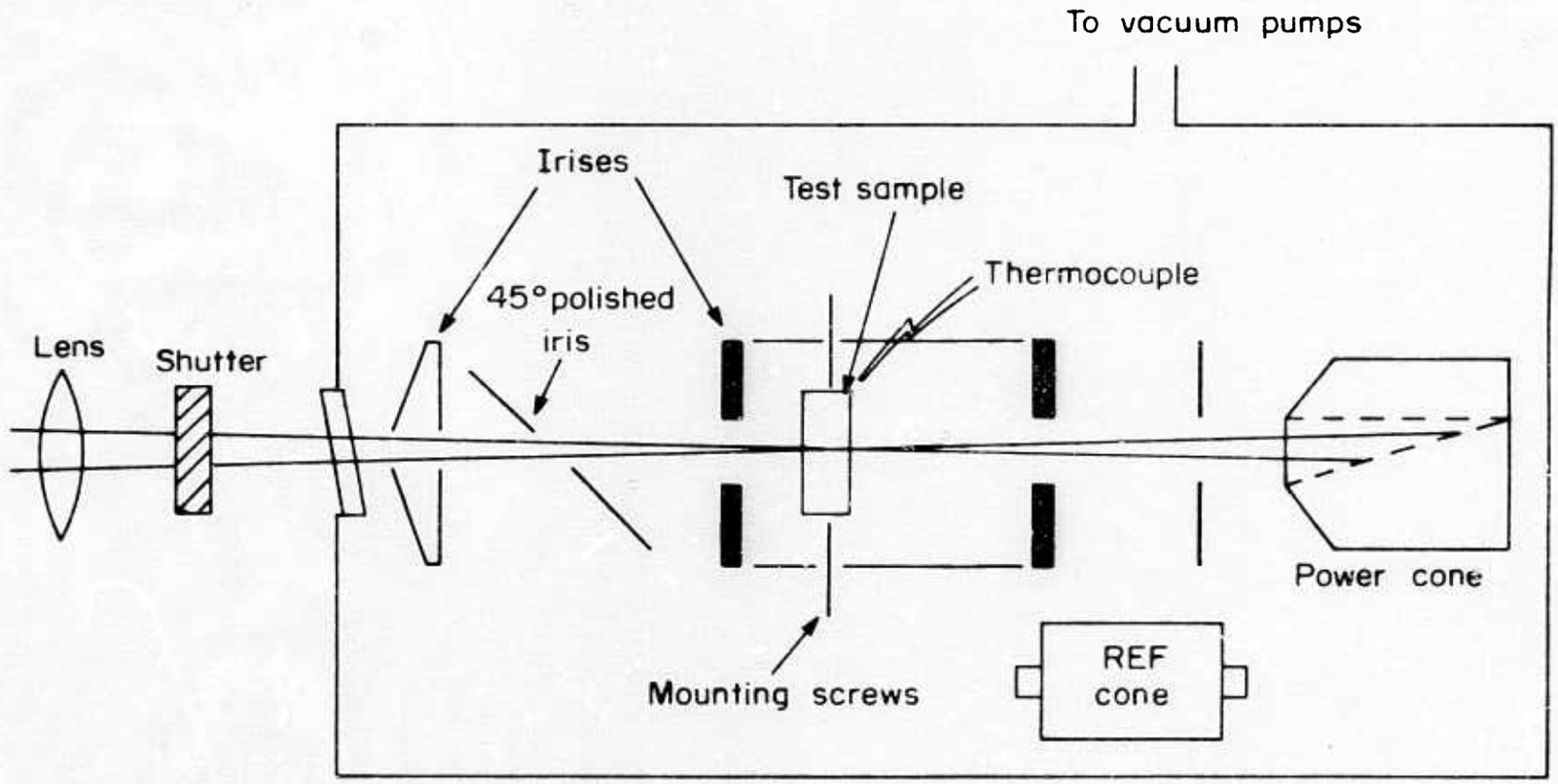


Fig. 6 5.25 Micrometer Carbon Monoxide Laser Calorimeter Chamber - Schematic.

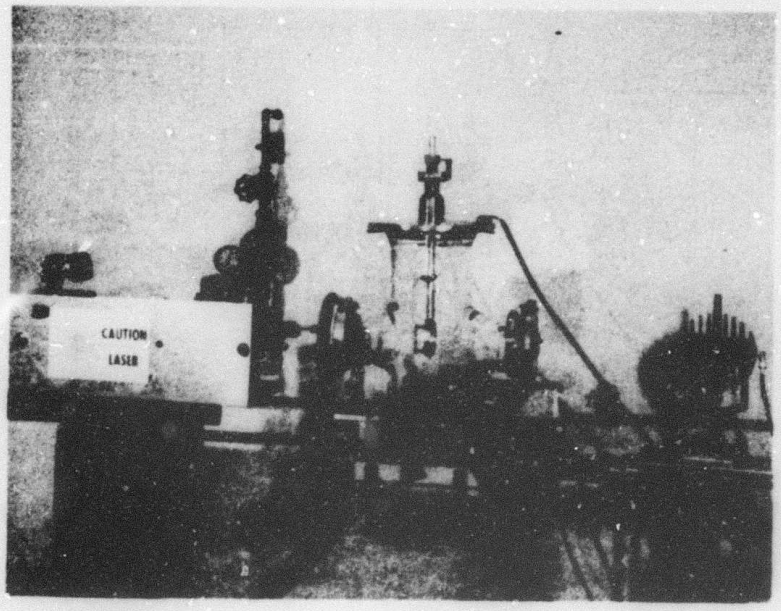


Fig. 7 10.6 μm Carbon Dioxide Laser Calorimeter.

polisned iris which is angled at 45° to the main beam and reflected onto the blackened chamber walls. The sample itself is mounted by three or four nylon screws within a 3-inch-diameter piece of aluminum tubing, the ends of which are closed off by irises. This prevents stray radiation which is not on the beam axis from reaching the sample thermocouple; the latter is further covered by a small piece of aluminum foil to reduce any direct absorption of stray radiation. The thermocouple is clamped inside the aluminum block, assuring good thermal contact and minimizing the turn on/turn off transients which can make the power cone temperature versus time curves hard to interpret. The cone was checked against the readings given by a CRL power meter at the same location within the chamber and the two techniques were found to agree to better than 5 percent.

The 10.6 micrometer laser calorimeter is shown in Fig. 7. This chamber is a pyrex cross with a 6 inch i.d. vertical arms and 4 inch i.d. horizontal arms. Evacuation of the chamber is accomplished through an opening in the base plate with a standard diffusion pump vacuum system. The side arms are fitted with KCl windows to allow entrance and exit of the laser beam. The sample is mounted in a ring attached to a rod which passes through a seal in the top plate. This rod may be moved vertically, and the entire chamber horizontally, to permit probing of different parts of the sample. The sample is mounted in the ring with four nylon screws, one of which also serves to press a thermocouple junction against the sample. The reference junction for the thermocouple is attached to a polished aluminum block also in the chamber but away from the laser beam, and the thermocouple leads pass through sealed holes in the top plate.

A Coherent Radiation Model 42 laser, capable of 50W at 10.6 μm, is used as power source, and a Coherent Radiation Model 201 Power Meter measures the power coming out of the exit window.

The outputs of the sample thermocouples of both calorimeters are amplified by Keithley Model 148 nanovoltmeters and displayed, along with the output of the power meters, on strip chart recorders. The absorption coefficient may be calculated either from the actual temperature rise of the sample or from the slope of the temperature rise, both appropriately

corrected for heat loss. To facilitate the calculations, a computer program has been written which requests the pertinent data, provides the refractive index and specific heat for commonly measured materials and performs the calculations. The computer program does not assume that the fraction of power absorbed is small, and the output gives the fraction absorbed and the absorption coefficient (uncorrected for any surface absorption). This program produces values for $\overline{\beta}_s$ and β_s. A second program, which calculates β_f using Eq. (21), was written for this project.

The substrate thicknesses were measured with a micrometer. Film thicknesses were determined by direct measurement with a surface profilometer.* Transmissivities at the laser wavelengths were measured by a Perkin-Elmer Model 457 spectrophotometer.

Immediately prior to its absorption measurement, each specimen was boiled in Freon-113** to remove hydrocarbon contamination. The Freon boils at approximately 47°C and will not affect the adhesion of a usable optical film.

The specimen was mounted in the calorimeter with the thermocouple fixed to the midpoint of one long side and calorimetric measurements were made on the long half opposite the thermocouple. For example, if the thermocouple were attached to the coated half, the uncoated portion of the specimen would be measured. The specimen was then rotated by 180° and the measurements were repeated on the opposite side. This procedure was adopted to preserve the symmetry of the heat flow.

Although no specific effort to randomize the order in which the specimens were measured was made, there was no significant pattern in the order in which the results were reported and calculated. For a significant portion of the time, specimens from more than one supplier were being evaluated. We believe, therefore, that the results obtained represent the absorptive behavior of the films, limited, as detailed below, by the variability of the substrate absorptivity.

---

* Dektak, trademark of Sloan Industries.

** Trademark, Dupont Co.

2.1.1.3 Laser calorimetry - results and discussions

The results of the calorimetric absorption measurements are summarized in Tables II-IV. With the exception of the films obtained from Vendor 2, the assignment of a films to deposition number one or two was done arbitrarily. Vendor 2 films are discussed separately below. For the most part, two measurements were made on the coated and two on the uncoated half of each substrate. Those cases where a larger number of measurements was used are noted in the tables. Absorptivities are reported as calculated from averages of the measurement pairs followed by a range which is in fact the range of values obtained from the individual measurements for those cases where only two pairs were taken and a standard deviation for larger numbers of measurement pairs. Occasionally an absorptivity is reported as being less than a certain quantity which is pronounced to be the minimum detectable limit. This limit was calculated for each film-substrate pair for which near-zero or negative absorptivities occurred by considering the variability of the substrate absorptivity. Equation (22) may be rewritten in the form

$$\beta_f = \frac{L_s}{\Delta L_f} \left[\overline{\beta}_s - K \beta_s \right] . \qquad (26)$$

The value of K is determined by the index and thickness of the films. It varied from approximately 0.75 to 1.3 for the films measured during this program. To calculate a minimum detectable absorptivity, we assume that the film contribution to the total absorption is $\overline{\beta}_s$ must be large enough to make the difference in the brackets above at least as large as two standard deviations of the variability of the uncoated measurements. The majority of the determinations of the uncoated side involved only two measurements in which case one half the total range was used to represent a "standard" deviation. This is actually statistically an underestimate of the true variability and probably a slight overestimate of the minimum detectable value. The values do, however, reflect reasonable, consistent estimates of the minimum detectable limits for these specimens. We consider minimum detectable limits for the procedure at the end of this section.

Examination of the tabulated data permits several generalizations to be drawn. First, with the exception of thorium fluoride films, all

TABLE II

ABSORPTION COEFFICIENT MEASUREMENTS: As_2S_3 FILMS

Substrate	Wavelength (Micrometers)	Absorption Coefficient (cm^{-1}) Deposition 1	Deposition 2	Supplier
BaF_2	5.25	0.48 ± .008	NM	1
		0.32 ± 0.01	2.05 ± 0.16	2
		5.00 ± 0.02	1.40 ± 0.20	3
ZnSe	5.25	0.47 ± 0.24	2.38 ± 0.06	1
		0.27 ± 0.05	1.23 ± 0.20	2
		1.30 ± 1.1	1.95 ± 0.1	3
ZnSe	10.6	2.50 ± 0.30	5.50 ± 1.10	1
		3.84 ± 0.81	8.46 ± 1.04	2
		< 2.35*	5.91 ± 1.2**	3

BULK ABSORPTION COEFFICIENT: As_2S_3

Wavelength (micrometers)	Absorption Coefficient (cm^{-1})
5.25	5×10^{-3}
10.6	0.01 - 1.0

* Minimum detectable limit

** Three pairs of measurements, range is standard deviation.

TABLE III

ABSORPTION COEFFICIENT MEASUREMENTS: ThF_4 FILMS

Substrate	Wavelength (micrometers)	Absorption Coefficients (cm^{-1}) Deposition 1	Deposition 2	Supplier
BaF_2	5.25	15.60 ± 0.35	3.45 ± 1.4	1
		3.18 ± 0.44	1.65 ± 0.04	2
		0.82 ± 0.12*	0.69 ± 0.09*	3
ZnSe	5.25	18.09 ± 1.44*	13.90 ± 5.5	1
		0.36 ± 0.01	< 1.35**	2
		3.30 ± 0.80***	< 2.88*	3
ZnSe	10.6	63.8 ± 2.9	58.0 ± 12.0	1
		21.33 ± 1.62	16.23 ± 0.53	2
		11.38 ± 2.73***	9.11 ± 0.82*	3

BULK ABSORPTION COEFFICIENT ESTIMATES: ThF_4

At 5.25 micrometers $< 1.0\ cm^{-1}$
At 10.6 micrometers $\sim 10\ cm^{-1}$

* Three pairs of measurements

** Minimum detectable limit

*** Based on standard deviation of 14 measurements

TABLE IV

ABSORPTION COEFFICIENT MEASUREMENTS: ZnS AND ZnSe FILMS

Film	Substrate	Wavelength (micrometers)	Absorption Coefficient (cm^{-1}) Deposition 1	Deposition 2	Supplier
ZnSe	BaF_2	5.25	2.02 ± 0.72	1.00 ± 0.83	1
			3.63 ± 0.34	< 0.5*	2
			1.32 ± 0.23	1.45 ± 0.37	3

BULK ABSORPTION COEFFICIENT: ZnSe

At 5.25 micrometers, 3×10^{-4} - 1×10^{-3}
(measured in CVD material)

ZnS	ZnSe	5.25	< 1.96*	10.7 ± 2.3	1
			1.32 ± 0.69	< 0.1*	2
			1.29 ± 0.04**	1.33 ± 0.36**	3
		10.6	20.05 ± 2.54	15.18 ± 1.11	1
			4.16 ± 1.53	< 1.5*	2
			1.00 ± 0.85	< 1.39*	3

BULK ABSORPTION COEFFICIENT: ZnS

At 5.25 micrometers $<< 0.1$
At 10.6 micrometers ~ 0.15

*Minimum detectable limit

**Three measurement pairs

the measurable film absorptivities all exceed the corresponding measured or estimated bulk values significantly. Judging from the great variability of the thorium fluoride measurements and the extent to which the less variable chalcogenide films exceed their bulk values, this estimate may need to be revised downward in the future as well.

Second, for As_2S_3 and ThF_4 films, which were deposited onto both substrate materials, the range and level of absorptivity is not influenced by the choice of substrate. Other factors are determining the absorption.

Third, there is a significant variability in the level of absorptivity obtained by the three vendors. The largest variation occurs for the thorium fluoride films. We show in the next section the probable cause for this variability.

There is also significant run-to-run variability of film absorptivity. Examples may be found in the results obtained for all three vendors. Of these, the films deposited by Vendor 2 are the most interesting because their procedure of depositing onto both substrate types simultaneously when ThF_4 and As_2S_3 films were being deposited made one additional comparison possible. Further, their record keeping permitted the sequence of the depositions to be correlated with the absorptivity measurements. The absorptivity measurements made on Vendor 2 films are grouped according to their deposition run numbers in Table V. The depositions were made in the order given by the last digits of the run numbers. Note that the depositions were carried out in the chamber in an order which placed the most contaminating As_2S_3 depositions last in line.

Vendor 2 reports that the repeated depositions were carried out under as nearly identical conditions of evaporation rate, substrate temperature, evaporant preheat time and temperature, and chamber base pressure as possible. Fresh charges of evaporant, taken from the same lot and batch, were used for both members of each deposition pair. The only detectable variation in deposition behavior occurred during the As_2S_3 deposition, during the second of which the optical thickness monitor indicated a lower reflectivity than it had during the first deposition.

TABLE V

CALORIMETRY OF INFRARED OPTICAL FILMS: VENDOR NO. 2

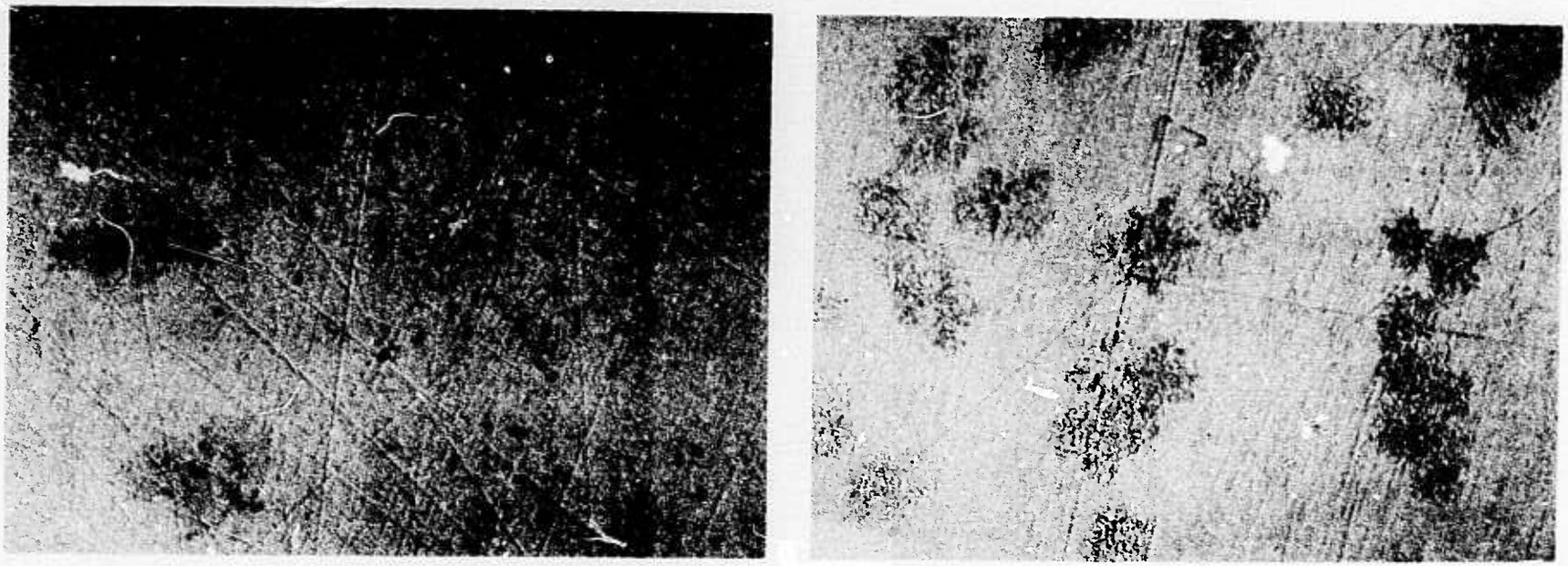
Deposition Run No.	Film	Substrate	Wavelength (micrometers)	Film β (cm^{-1})
543-002	ZnS	ZnSe	5.25	1.3
			10.6	4.1
543-003	ZnS	ZnSe	5.25	< 0.1*
			10.6	< 1.5*
543-005	ZnSe	BaF_2	5.25	3.6
543-006	ZnSe	BaF_2	5.25	< 0.5
543-008	ThF_4	BaF_2	5.25	3.18
		ZnSe	5.25	0.36
			10.6	21.3
543-009	ThF_4	BaF_2	5.25	1.65
		ZnSe	5.25	< 1.35*
			10.6	16.2
543-012	As_2S_3	BaF_2	5.25	0.32
		ZnSe	5.25	0.27
			10.6	3.8
543-013	As_2S_3	BaF_2	5.25	2.0
		ZnSe	5.25	1.2
			10.6	8.4

* Estimated minimum detectable limit for the film-substrate pair.

The data in Table V demonstrate sizable variations in film absorptivity may occur among consecutive deposition runs even when all the deposition parameters normally associated with good thin film deposition practice are monitored and held constant. Bear in mind that the absorption data were collected in two calorimeters, one for each wavelength. Two of the deposition pairs, 008-009 and 012-013 contained both substrate types. In no case is the ranking of the absorptivity level reversed for a film or substrate pair.

While any attempts to explain the variations are pure speculation, it is interesting to note that in each of the first three deposition pairs, the second deposition had the lower absorptivity. Such behavior may be plausably explained by assuming that the material from the first deposition acted as a getter for some absorbing species in the residual gas and that the gettering action was sufficiently strong that opening the chamber to change substrates and replenish the evaporant charge did not destroy it. Certainly two conclusions follow logically from these observations. First, a careful correlation of the level and composition of the residual atmosphere in the deposition chamber, the deposition rate, and the absorptivities of optical films should be carried out. Second, on a more immediately practical level, it would be well to make use of whatever gettering action is produced by the film material by beginning each the deposition onto as large an area of the chamber itself as is practical and exposing the substrates to the evaporant after a "gettering period." This approach might require alterations in the shuttering technique for large area depositions.

The single instance in which the higher absorptivity occurred in the second of the deposition pairs was deposition 013, the As_2S_3 film which was reported to have a lower reflectivity than its predecessor. Nomarski interference photomicrographs of the two As_2S_3 films on BaF_2 substrates are shown in Fig. 8. The larger defect density on the film which had the higher absorptivity is apparent. While we have not identified the defects, it is reasonable to suspect that they contribute to the film absorptivity. Only the As_2S_3 films contained features which could be distinguished from their substrate in the optical microscope. Certainly these features would scatter the light of the optical thickness monitor and cause the reflectivity reduction which was observed.



a) Low Absorption Coefficient Film

b) High Absorption Coefficient Film

Fig. 8 Micrographs of Vendor No. 2 As_2S_3 Films on Barium Fluoride.

In summary, the film calorimetry experiments have shown that the film absorptivities are for the most part substantially higher than the corresponding bulk values. It appears most likely that the differences are produced more by some portion of the deposition process rather than by any fundamental limitations of thin films. Large variations in the film absorptivities occur both among suppliers and from deposition-to-deposition for single suppliers.

We note that with the exception of some of the zinc sulfide films, the minimum detectable limit for the film-substrate pairs measured during this project was set by the variability of the substrate absorptivity. This effect was more pronounced for the CVD zinc selenide substrates than for the barium fluoride. The selenide material was apparently taken from several of the earlier CVD production runs and as a result, some of the finished substrates contained inclusions which were visible to the unaided eye. The densities of these inclusions were ranked subjectively as "none", "few", "moderate", and "many" and a rough, though by no means complete, correlation between density and level and variability of substrate was noted. The effect of this variability was to raise the minimum detectable levels to higher absorptivities for films deposited on typical zinc selenide than for those on barium fluoride. Higher quality CVD zinc selenide material is now available and should be used for future experimentation. Further, the surface finishes of both the substrate materials could be substantially improved by application of the techniques discussed in Paragraph 3.1 of this report. Future work should be performed on the best obtainable surfaces as well as the best obtainable material. The effectiveness and uniformity of surface cleaning procedures should be optimized by laser calorimetry before they are applied to the substrates. We estimate that these precautions should lower the minimum detectable absorptivities for 1-2 micrometer thick optical films to the order of one tenth of a reciprocal centimeter.

Finally, the absorptivities of the arsenic trisulfide films at 10.6 micrometers compare well with the value of 5.5 cm^{-1} determined by Gibbs and Butterfield[4] on one of their own films. They also report an absorptivity of 33.2 cm^{-1} for zinc selenide films at the same wavelength. Since our zinc selenide films were deposited only onto barium fluoride substrates

which are essentially opaque at 10.6 micrometers, we cannot compare our results directly. Their absorptivity is, as they report, very substantially larger than the selenide bulk values. We find the 10.6 micrometer absorptivity of the similar chalcogenide zinc sulfide to be extremely variable (Table IV) and probably strongly influenced by subtle changes in the deposition process. Zinc selenide films should behave similarly.

2.1.2 Attenuated total reflection spectroscopy

The sensitivity of any absorption spectroscopic technique may be increased by increasing the pathlength of the light through the absorbing medium. Attenuated total reflection (ATR) spectroscopy makes use of this approach by permitting the evanescent wave (that portion of the radiation which extends beyond the physical surface during total internal reflection) to interact with the absorbing medium as the primary beam is repeatedly reflected down a nominally lossless medium. The method has been extensively developed by N.J. Harrick, whose book[5] on the subject discusses theoretical and experimental aspects of a variety of applications. During earlier phases of this project,[2,3] internal reflection spectroscopy was used extensively to study surface contamination and cleaning of alkali halide and alkaline earth fluoride materials.

The spectroscopy performed during the past year has emphasized the study of the optical films, although some surface cleaning experiments are reported in Sec. 3.

An internal reflection plate is shown in cross section in Fig. 9. The number of reflections the probe beam makes during its passage can be calculated, as can the penetration of the beam into a surface layer of known index of refraction and thickness. An attachment which permits an internal reflection specimen to be examined in a standard infrared spectrometer is shown schematically in Fig. 10. For the purposes of this project, the attachment was modified to permit light to pass only along the lower half of the specimen as viewed in the upper portion of Fig. 10. The films deposited by the vendors covered only one half the surface of the substrates, as shown in Fig. 1, so spectra of film and substrate could be obtained separately. The logical extension to double

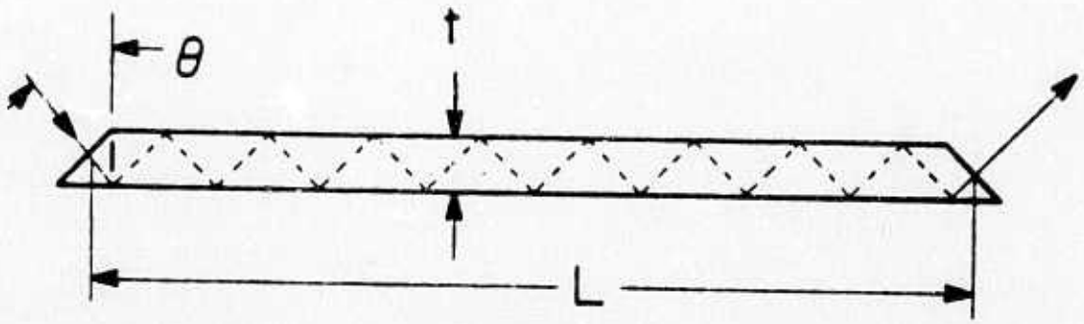


Fig. 9 Internal Reflection Plate.

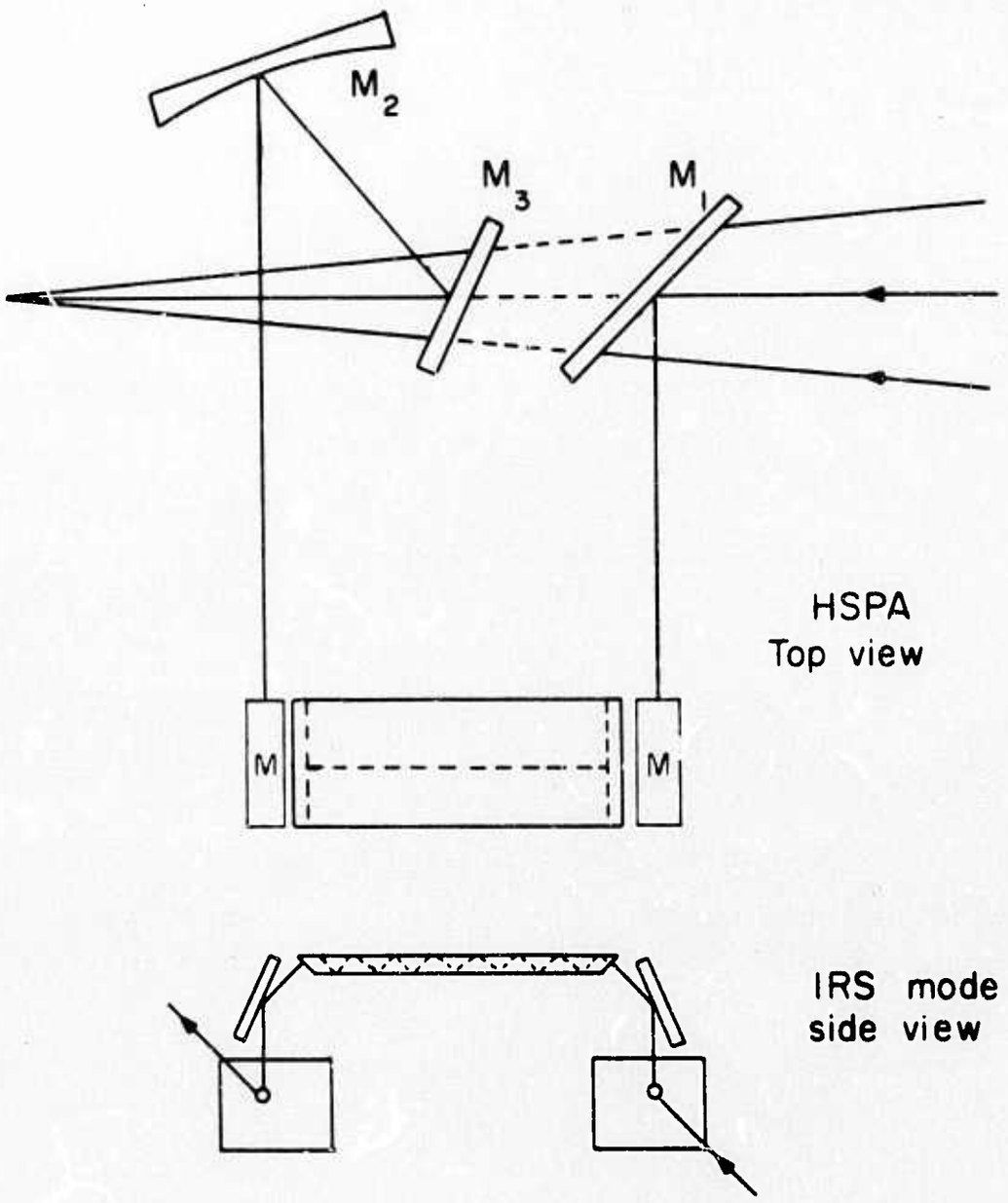


Fig. 10 Schematic Diagram of Harrick Scientific Horizontal Single Pass IRS Attachment.

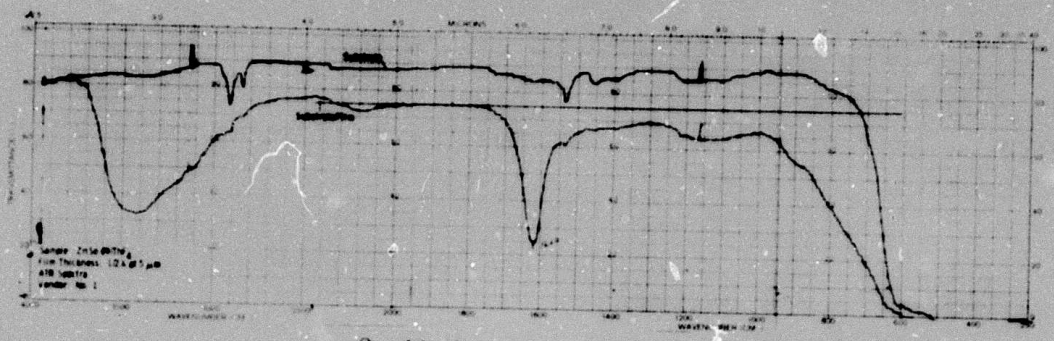
beam techniques, sending the probe beam down the coated half and a reference beam along the uncoated half of the specimen was considered, but thought to be sufficiently difficult to be beyond the scope of this project.

2.1.2.1 Experimental procedures

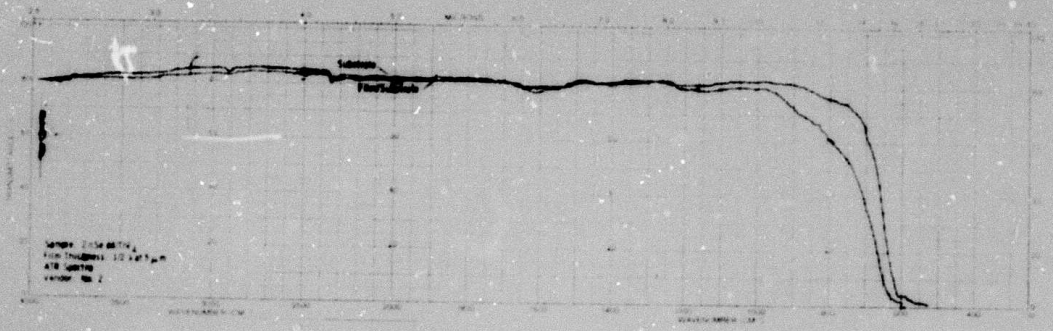
The modified ATR attachment was used in a Perkin-Elmer Model 457 spectrometer to obtain spectra of the as-received films and their substrates. The spectrometer is a double beam instrument, so a variable aperture was placed over the reference beam to adjust the position of the spectrum on the chart paper. For these measurements, the signal from the specimen was first maximized by adjusting the specimen and mirror positions with the variable aperture removed. The aperture was inserted and adjusted to produce a "transmission" of 80 percent at 2.5 micrometers. The sample chamber was closed, sealed and flushed with dry nitrogen. Since the path lengths in air of the two beams differ, atmospheric carbon dioxide and water vapor present in the sample chamber produce apparent absorptions. Spectra of the coated and uncoated halves of each substrate were obtained.

2.1.2.2 ATR spectroscopy; results

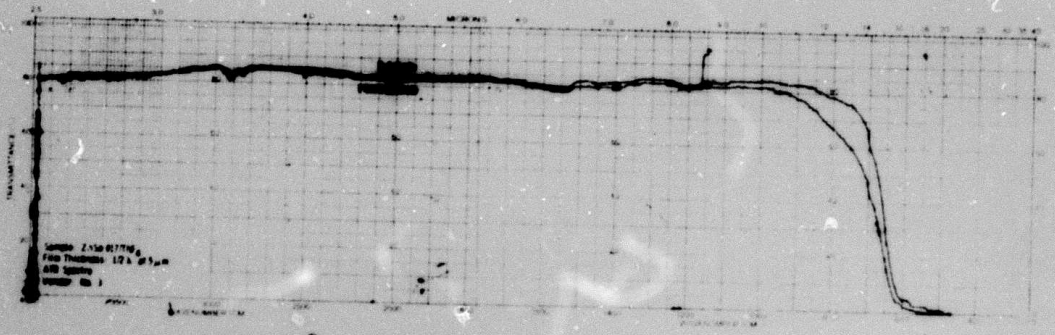
ATR spectra of thorium fluoride films deposited onto zinc selenide and barium fluoride substrates appear as Figs. 11 and 12. In these and the succeeding ATR figures, the spectra are arranged in order of vendor with Vendor 1 at the top. The absorptivities determined by laser calorimetry are printed at the proper wavelength below the spectra. The ThF_4 films exhibited the largest vendor-to-vendor variability of absorptivity during the laser calorimetry measurements and this variability is carried over to the ATR spectra. The strong absorptions at 3400 cm^{-1} and 1620 cm^{-1} in spectrum of the film from Vendor No. 1 are most likely caused by some interaction of the film material with water vapor. The similarity between this spectrum and the published spectrum of $ThF_4 \cdot 4\ H_2O$ [6] (Fig. 13) is striking. Thorium fluoride depositions carried out at the Research Division determined that the major differences in the spectra



$\beta = 18.1$ $\beta = 63.8$



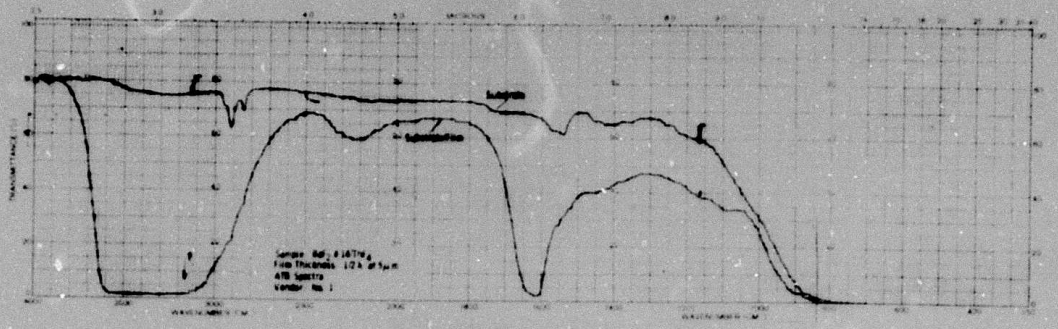
$\beta = < 1.35$ $\beta = 16.0$



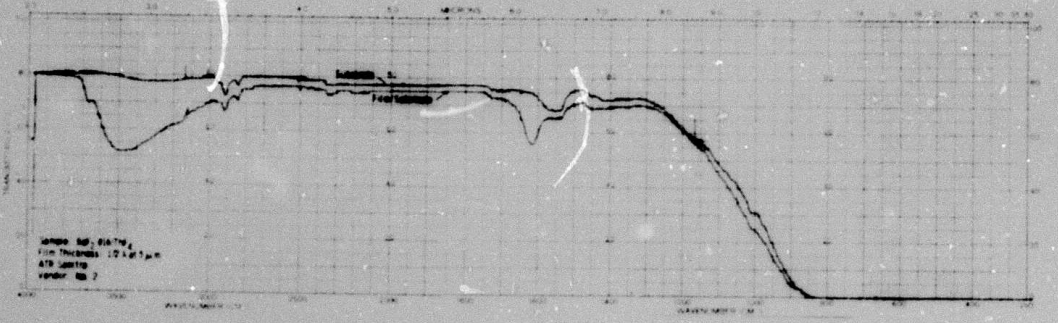
$\beta = < 2.88$ $\beta = 9.1$

Reproduced from best available copy.

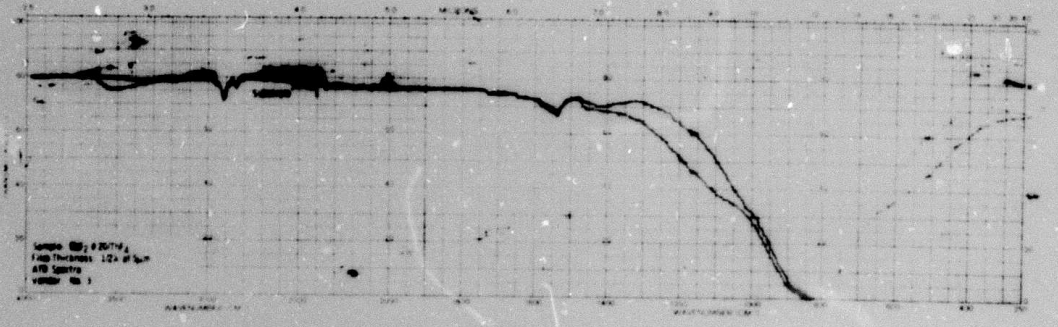
Fig. 11 ATR Spectra of Thorium Fluoride Films on Zinc Selenide Substrates.



β = 15.6



β = 3.2



β = 0.69

Fig. 12 ATR Spectra of Thorium Fluoride Films on Barium Fluoride.

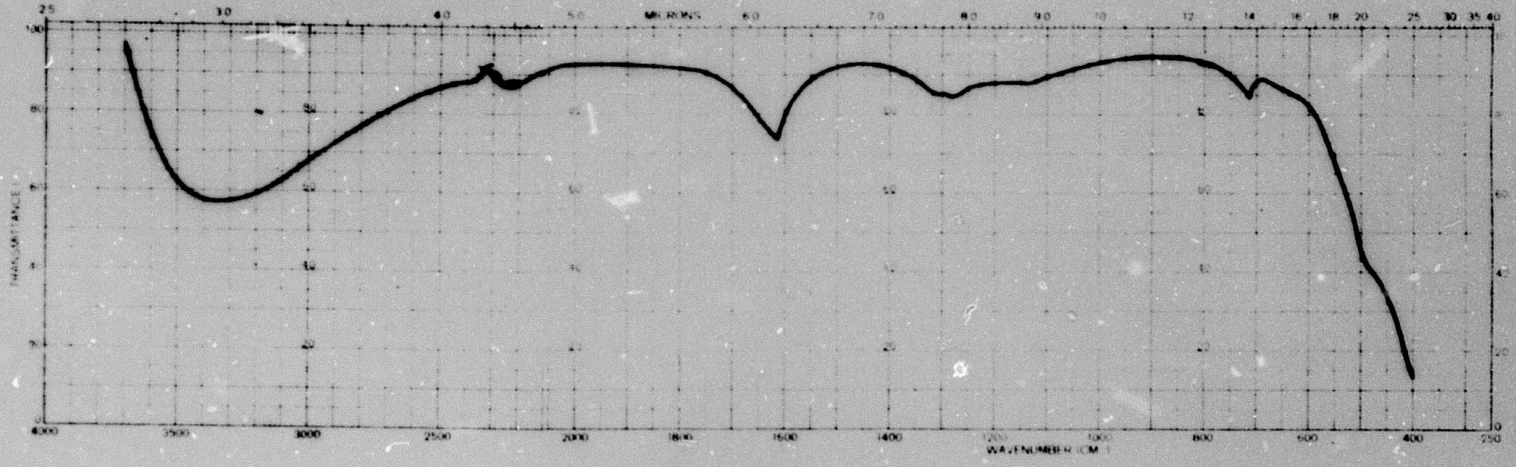


Fig. 13 Infrared Absorption Spectrum of $ThF_4 \cdot 4\ H_2O$.

from the three vendors were produced by substrate temperature variations during deposition. Room temperature substrates produce films having the absorptive, hydrated spectrum; substrate temperatures on the order of 150°C will produce films with little or only very weak absorptions at 3400 and 1620 cm^{-1}. Recent results obtained at the Honeywell Research Center demonstrate that the deposition rate variations may also be used to produce variations in thorium fluoride film absorptivities.[7] In a second experiment, one of the thorium fluoride films supplied by Vendor 3 was held for two hours at 120°F in 95 percent humidity. This treatment essentially destroyed the adhesion of the thorium fluoride film but did not produce the water-associated absorptions in its ATR spectrum. The ATR spectra and calorimetry of thorium fluoride films, taken together with the parallel deposition experiments and environmental testing, strongly suggest that water vapor which is present in the residual atmosphere of the deposition chamber plays a major role in the determination of the absorptivity of the film. Whether residual water vapor helps to determine the absorptivities of the other film materials should be determined by experiment.

The spectra of the thorium fluoride films deposited onto barium fluoride substrates all appear to have stronger water-related absorptions. The "stronger" absorptions actually are produced by the close index of refraction match between the film and its substrate. More of the probe radiation is coupled into the thorium fluoride on the barium fluoride substrate than the film on the higher index zinc selenide substrate. Of the three films on barium fluoride, the one produced by Vendor No. 3 had the least absorption at 3400-3500 cm^{-1}; these films also had the lowest absorptivities at 10.6 micrometers, measured calorimetrically. Such apparent correlations deserve further study.

The absorptions at 2915 cm^{-1} and at 2845 cm^{-1} are caused by hydrocarbon contamination of the specimen surfaces. Since all the ATR spectra were determined on the as-received specimens, the intensities of the absorptions may be related to some accumulation of the cleaning, handling, and shipping procedures of the vendors. Since Vendor No. 1 and 3 reshipped the coated specimens in what appeared to be their original containers, the variability of the absorption levels probably reflects differences in handling procedures.

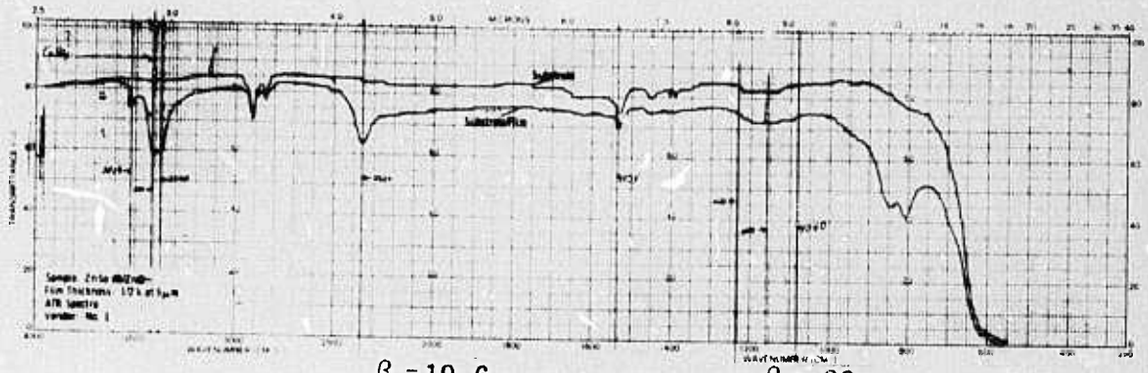
This hydrocarbon contamination is a significant feature of the surfaces for several reasons. First, a review of hydrocarbon absorption spectra reveals that their absorptivity at 3.8 μm, (the DF laser wavelength) is typically five percent of the maximum absorptivity at 2915 cm^{-1}. Hydrocarbon contamination may contribute to the surface absorptivity of chemical laser optics. Second, if it is not removed prior to deposition of the antireflection coating, the trapped contamination layer may contribute to the degradation of the AR coating during high-power laser illumination. The implications of the contamination layer for the adherence and durability of the coatings are obvious. While boiling Freon-113* will essentially remove these hydrocarbon absorptions from ATR spectra, indicating that they exist largely on the exposed surfaces of the specimens, lesser quantities trapped at the film-substrate interface cannot be precluded.

Finally, the absorption at 1500 cm^{-1} is characteristic of the barium fluoride surface, probably a hydration product. The absorption may be seen in both the "substrate" and "film" spectra. Note that no information about the film-substrate interface may be drawn from this observation because half the reflections of the probe beam as it traverses the "film" side of the specimen take place at the uncoated back face.

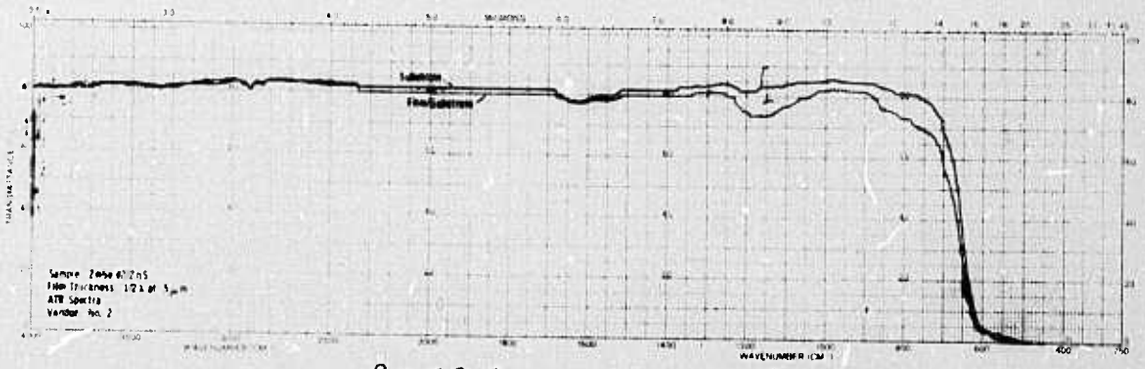
The spectra of zinc sulfide films on zinc selenide are presented in Fig. 14. In this case, we believe the extra strong absorptions in the upper spectrum are caused by impurities in the evaporant. The association with the higher absorptivities at the laser wavelengths is apparent.

Spectra of zinc selenide films on barium fluoride appear in Fig. 15. In this case, the only hydrocarbon and substrate absorptions occur. Absorptivities determined at the laser wavelengths are low for all the films.

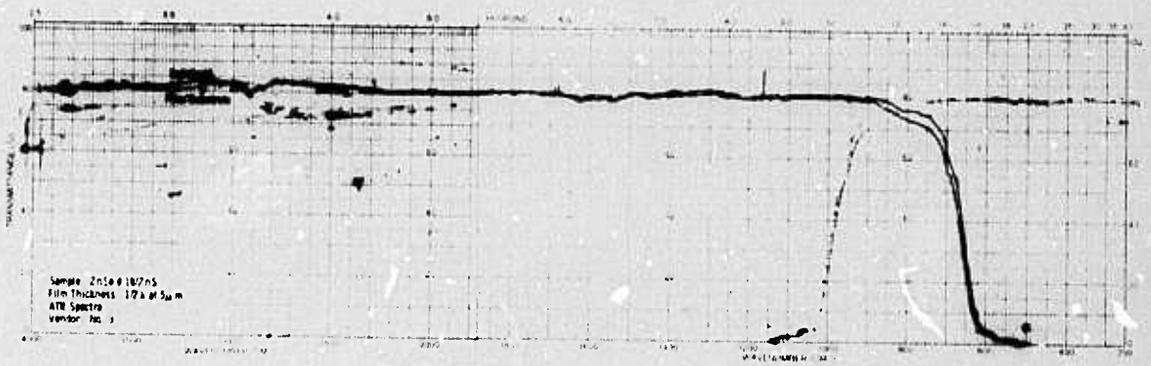
ATR spectra of the arsenic trisulfide films appear in Figs. 16 and 17. There is no obvious correlation between the laser calorimetry results and the spectra. The variability of the absorptivities measured at 5.25 μm (where the spectra have no distinguishing features) is larger than that at 10.6 μm, close to obvious variations in the cut-off behavior. The broad absorption which peaks at 1200 cm^{-1} in the specimen from Vendor No. 3 (possibly due to oxygen impurities) does not seem to have a large influence on the 10.6 μm absorptivity.



$\beta = 10.6$ $\beta = 20$



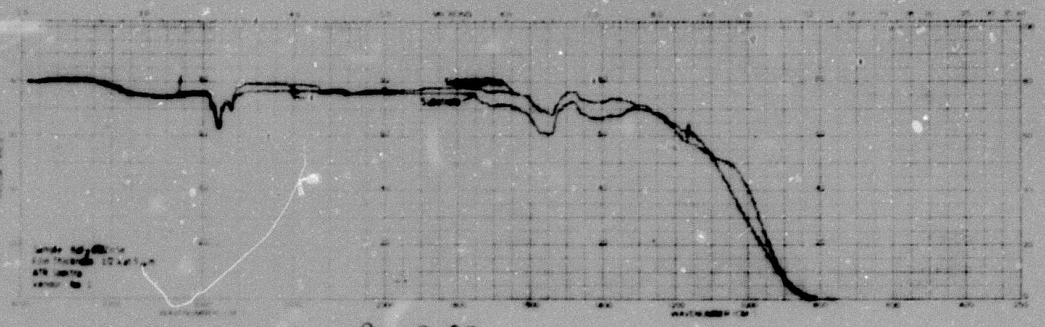
$\beta = < 0.1$ $\beta = 0.60$



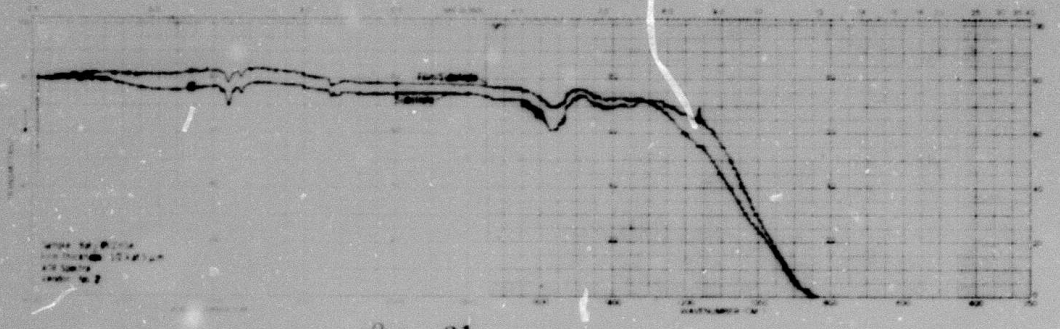
$\beta = 1.3$ $\beta = 1.0$

Reproduced from best available copy.

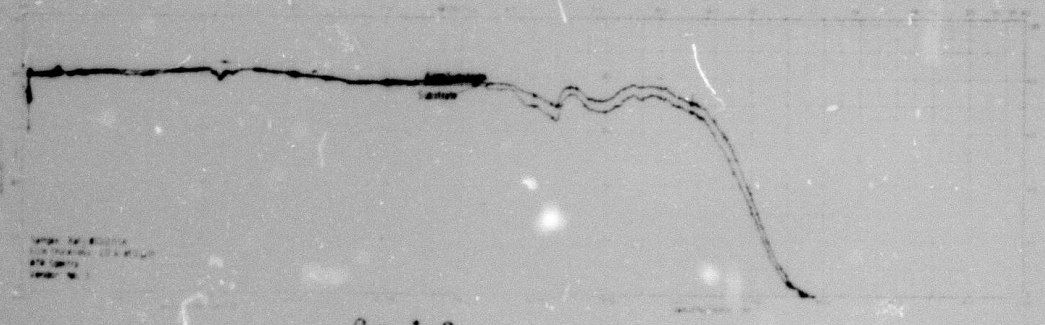
Fig. 14 ATR Spectra of Zinc Sulfide Films on Zinc Selenide.



β = 2.02

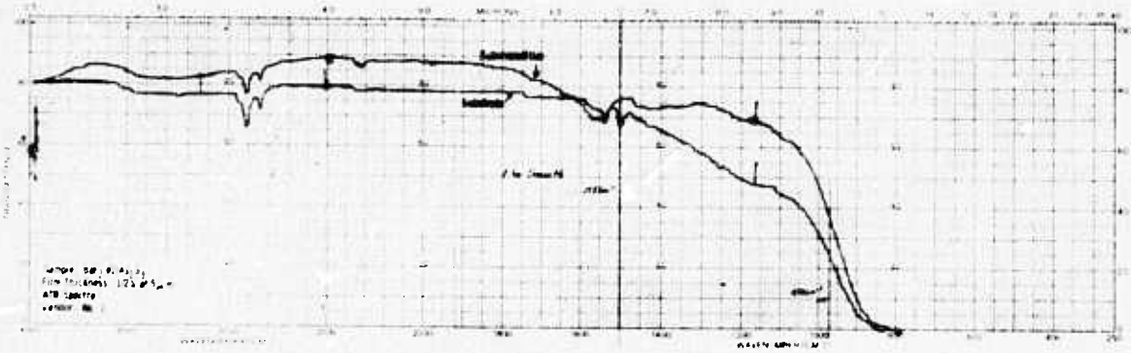


β = .21

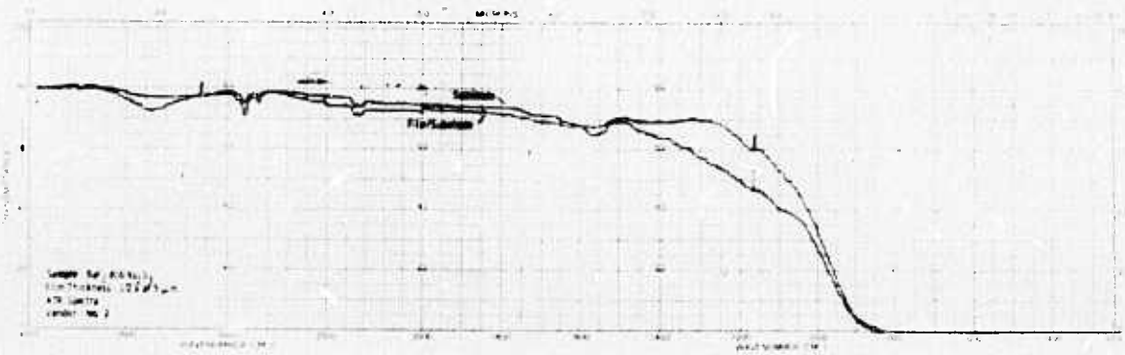


β = 1.3

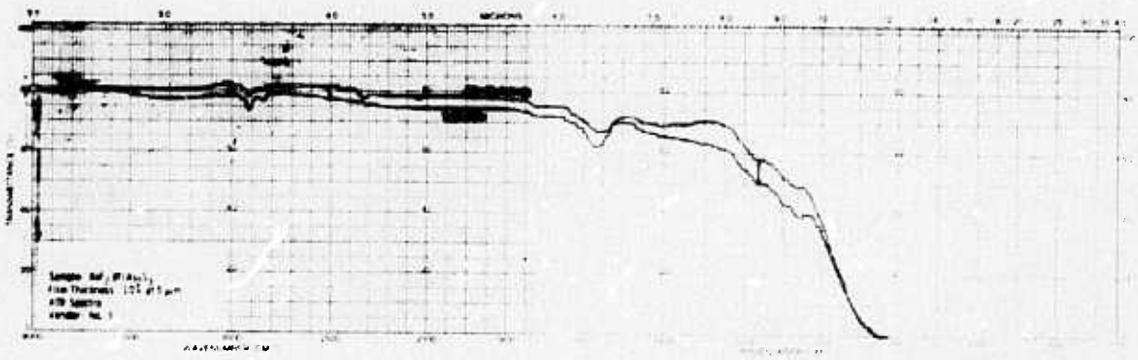
Fig. 15 ATR Spectra of Zinc Selenide Films on Barium Fluoride.



β = 0.48



β = 0.32



β = 5.0

Reproduced from best available copy.

Fig. 16 ATR Spectra of Arsenic Trisulfide Films on Barium Fluoride.

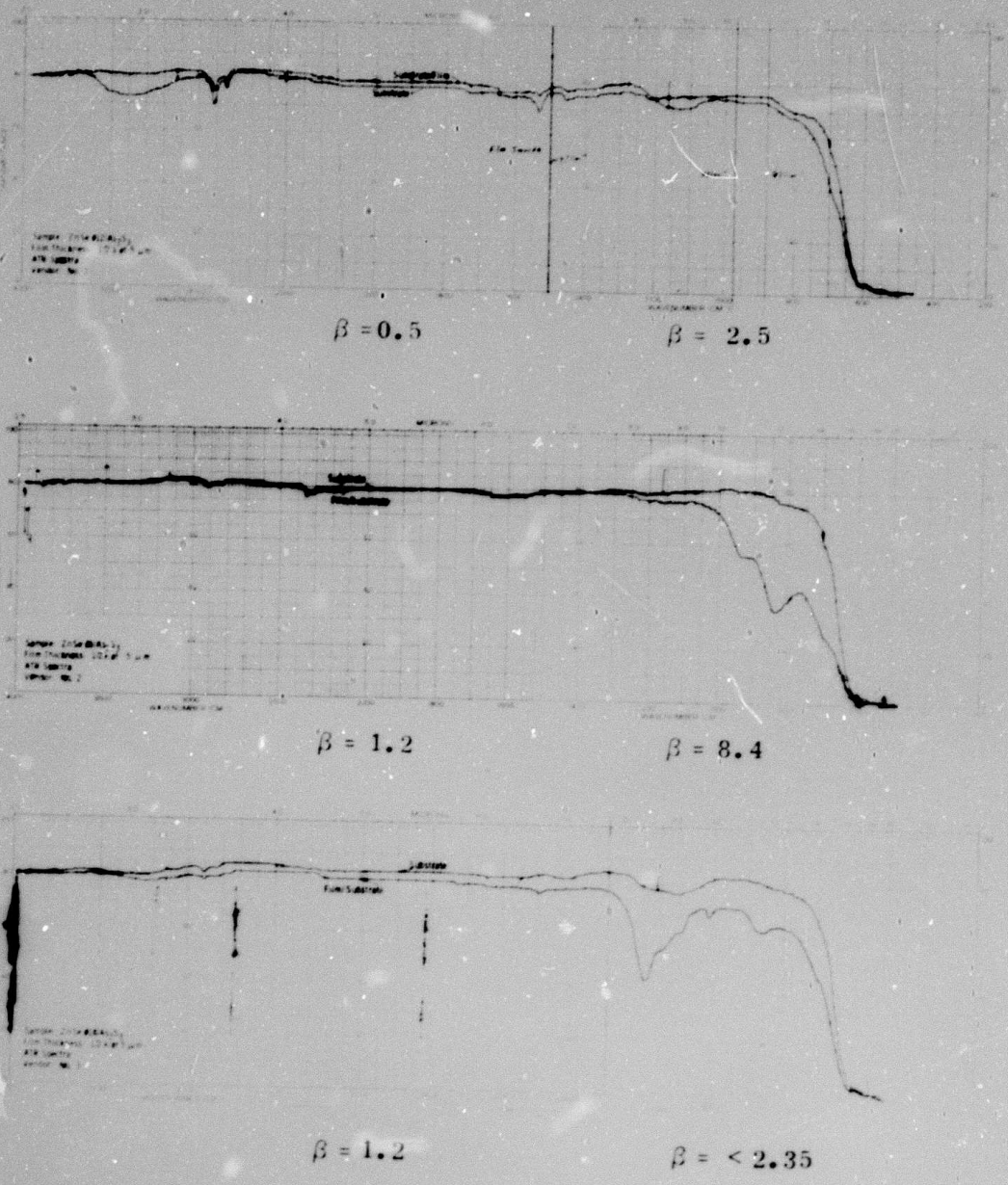


Fig. 17 ATR Spectra of Arsenic Trisulfide Films on Barium Fluoride.

Reproduced from best available copy.

Summarizing, the ATR spectra of the vendor-supplied optical thin films have been used to determine their major absorptions at wavelengths between 2.5 μm and the substrate cut-off. In all cases, hydrocarbon contamination could be detected on the as-received specimens.

Absorptions occurring away from the laser wavelengths were correlated with higher absorptivity at the laser wavelengths for zinc sulfide and thorium fluoride but not for arsenic trisulfide films. The spectra and absorptivity of thorium fluoride films were correlated with their deposition coefficients in preliminary experiments. No quantitative absorption coefficient information appeared extractable from these spectra. For the most part, the spectra were featureless at the important laser wavelengths, and the "base line" levels of the spectra were determined by such other factors as index mismatches, film thickness, and sample alignments in the spectrometer.

2.1.3 Integrated optics experiments

Under the proper conditions, thin transparent films may be made to act as waveguides for light propagating parallel to their substrates. This effect is presently put to use in the rapidly expanding integrated optics technology where light propagating in thin film waveguides can be manipulated by a variety of devices. Since the integrated optics technology is directed towards various communications and optical signal processing applications, the determination of the attenuation of the light beam propagating in the waveguide is of considerably practical importance.

Integrated optics techniques have been used to measure losses in thin films.[8,9] These procedures are generally performed at single laser wavelengths and are used to measure not only the losses due to absorption but those due to scatter centers and other film inhomogeneities.

During this project, exploratory efforts were made to extend these techniques to the measurement of absorptive and scattering losses at all infrared wavelengths rather at discrete laser wavelengths.

The eventual goal of the work was the development of a substantially more sensitive technique for the determination of film absorptivities and

scattering levels as a function of wavelength in the infrared. The integrated optics approach to the problem should increase the sensitivity by substantially increasing the pathlength of the light in the film which would be traversed parallel to a long dimension rather than through its thin cross section, as it would be for a conventional transmission measurement.

The potential advantage of the technique, in addition to the increased sensitivity, is the generation of light scattering as well as absorption behavior. Light scattering in thin films may prove to be particularly interesting in view of the apparently significant role which inclusions have in determining their damage thresholds.

The experimental apparatus which was designed and partially constructed for the project is shown schematically in Fig. 18. The light from a black body radiator is coupled into the film by means of prism coupling which is oriented so that a small wavelength range is most efficiently coupled into the film. Scattered light from a region in the film is imaged into the monochrometer/detector. The intensity of the scattered light may in principle be determined as a function of wavelength and position in the film, by varying the orientation of the prism and positioning of the collecting optics. A second prism coupler may be used to examine the intensity of the transmitted beam for determination of the total absorption plus scatter losses. In both cases one would measure the losses as a function of distance along the film in order to eliminate the effect of input coupling losses.

This apparatus requires a broad band infrared radiation source which is reasonably intense. Since the beam must be focussed, collimated and refocussed by the apparatus, the illuminator must be a point source. Such commonly used infrared sources as globars are not acceptable.

The high intensity infrared point source, shown schematically in Fig. 19, was constructed for use with the thin film spectrometer. It consists of CW $YAlO_3$:Nd laser which is focused onto the end of an alumina rod and focussing optics to introduce the block-body radiation into the spectrometer. The laser was capable of heating the alumina

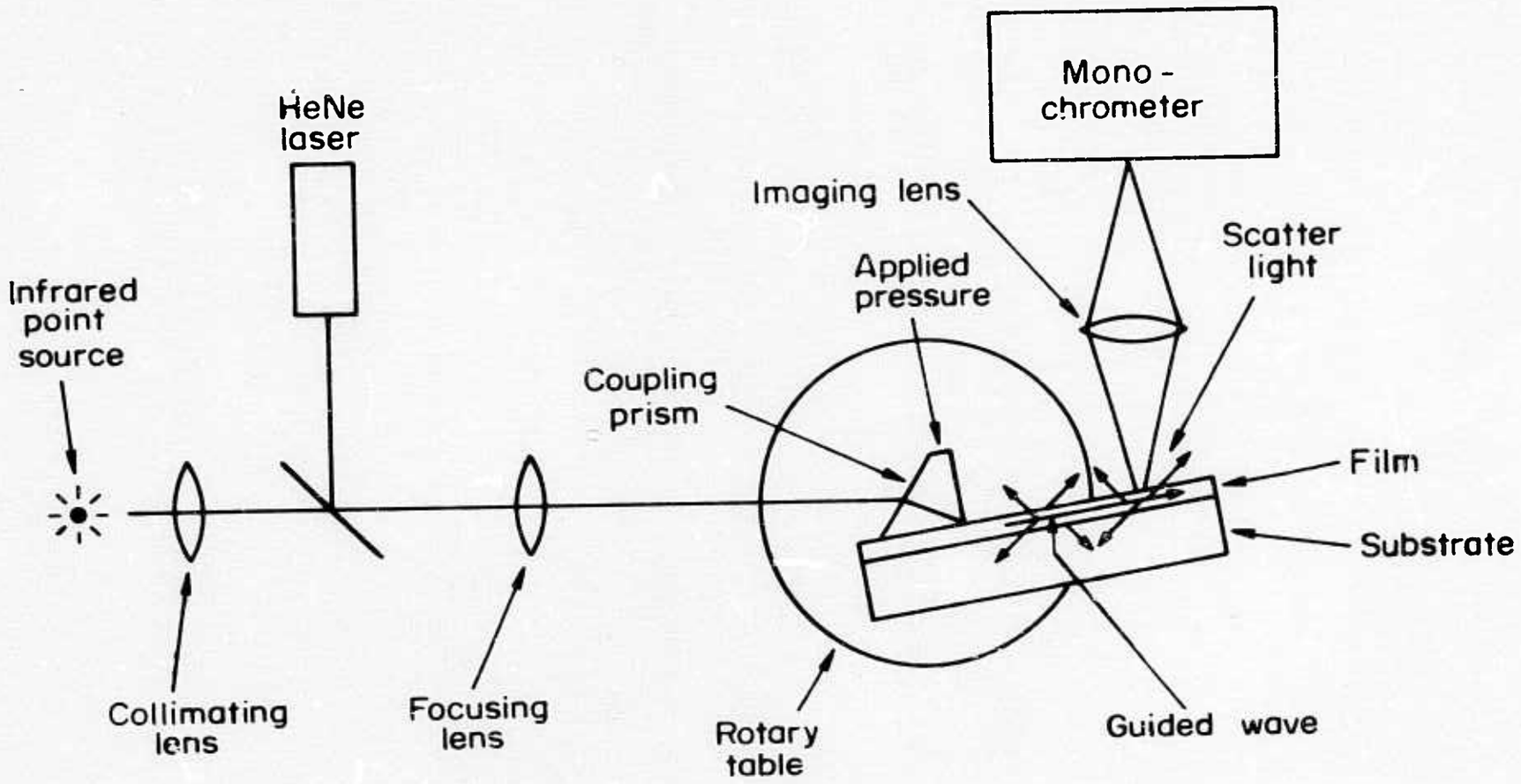


Fig. 18 Thin Film Absorption Spectrometer - Schematic.

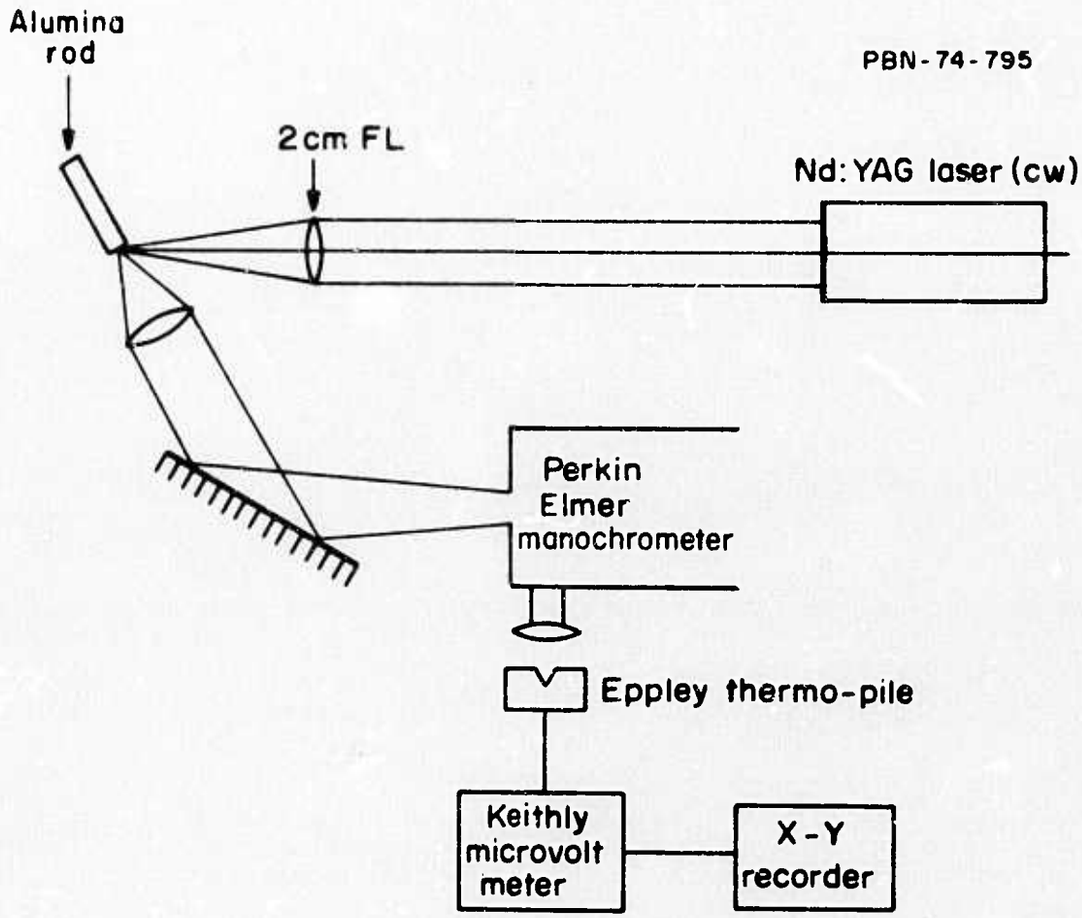


Fig. 19 High Intensity Infrared Point Source.

in the focal spot to approximately 2200°C, above its melting point. The spectral distribution of the radiation from this source is given in Fig. 20.

Unfortunately, our attempts to couple even coherent light from a helium-neon laser (6328 angstroms) into the vendor-supplied films were unsuccessful. Several factors probably contributed detrimentally to the experiments. First, the poor surface quality of the vendor-supplied (Fig. 21) substrates caused the beam to be strongly scattered. Further, the zinc selenide, which was used for the coupling prism also scatters 6328 angstrom light strongly. These conditions may both be corrected. The surface preparation techniques of Sec. 3 of this report will produce substantially higher quality surfaces, and more nearly scatter-free zinc selenide is now available for prisms. Germanium prisms could also be used to minimize scatter introduced by the apparatus at infrared wavelengths. With these refinements, a better assessment of the approach could be made.

Two additional difficulties with the approach bear mentioning. First, since the efficiency of coupling by either prisms or gratings is extremely angle-sensitive, the alignment of the illuminator-coupler-sampler system is critical and the rotation of the system to vary the wavelength range of the light in the film must be very carefully designed. Second, since the film is required to act as a waveguide, its index of refraction must be higher than that of the substrate. This effectively limits the technique to the study of the higher index films.

We believe this approach, within the limits set forth above, can be used to determine the wavelength dependence of absorption and scattering in infrared optical films. It will require a very careful experimental touch, however, and therefore should be made the object of a more single purposed study so that a more strongly directed effort can be made.

2.2 Mechanical Property Characterization

Thin film mechanical properties may be considered from several points of view. The user requires adhesion above all. The film cannot

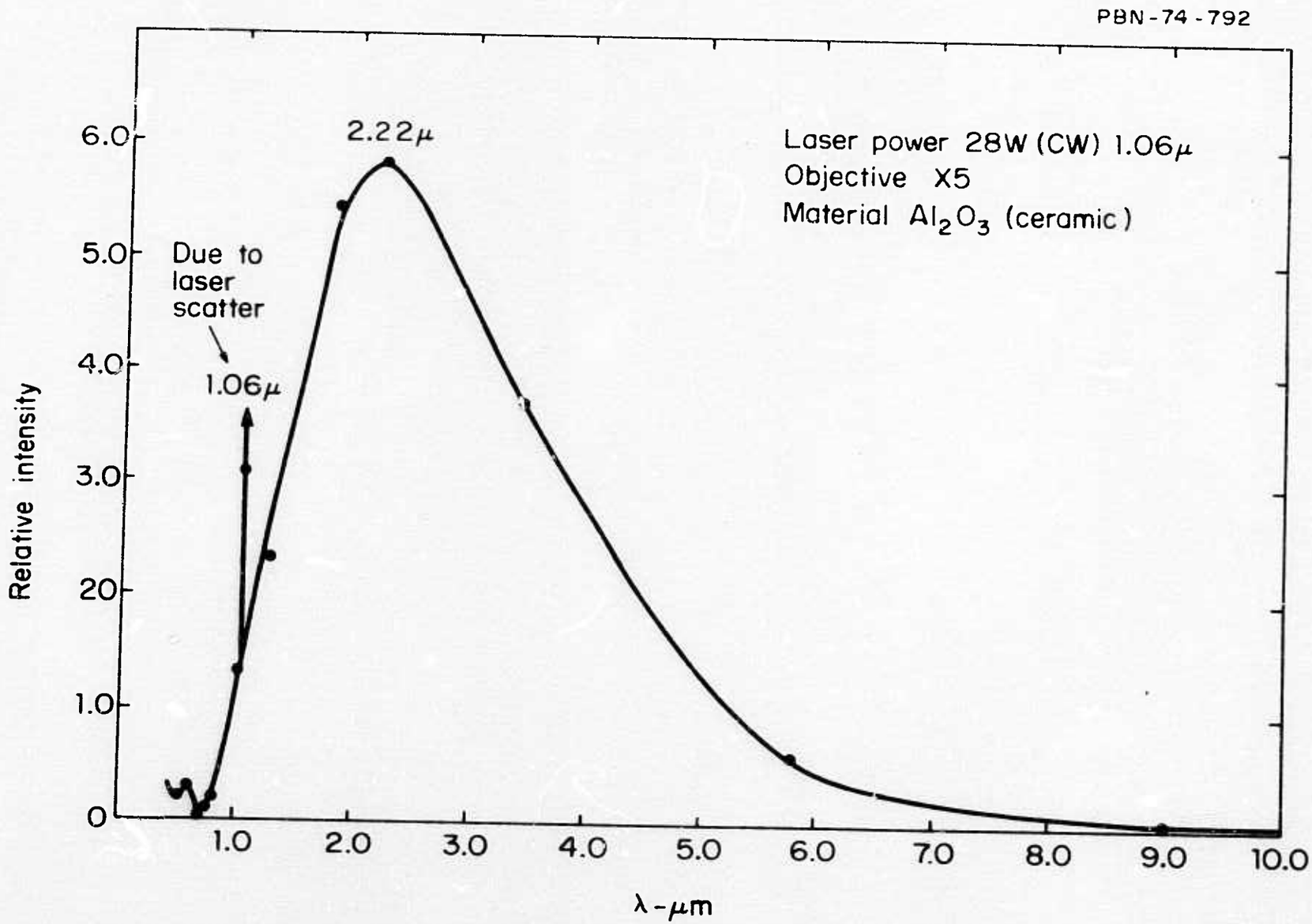
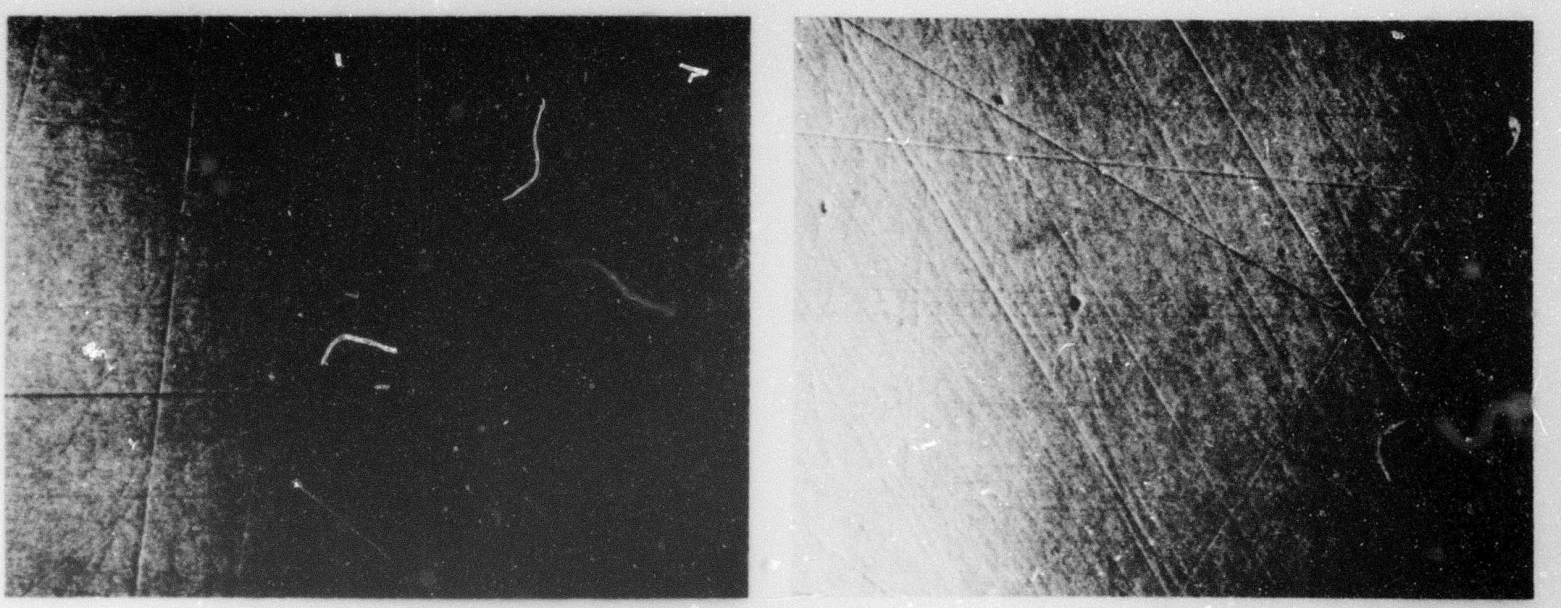


Fig. 20 Output Spectrum of Alumina Point Source.



25 μm

a) Sample No. BaF_2 - 7

b) Sample No. ZnSe - 14

Fig. 21 Nomarski Interference Microscopy of Surfaces of Film Substrates.

peel under its intended use conditions. The user will then typically require further evidence of film durability. Abrasion resistance is important if the film must be cleaned. Thermal shock resistance may be important. Films which coat hygroscopic or water-soluble materials must be truly pinhole-free, a condition which is seldom met for large-area films even in the semiconductor industry, which of necessity operates largely in a cleanroom environment more conducive to such films than do most optical film producers. Finally, the user will require that these or other properties be maintained at useful levels as the film is exposed to its use environment. We note here that the user of high power laser optical coatings is also very concerned about the degradation of the coating optical properties with time or environmental exposure. Environmentally produced optical property degradation of thin films has received little or no attention to date.

For the user, pass-fail tests [1] can frequently provide the required characterization. If the film falls off the substrate or scratches or permits the substrate to be dissolved after the film has been subjected to the test treatment, it is said to have failed the test. Most characterizations of thin film mechanical properties are of this type.

The thin film physicist prefers a different characterization. The nature and strength of the atomic interactions which hold the film to its substrate are of more interest than whether the film can be removed by a piece of cellophane tape. The state-of-stress in deposited films, their elastic constants, strengths and deformation behavior are the subjects of interesting and fruitful research. For much of this, the experimental techniques require films which are of little practical importance.

The characterization work begun during this project has been carried out from a point of view intermediate between these two. The techniques were to be more quantitative than simple pass-fail tests to permit comparison of films with one another, with themselves during environmental testing, and with the results of simpler pass-fail testing. The techniques were in addition required to be applicable directly to the

optical films of interest. The adhesion and microhardness of the films were chosen for study during this project, adhesion because of its paramount importance among film properties and microhardness because it appeared to be a quantitatively determinable quantity which could be measured for the films themselves and then, perhaps in combination with adhesion measurements, be correlated with the user-oriented film durability tests.

2.2.1 Adhesion measurements

The macroscopic adhesion strength of thin films is determined by a complex combination of atomic bond strengths, physical interlocking and chemical interdiffusion of the film and substrate, film stresses, and the mechanical strengths of the film and substrate. Although the area has received considerable research attention [10, 11] no generally acceptable procedure for defining or measuring thin film adhesion exists. During this project, exploratory attempts to adapt direct pull techniques and scratch tests to optical films were made. At the end of the project, the vendor-supplied films were subjected to "Scotch tape"* tests.

2.2.1.1 Direct pull testing

In these methods, a "handle" of some sort is fixed to the thin film and the force applied to the handle required to pull the film from its substrate is taken to be the adhesion strength. Several excellent reviews of the approach [11, 12] which present its many experimental embodiments in detail are available. Direct pull experiments are essentially extensions of the "Scotch tape" test, which incorporate some quantitative measure of a breaking strength. As a class, they suffer from a common set of experimental limitations. These include:

1. Specimen alignment - The force applied to the film substrate interface for a given externally applied force may be a strong function of the test fixture alignment. Nonuniform force applications may be undetectable and interpretation of the applied force-to-fracture in terms of the film adhesion becomes impossible.

---

*Trademark, 3M Co.

2) Bonding agent - Film interaction - The changes which occur in the film as a result of the adhesive used to affix the pulling device are generally unknown. This problem is circumvented in some tests which peel the film from its substrate, but these require films which are thick and strong enough to support themselves during the test.

3) Determination of the fracture mechanism - Films may be removed from only a portion of the test area. In these cases, the total failure will have taken place by a complex process which involved both film-substrate debonding and film adhesive debonding and may have included film-film fracture. Further, misalignment of the test fixture may cause large variations in failure modes.

Nevertheless, direct pull methods may, in principle, be used to rank adhesion strengths of films more quantitatively than simple pass-fail adhesion tests. They were considered to have sufficient merit to warrant exploratory work during this project. The test fixture, shown in Fig. 22, was constructed for the experiments. The fused silica pulling rod attached to the film is fabricated with ends polished flat to within one tenth wave (in the visible) and normal to the rod axis to within 3 sec. of arc.

Pulling rods were cemented to the films in a jig which held the contacting surfaces parallel and produced a uniformly thick adhesive layer. The force was applied to the film by pulling the substrate surface against the machined pull rod guide in an Instron mechanical testing apparatus. After some experimentation, Boxer Epoxy* was selected as the adhesive. This is an unfilled, room temperature curing epoxy which was strong enough to insure failure of the films tested at the interface. Epoxies which required elevated temperature and RTV-type compounds which release acidic byproducts as they cure were rejected because of possible interactions with the films. Cyanoacrylates such as Eastman-910** were used, buth they did not bond reliably in the test jig used to promote alignment of the pull rod and film. The results of a typical series of experiments are summarized in Table VI. The test specimen was an arsenic trisulfide film deposited onto a strontium fluoride substrate. Each data point corresponds to a single test.

---

* Obtained from Edmunds Scientific.

** Trademark, Eastman Kodak Co.

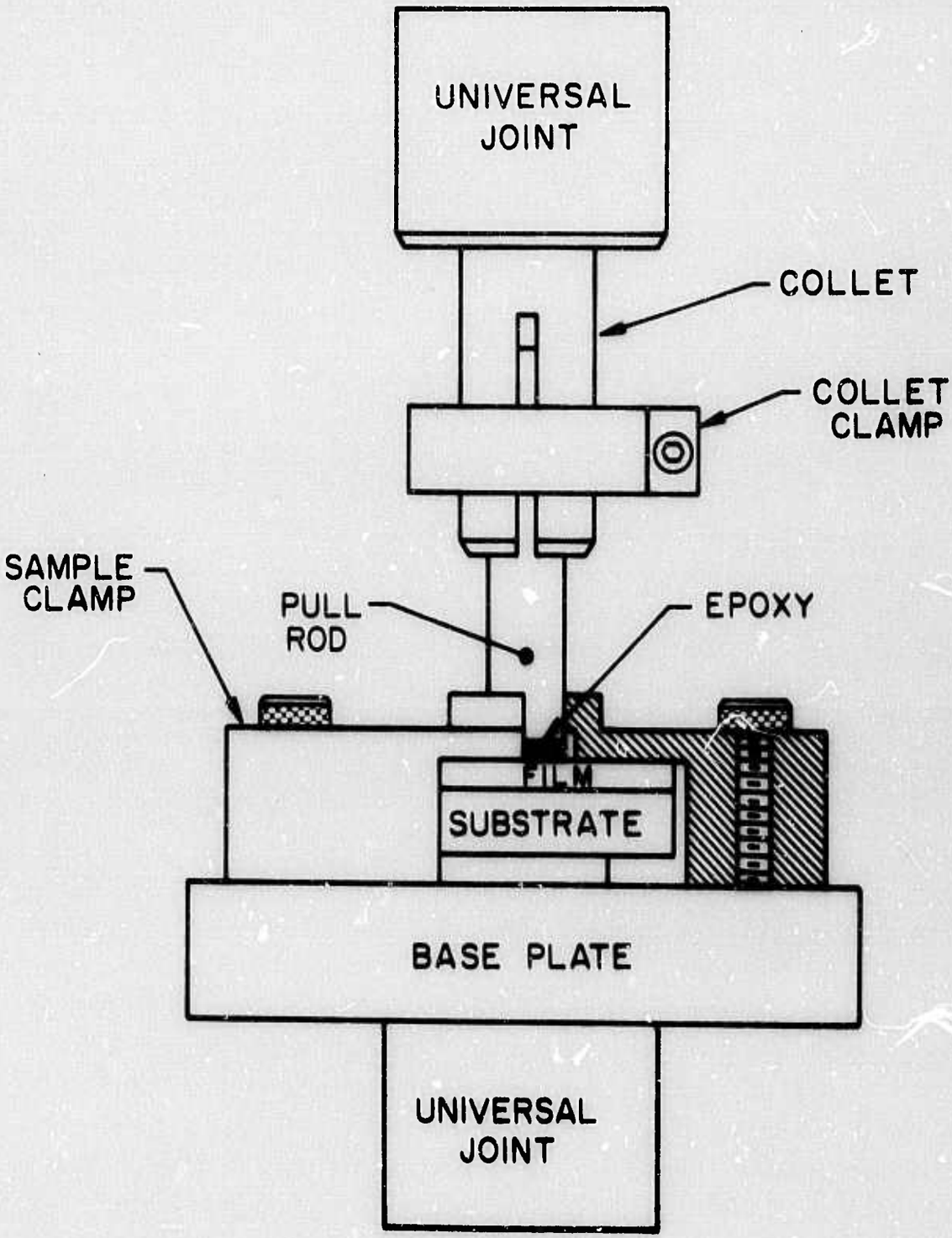


Fig. 22 Test Fixture for Direct Pull Adhesion Tests.

TABLE VI

DIRECT PULL ADHESION TESTING: As_2S_3 FILM ON SrF_2

Fracture Strength (psi)	Comments
1982	No fracture, sample intact
274	Most of film removed by test
~0	Most of film removed by test
221	Most of film removed by test
263	Most of film removed by test
408	Most of film removed by test
243	Removed all of film

No usable film adherence strength can be extracted from these data. The variability of the results was shown to be due at least in part to the stiffness of the universal joints which aligned the test fixture in the Instron apparatus. Films failed at applied loads which were too small to properly align the fixture in the apparatus. While this problem could probably have been alleviated by applying the force through long flexible wires to the fixture, the direct pull experiments were terminated in favor of the more promising microhardness work discussed in paragraph 2.2.2.

2.2.1.2 Scratch tests

The force required to scrape a film from its substrate may also be used as a measure of its adhesion. In this approach, a tool with a known (usually spherical) point geometry is dragged across the film under various loads and the smallest load which removes a strip of film, is taken as the adhesion measure. Interpretation of the results in terms of actual adhesion strengths has received considerable attention and is now the subject of some controversy.[10] The method has been used to measure reproducibly various time-dependent adhesion effects which occur for metallic films and to demonstrate the increase of adhesion caused by the diffusion of aluminum through a gold thin film to the substrate surface.[10]

The scratch tester shown schematically in Fig. 23 was constructed for use during this project. The force is applied through a

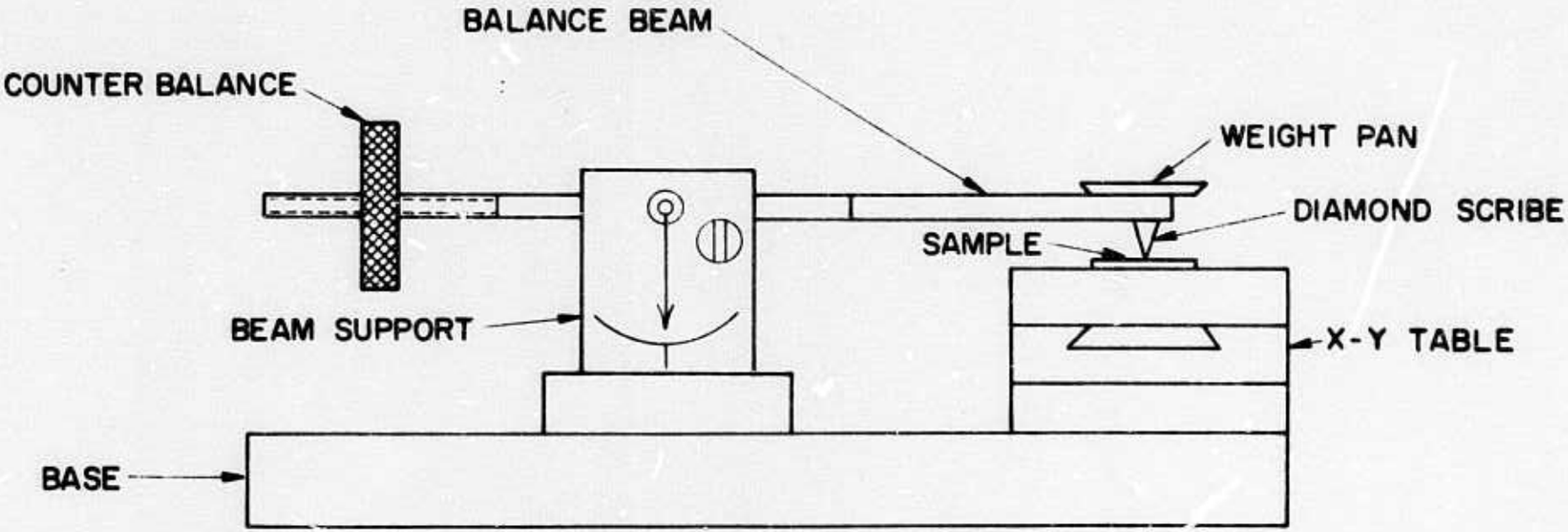


Fig. 23 Apparatus for Scratch-Adhesion Testing.

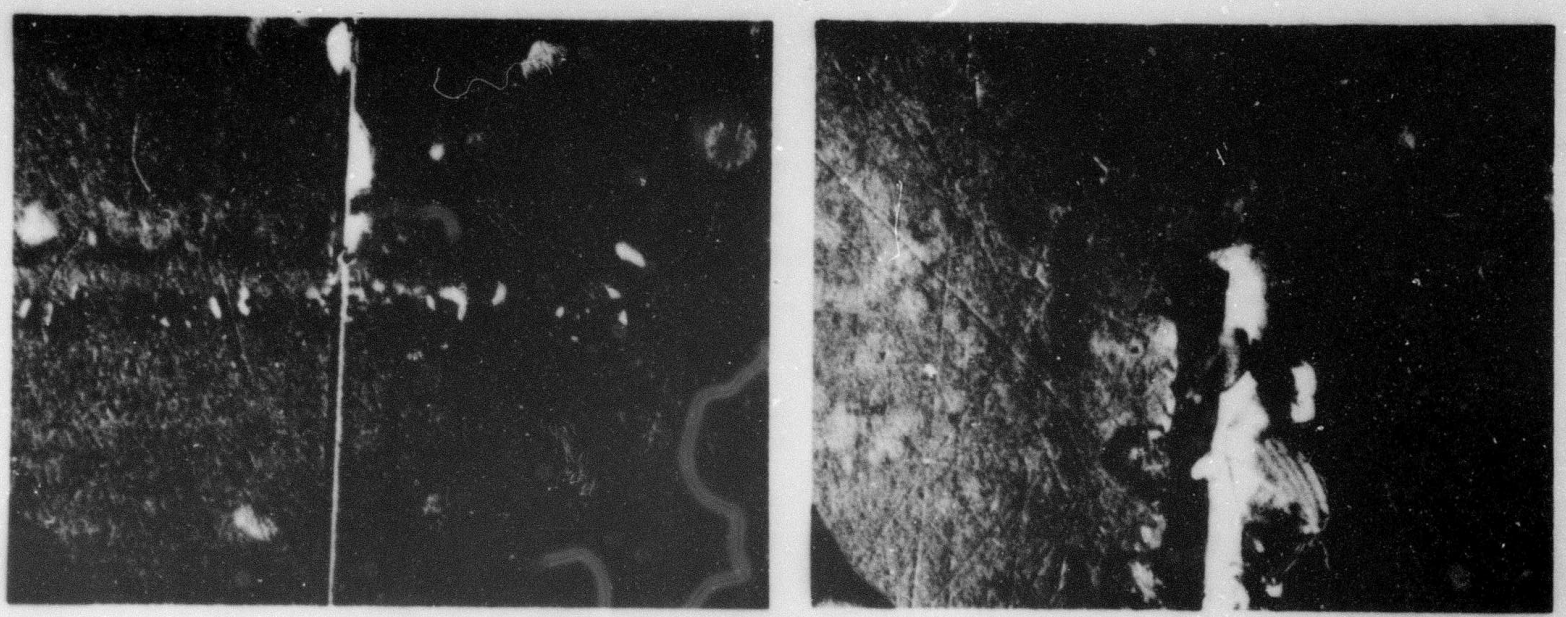
spherical diamond point of 0.001 inch radius by loads added to the counter-balanced beam. The sample holder is a small compound vice movement. Both sample table and beam are mounted on a section of optical bench rail. Scratches are produced in the specimens by resting the loaded indenter gently on the film surface and sliding the sample table on its compound vice movement in a direction away from the beam pivot. Specimens are examined by Nomarski interference microscopy. Figure 24 contains photographs of scratches in arsenic selenide films on zinc selenide substrates. A twenty gram load produced the larger scratch, a one gram load the smaller. In both cases, the only film damage detectable in the optical microscope is associated with fracture and lifting of along the groove edges. It was not possible to detect the onset of film removal within the groove itself, where the applied load can be correlated with the force at the film-substrate interface. We believe scanning electron microprobe techniques should be capable of determining the onset of film removal by analyzing the chemical compositions of the scratch and its surroundings.

The technique has been applied to metallic films on metallic substrates.[13] Time limitations have prevented our application of the microprobe/scanning electron microscope techniques to these films. The apparatus for the experiments has, however, been constructed and shown to produce repeatable defects on the surfaces of zinc selenide and alkaline earth fluoride specimens. Further exploitation of the technique at this point would not be difficult. An energy dispersive X-ray analysis capability has recently been installed on the Research Division scanning electron microscope and is available for the work.

Scratch testing has, in the past, been chiefly used to study the adhesion of metallic films on glass, or other hard brittle substrates. Optical films on softer substrates may deform by different mechanisms. The increased sensitivity of the microprobe detection of film removed is required to assess the technique properly.

2.2.1.3 Pass-fail testing

At the end of the project, adhesive tape adherence test of MIL-M-13508C was applied to the vendor-supplied films. At that time, the



a) One Gram Load

b) Twenty Gram Load

Fig. 24 Scratch Test of Arsenic Trisulfide Film on Zinc Selenide.

films had been exposed to the atmosphere for approximately eight months. They had been cleaned several times by boiling in Freon-113 and evacuated and re-exposed to the atmosphere several times during the calorimetry experiments.

In the test, a piece of Scotch* tape is placed on the film, pulled down over the edge of the specimen, rubbed into close contact with the surface, and removed by a slow, steady pull. Three of the arsenic trisulfide films failed the test, one each on barium fluoride and zinc selenide substrates from Vendor 2 and one on barium fluoride from Vendor No. 3.

2.2.2 Microhardness measurements

All of the characterization techniques discussed to this point have, in fact, measured properties which were determined by both the film and its substrate. Separation of a true film property from them was possible only for the calorimetric absorption determinations, the physics of which is well understood. This section of the report discusses the application of microhardness measurements to thin films. To a much larger extent than is possible with other mechanical property characterizations, this approach may be used to distinguish film from substrate properties.

Microhardness measurements are made by pressing a diamond point into the test specimen under a known load, commonly between 50 and several hundred grams, and measuring the size of the indentation produced. Various standard indenter shapes have been adopted and commercially-available microhardness test equipment is widely used both for laboratory and industrial materials evaluation. Important applications[14] include commercial uses such as qualification of materials and fabricated parts and basic studies of deformation behavior of crystalline and amorphous solids.

Microhardness indentations produced by the normal range of loads are typically several micrometers deep. Very light loads are difficult to apply reproducibly and hardness data taken at light loads is frequently

* Trademark, 3M Company.

inconsistent and difficult to interpret. For these reasons, then, very little information about the microhardness of thin films exists. Two reports which have been published treat films which are thick enough to behave as bulk materials to standard microhardness test equipment. These are tens to hundreds of micrometers thick, substantially thicker than the optical films considered here, but they offer interesting insight into the potential of the technique. Palatnik and Gladkikh[15] show increasing hardness in metallic films with decreasing substrate temperature. This effect can probably be explained by a film grain size which decreases with the substrate temperature. More recently, Furuuchi and Sakata[16] have demonstrated a dependence of the hardness of SiO_2 films on both the evaporation technique and the pressure of the residual atmosphere in the chamber during evaporation.

In the following sections, we discuss the construction of a microhardness tester which can be used to examine micrometer-thick films and present some preliminary data taken with it.

2.2.2.1 Microhardness tests; experimental apparatus

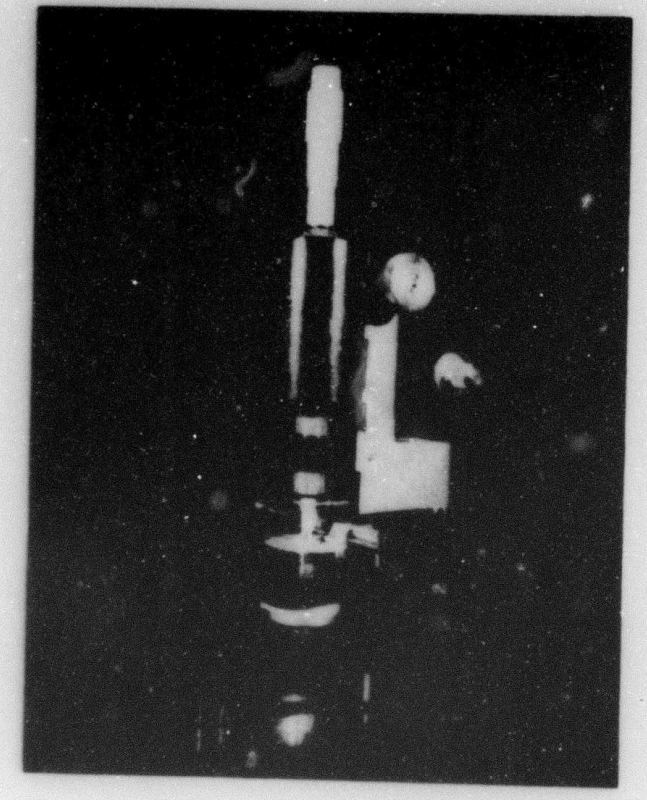
In order to represent the properties of the film alone, the depth of a microhardness indentation must be substantially less than the film thickness. Estimates of the appropriate thickness to depth ratio range from six to fifteen. For the micrometer-thick films, indentation depths on the order of 1000 angstroms are required.

Figure 25a is a photograph of the microhardness tester constructed during this project. Figure 25b shows in cross section the operation of the indenter. Figure 26 is a block diagram of the tester and its electronics. The instrument, housed in a modified optical microscopy frame, consists of a specimen table, a piezoelectric micropositioner mounted below the specimen table, and a diamond indenter point mounted at the end of an aluminum cantilever beam above the micropositioner. The position of the indenter point may be determined by either the semiconductor strain gauges on the beam or the linear voltage differential transformer (LVDT)*

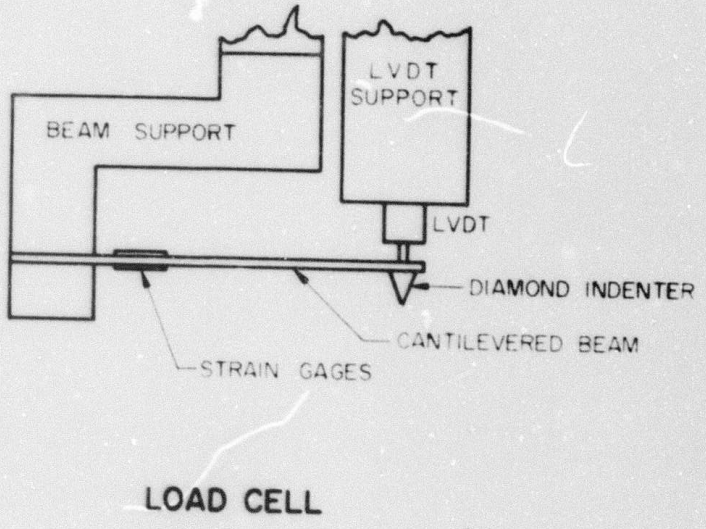
---

* Robinson-Halpern No. 70-3051F. This is the LVDT used by Sloan Instruments in their Dektak surface profilometer which has a sensitivity of the order of tens of angstroms.

PBN-75-580



a) Photograph of Instrument.



b) Operation of Instrument.

Fig. 25 Ultramicrohardness Tester (a) Photograph (b) Cross Section of Operation.

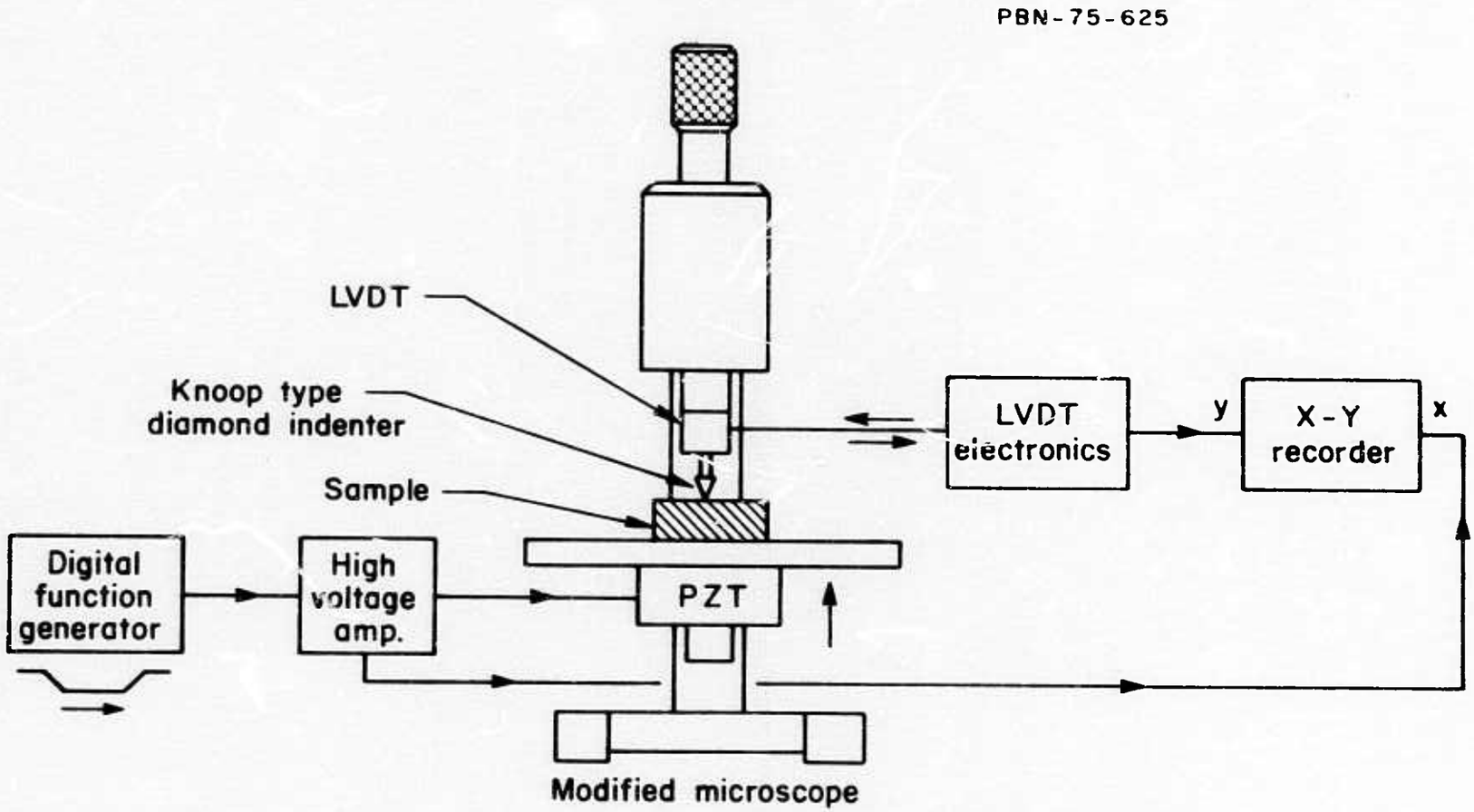


Fig. 26 Block Diagram of Ultramicrohardness Apparatus.

mounted above it. During the development of the apparatus, the LVDT proved to be more reliable and less noisy than the strain gauges. All experimental data were taken using the LVDT. The position of the specimen is determined by the voltage applied to the piezoelectric micropositioner.

During operation, the sample to be measured is placed on the specimen table. The table is raised and the indenter lowered manually with the coarse and fine control knobs on the microscope housing until the sample is within range of the piezoelectric micropositioner. A digital function generator provides a trapezoidal wave form, with a rise and fall time of 50 seconds and a hold time of approximately 30 seconds (all are variable), to a high voltage linear amplifier which provides the drive to the micropositioner, raising and lowering the sample into the diamond indenter. The drive voltage to the micropositioner is used to drive the x input of an x-y recorder. The position of the diamond indenter (beam position) is monitored by the LVDT and this signal is applied to the y input of the recorder which now plots signals proportional to the displacements of the sample and the indenter during the indentation process. These may be expressed in terms of load applied to the indenter and displacements of the sample by means of suitable calibrations.

Figure 27 is the voltage-displacement calibration obtained for the piezoelectric translator. Since the total displacement range of the device was only nineteen micrometers, the displacement was measured interferometrically. The difference in displacement for increasing and decreasing voltages is produced by hysteresis in the piezoelectric material. The microhardness data were taken using only the increasing voltage leg of the curve for which a constant of 0.019 μm/volt was taken from the calibration curve.

The beams fabricated for the apparatus were calibrated directly by measuring the LVDT signals produced by various beam loadings. Figure 28 is a calibration curve for a $2.25 \times 12.70 \times 88.90$ millimeter aluminum beam for which the calibration constant was 0.699 volts/gram.

Since the apparatus measures small deflections of a cantilevered beam, it is very sensitive to room vibrations. For the experiments

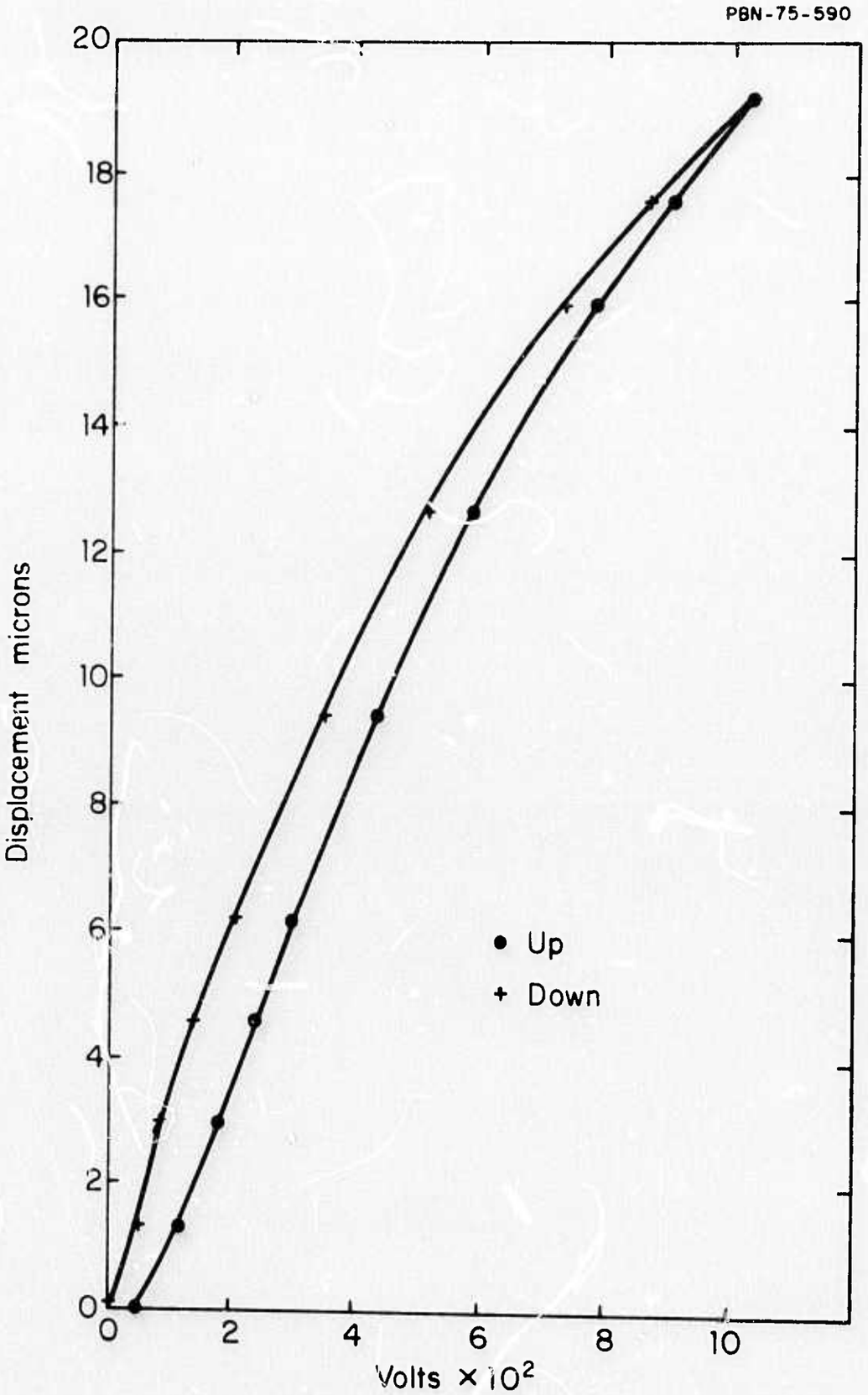


Fig. 27 Voltage-Displacement Calibration of Piezoelectric Translator.

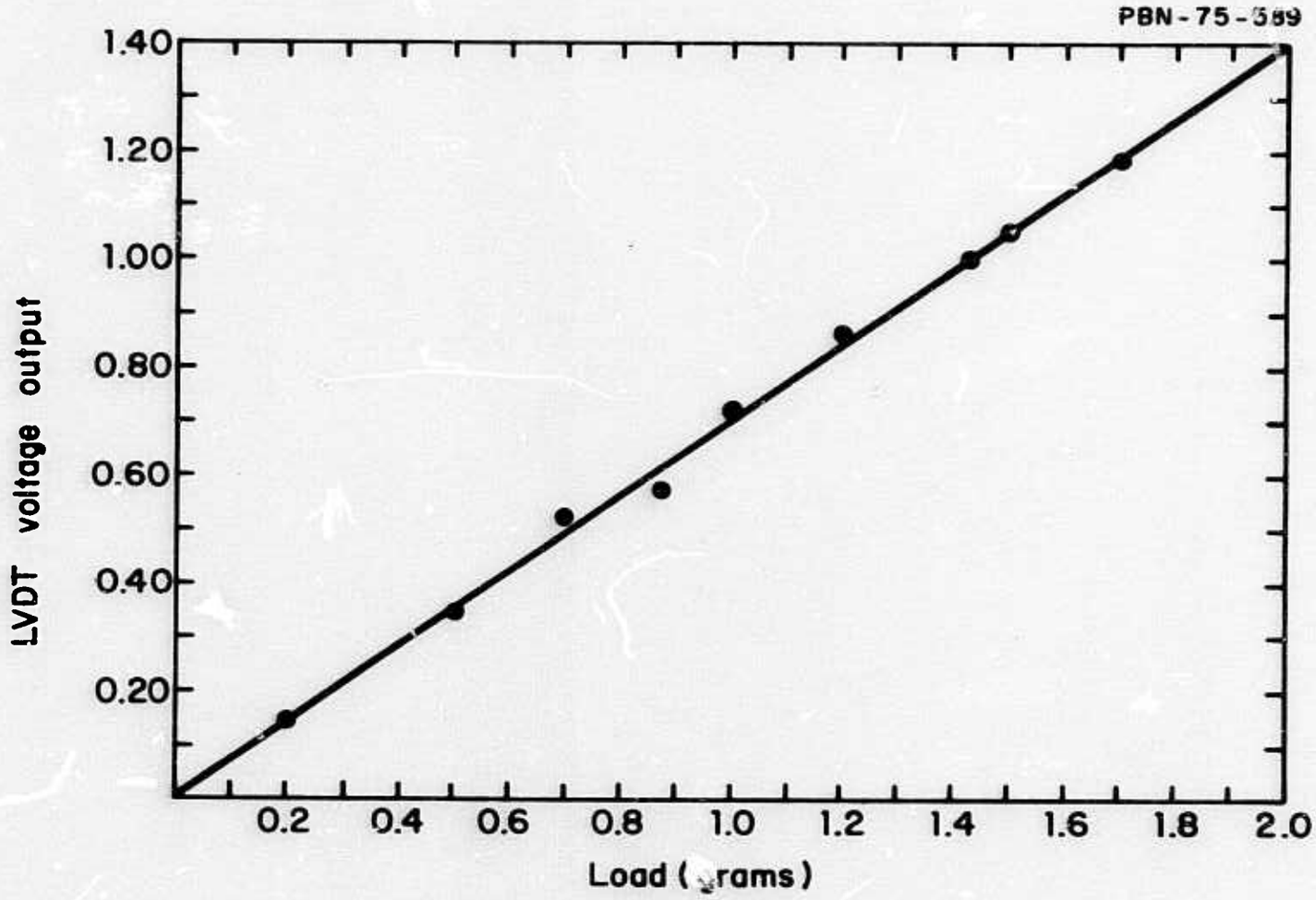


Fig. 28 Load-Position Calibration of LVDT - Beam System.

discussed in this report, the microhardness apparatus was mounted on a 2 × 4 foot air-suspension optical bench which was in turn set on a heavy granite-top table. A commercial microhardness apparatus (Kentron) was placed on the same table.

Figure 29 shows schematically the data taken during a typical microhardness experiment. As the sample is raised for the first sweep, it makes contact with the indenter at Position 1. As the sweep continues, the load and specimen displacement were given by the y and x axes of the plot. Position No. 2 of the figure corresponds to the point of maximum load and specimen motion during the sweep. The voltage to the sample translator is returned to its original value and the specimen is pulled away from the indenter and returned to its original position. This portion of the cycle is not shown in the figure because the hysteresis of the translator complicates its appearance. The specimen is raised into the indenter for a second time and a new point of contact (position 3) is recorded. The indentation depth is taken as the difference in displacement between the first and second contact points (positions 1 and 3) and the load as the maximum y value during the first sweep (position 2).

The apparatus discussed above was, in fact, the second microhardness tester constructed for the program. The first one, shown in Fig. 30, was a modified analytical balance in which the indenter replaced one pan position and a solenoid core the other. The instrument had at one time been a portion of an automated thermogravimetric analysis apparatus. The attitude of the balance beam is sensed by a position-sensitive photocell which receives a light beam reflected from the mirror at the balance point. Two approaches to microhardness determination were attempted with the balance. In the first, the photocell signal was used in a feedback loop to control the current in the solenoid so as to keep the position of the indenter constant as the sample was raised into it (by the piezoelectric translator). The coil current was measured to determine the indenting load and the indentation size was determined in an optical microscope. Unfortunately the contact of the indenter with the rigid specimen caused the characteristics of the feedback loop to change to the extent that the system broke into oscillation. None of the many

PBN-75-583

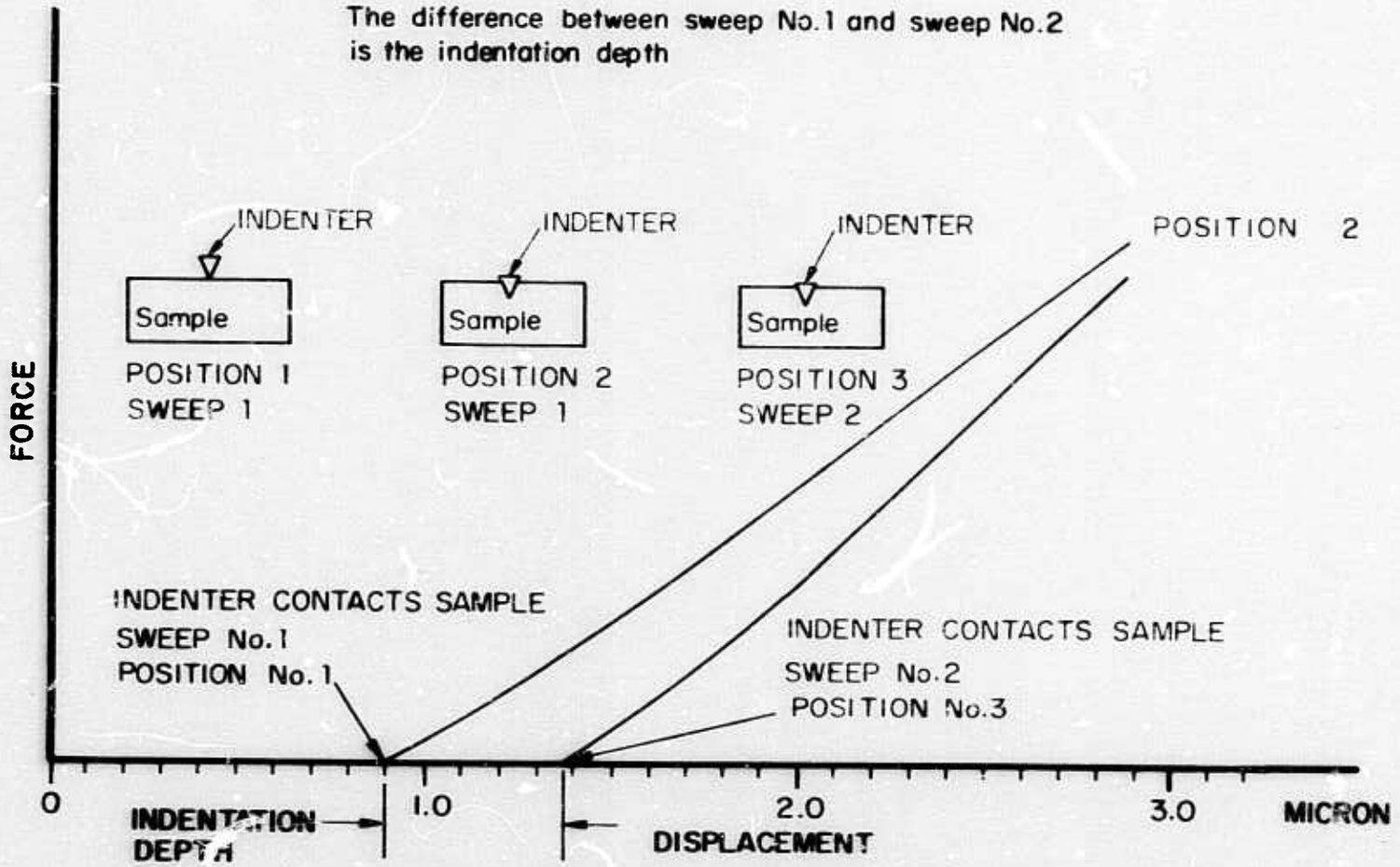


Fig. 29 **Recorder Trace of Typical Microhardness Experiment.**

PBN-75-582

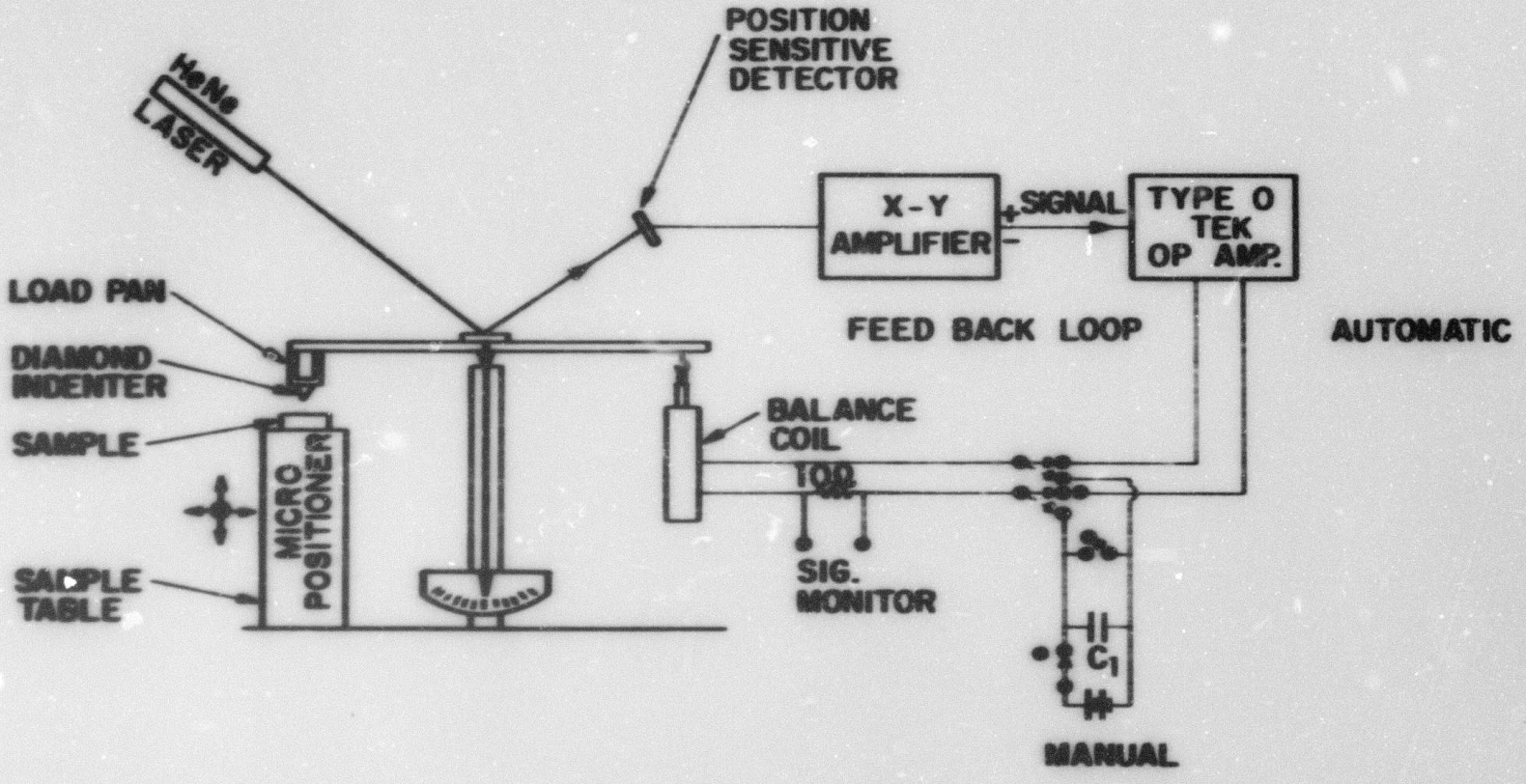


Fig. 30 Balance Beam Microhardness Tester - Schematic.

modifications made to the feedback approach substantially changed its behavior. The second approach used the balance as a loading device by weighting the indenter end of the beam which was balanced by the solenoid, positioning the specimen within 0.001-0.002 inches of the indenter, and decreasing the current in the solenoid coil (thus loading the specimen) by discharging a capacitor through the coil. Indentation sizes were again determined optically. This technique was used to apply loads as small as 150 milligrams to specimen surfaces, but the vibration sensitivity of the apparatus and the requirement of optical microscopy for indentation characterization were considered to make it unacceptable.

Finally, a commercial microhardness tester* was used to provide data against which the operation of the new apparatus could be compared. In this apparatus, the load is applied to the indenter by the motion of a weighted beam which is controlled by an oil-filled dash pot. The specimen is mounted on a two-position stage. One position holds the specimen under the indenter and the other holds the indentation in the field of view of an optical microscope for measurement. The applied load may be adjusted between one gram and ten kilograms. In practice, loads between approximately fifty grams and several hundred grams are most commonly used. Lighter loads usually produce erratic results and are avoided. One of the findings of this work was that room vibrations played a larger role in this nonreproducibility than was previously supposed. The hardness of zinc selenide bulk specimens determined by 50-gram loads was found to depend strongly on whether a large floor-mounted vacuum pump located several laboratories away was turned on or off. Measurements using the smaller loads required for thin film determinations were impossible. After this observation, the Kentron unit was placed on the air suspension table along with the experimental ultramicrohardness tester. The results reported in the next section were taken with both units on the air-suspension table.

2.2.3.2 Microhardness tests; results and discussions

Microhardnesses are reported as hardness numbers which have the units of pressure, kilograms per square millimeter. These are

---

*Kentron Model AK208

determined by the load applied to the indenter (in kilograms using mass for force) and the cross-sectional area of the indentation at the specimen surface (in square millimeters). Microhardness indenter shapes have been standardized and very accurately fabricated indenters are available. The Knoop indenter was used for all experiments reported here. The Knoop indenter is a pyramidal point with included angles of 130° and 172° 30' between the two pairs of faces. It produces a diamond-shaped indentation with one diagonal approximately seven times longer than the other. The long diagonal is thirty times the depth of the indentation. The other common indenter point, the Vickers, produces a square indentation of a depth one sixth of its diagonal. Microhardness numbers are obtained by measuring the applied load and a linear dimension of the indentation which is squared and converted to an area by multiplication by a constant for the indenter type used in the experiment. For the Knoop indenter, the square of the long diagonal of the indentation (in square millimeters) is multiplied by 0.07028.

The indentation behavior that the apparatus should produce may be deduced by considering a typical stress-strain curve for a solid undergoing plastic deformation (Fig. 31). During the first loading, the strain increases rapidly and linearly with stress until the elastic limit is exceeded and more slowly thereafter as material work hardens. Work hardening is the increase in yield strength produced in a material by plastic deformation. For this discussion, the important feature of the phenomenon is given by the second loading (curve 2), which shows that a higher load is now required to produce further plastic deformation in the material. Considering now the indentation process, we see that the first sweep of an indentation experiment corresponds to the first loading of Fig. 31. During this step, deformation and work hardening occur. The second sweep, since it does not produce any higher indenter load, should not cause any further indentation. Load-displacement traces of subsequent sweeps should fall on top of the second sweep. This expected behavior was commonly found to occur. An example is given by the lower traces in Fig. 32, data taken during indentation of a fresh chemically polished potassium chloride surface. In this case, the indentation depth is calculated to be 1.07 micrometers which should correspond to a long diagonal length thirty times longer or 32.1 μm.

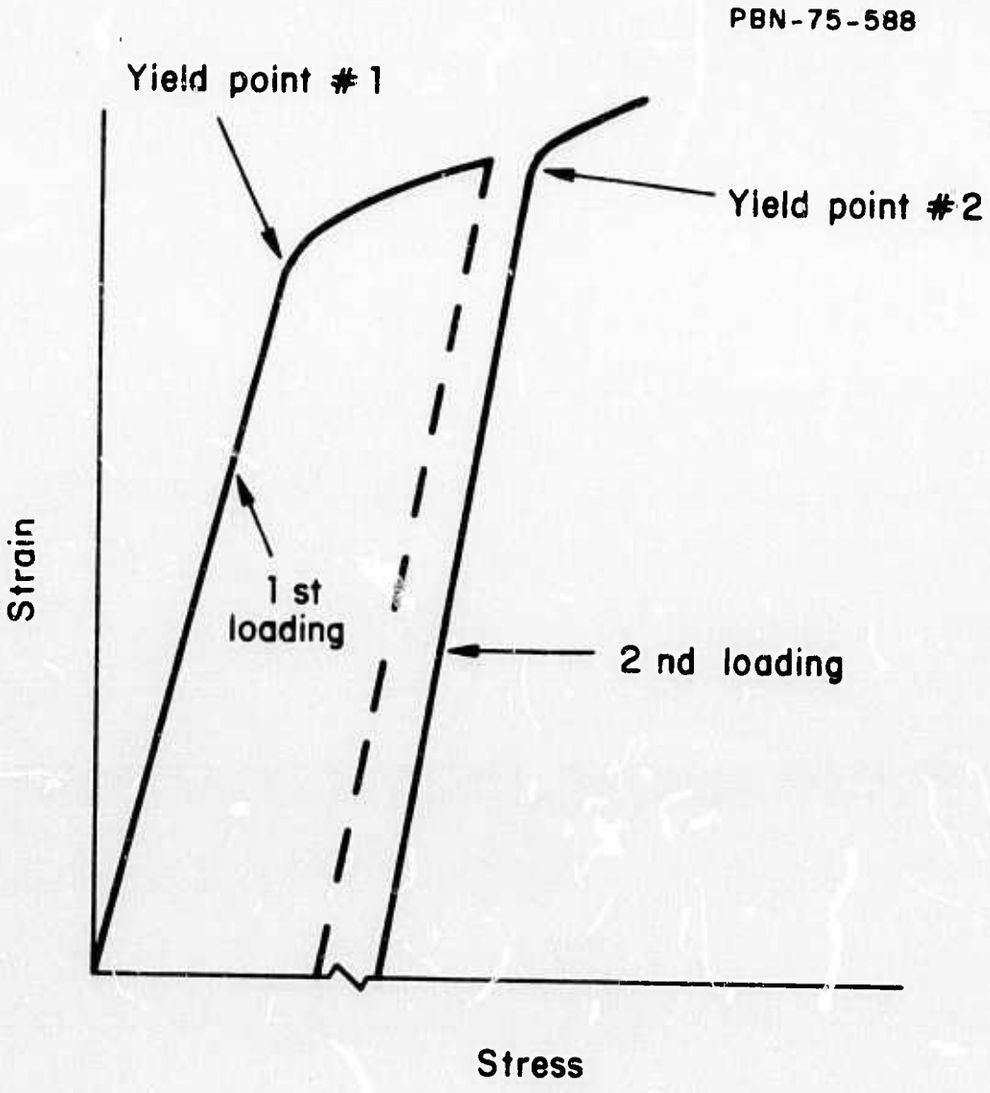


Fig. 31 Stress-Strain Curve for Material Undergoing Work Hardening.

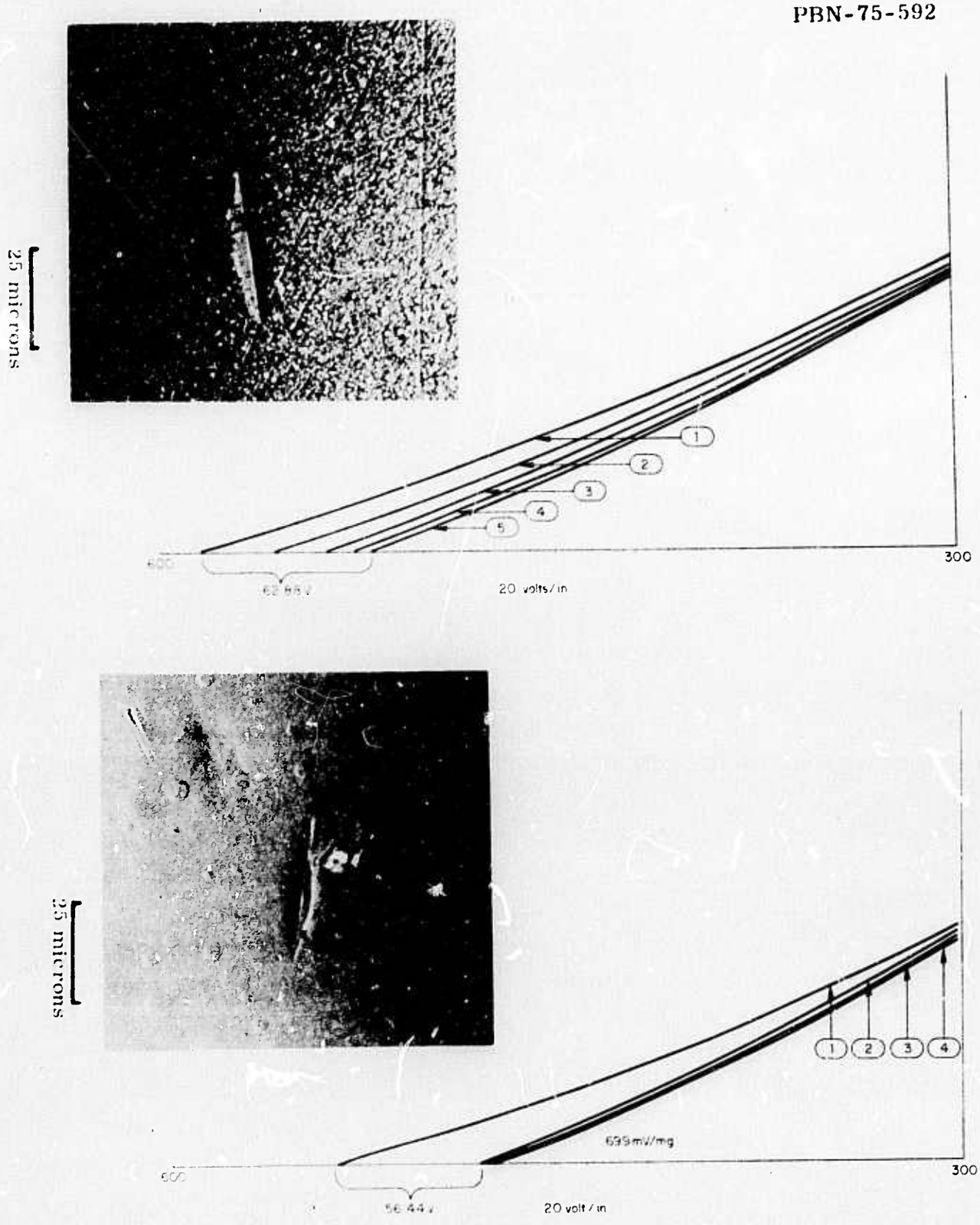


Fig. 32 Indentation Behavior of Potassium Chloride Surfaces.

The indentation, measured subsequently in an optical microscope, was 36.9 micrometers, which is within 15 percent of the calculated value. An example of anomalous behavior may be seen in the upper traces of Fig. 32, indentation traces of the same specimen which produced the "proper" behavior, but before the chemical polishing treatments. In this case, each succeeding indentation sweep produced further deformation. Although we have, at present, no explanation for the behavior, it is clearly produced by the state of the surface being indented. Hanneman and Westbrook[17] have reported a dependence of the hardness of a variety of crystalline and amorphous materials upon the extent of their absorption of water from the atmosphere. These observations suggest that low-load microhardness behavior could be used to follow the effects of environmental degradation of the mechanical properties of surfaces (and by extension, films) one of the primary goals of our characterization experiments. These indentations were made by loads of 1.3 grams on the chemically polished and 1.6 grams on the "dirty" surface.

A second form of anomalous behavior, this one produced by an instrumental difficulty, is given in Fig. 33. In this case, the contact point of the second sweep is seen to occur before that of the first sweep. The apparent interpretation of this is that the first indentation actually produced a convex dimple rather than a hole in the surface. The actual cause is seen in the photograph inset. During the second sweep, the indenter has actually missed the center of the indentation and made contact at a higher elevation with the deformed material beside the original indentation. The effect produced two important actions. First, during the experiments discussed in this report, each indentation was subsequently located and examined in an optical microscope. This procedure made the microhardness measurements substantially more tedious and time consuming than was desirable and decreased the opportunity for gathering statistically interpretable microhardness data. Second, it prompted a design for a revised version of the instrument in which the motions of the sample and indenter are measured separately by two LVDT's and the piezoelectric translator is used only to provide the specimen motion. We believe the translator hysteresis makes the specimen position insufficiently predictable during the downward motion and use the two cycle approach in order to begin with the translator in the same state for both the indenting and



25 μm

Double-Struck
Indentations

1. First Sweep Sample Indentation
2. Abnormal Second Sweep
3. Normal Second Sweep

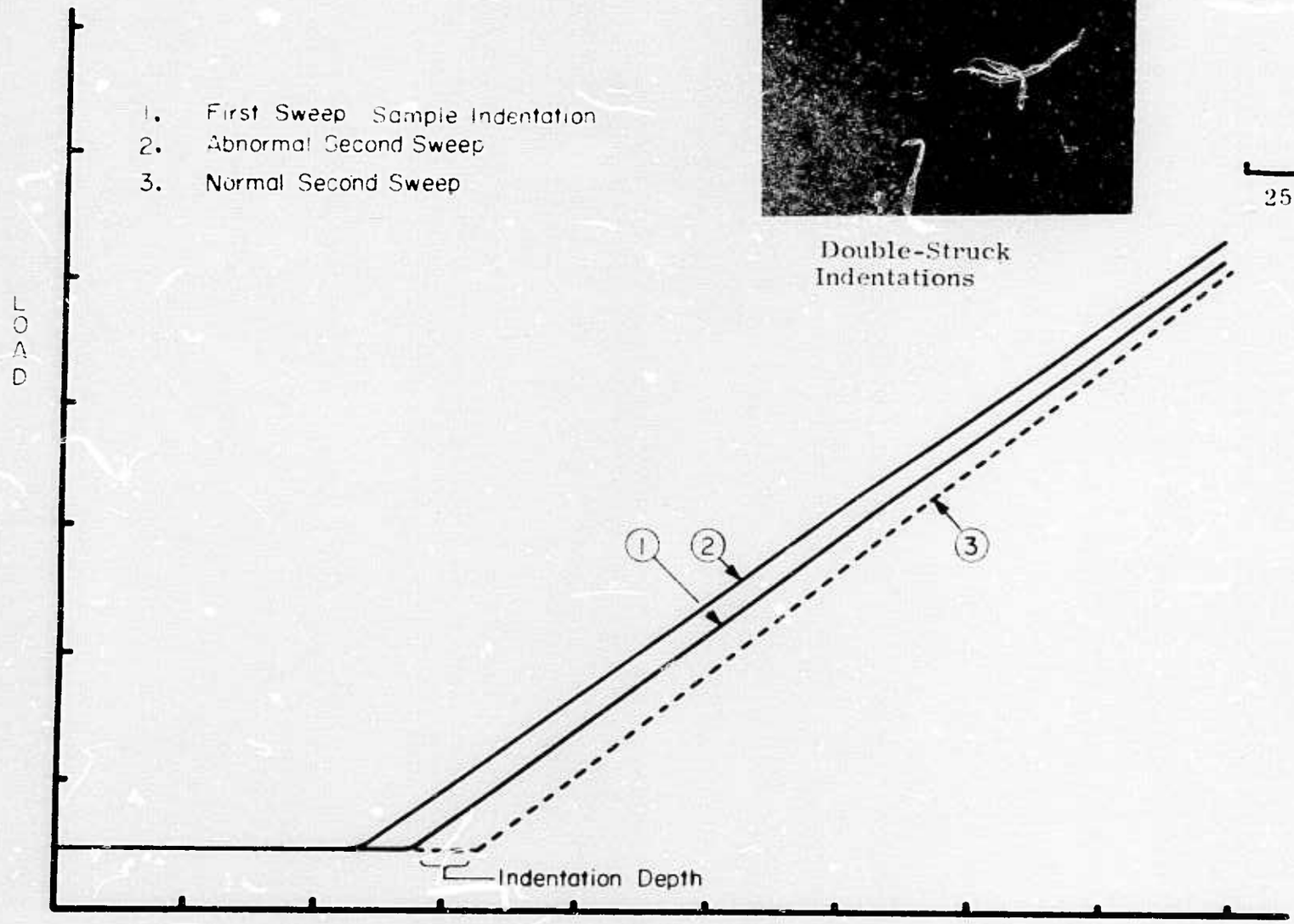


Fig. 33 Anomalous Indentation Behavior.

measuring steps. The revised version of the apparatus will require only a single sweep to generate the indentation depth information. The offset between the indentations in Fig. 33 was probably produced by a very small lateral sample motion between indentation sweeps.

To assess the value of the apparatus as a quantitative microhardness tester, it is necessary to consider the microhardness measurement itself in more detail. Since microhardness is supposed to be a material property, the numerical value of microhardness determined for a material should be independent of the load. To the extent that this is true, the size of the microhardness indentation which should be produced by any load may be calculated, given the hardness number. Recall that the hardness number is defined as the ratio of the applied load (in kilograms) to the area of the indentation (in square millimeters) and that the square roots of the areas and the liner dimensions of microhardness indentations are related by constants for each indenter type. For loads in excess of approximately 50 grams, the microhardness of a large variety of materials does exhibit this expected independence of load. For lower loads, large deviations from the idealized behavior are frequently observed. While these deviations may be produced by true surface hardness variations, instrumental errors are more commonly the cause. The importance of vibration isolation has already been discussed. When very light loads are used, the accuracy of fabrication of the indenter also becomes critical. For the measurements reported here, both the depth and length of each indentation were measured. Those two dimensions should be in the ratio of 1:30 for Knoop indentations. The dimensions of some typical indentations produced by the diamond indenter used for the microhardness tester are tabulated in Table VII.

TABLE VII

DEPTH CORRECTIONS FOR MICROHARDNESS INDENTATIONS

Sample	Load (gm)	Indent Length Optically (μm)	Indent Depth Length × 1/30 (μm)	Measure Depth UHMT (μm)	(μm) Difference
Bulk KCl DB-1	1.28	36.88	1.229	1.071	0.158
Bulk As_2S_3	1.59	12.21	0.407	0.280	0.127
Bulk KCl DB-1	1.59	40.67	1.356	1.195	0.1610
ZnSe 15/As_2S_3	1.66	11.75	0.3900	0.19	0.2017

The data in Table VII demonstrate that the indenter behaves as though its tip were slightly blunted. The apparent difference between the actual and the expected position of the tip of the indenter ranges from 1200 to 2000 angstroms. This discrepancy may be produced by an actual dimensional inaccuracy of the indenter tip, by elastic recovery of material beneath the indentation, or by some combination of the two. As a practical approach, however, an estimate of the indentation diagonal length which should be produced may be calculated from the indentation depth by Eq. (27).

$$\text{Indentation length} = (\text{measured depth} + 1600\text{Å})\ 30\ . \qquad (27)$$

This length should scale as the square root of the applied load. These observations make a comparison of the operation of the ultramicrohardness tester constructed for this program with the commercial Kentron unit possible. Tables VIII and IX present data obtained by the two units on a variety of bulk and thin film materials. To provide the comparison, the Kentron measurements were performed using a one gram load. Two or three measurements are averaged to provide an indentation length. The same specimens were then tested with the ultramicrohardness tester (UMHT) and the load and depth, corresponding to a single, well-behaved indentation cycle* determined for each specimen. The Kentron data were then scaled by the square root of the ratio of the (UMHT) load to the Kentron load to determine the size indentation the Kentron instrument would have produced if it had been used with the same load as the UMHT apparatus applied. This value appears in the tables under the column "Kentron Indentations." The depths measured for the UMHT indentations were then used to calculate the size indentation which have been produced (Eq. (27)). These values appear as "Calculated Indentations." Finally, the indentations were located and measured in an optical microscope to produce the column of "Measured Indentations."

While these are preliminary data, limited in statistical significance by the necessity of optically inspecting each indentation, the results obtained by the two instruments show good general agreement. In eight of the

---

*In this context, well-behaved is taken to mean that no unusual behavior (such as a double struck indentation) was produced in the x-y plot of the indentation cycle.

TABLE VIII

COMPARISON OF ULTRAMICROHARDNESS AND KENTRON MEASUREMENTS OF BULK MATERIALS

Sample	Load (gm)	UMHT Indentations		Kentron Indentations (μm)
		Calculated (μm)	Measured Optically	
KCl (dirty)	1.59	40.65	40.67	39.51
KCl (clean)	1.28	36.90	36.88	35.45
As_2S_3	1.59	13.20	12.21	13.79
ZnSe	1.7	10.02	14.82	11.0
ZnSe	1.45	6.71	13.84	10.16
ZnSe	1.895	14.12	16.45	11.62
ZnS	1.757	9.20	14.75	9.0
ThF_4	1.70	20.13	9.66	12.18

TABLE IX

COMPARISON OF ULTRAMICROHARDNESS AND KENTRON MEASUREMENTS OF FILM MATERIALS

Film	Substrate	Load (gm)	UMHT Indentations		Kentron Indentations (μm)
			Calculated (μm)	Measured Optically	
As_2S_3	ZnSe	1.66	10.50	11.75	11.78
ThF_4	ZnSe	1.543	11.66	14.95	10.31
ZnS	ZnSe	1.61	6.88	7.44	5.86
ZnSe	BaF_2	1.0	7.30	6.33	6.95
ZnSe	BaF_2	1.79	8.07	9.14	9.3
ThF_4	ZnSe	1.55	7.88	10.64	10.57
ThF_4	ZnSe	1.52	7.43	12.01	10.21
ThF_4	ZnSe	1.59	7.82	12.34	10.44
ThF_4	ZnSe	1.06	7.57	9.14	8.53
As_2S_3	BaF_2	1.54	8.8	14.36	15.07

eighteen specimens examined, all three determinations agree to within plus or minus one micrometer of each other. Among those for which the agreement of all three values was not so close, the directly measured and calculated values obtained with the ultramicrohardness unit showed the better agreement with the Kentron data with approximately the same frequency. We believe the principle of operation of the ultramicrohardness tester has been demonstrated to be valid by these experiments. Further work will be required to characterize the instrument completely. The reproducibility and speed of operation of the unit should both be improved by the addition of a second LVDT to permit single rather than double sweep operation. Note that the loads selected for the UMHT for these experiments were purposely made large so that the results could be compared with those taken with the Kentron apparatus. The new apparatus should be capable of determining indentation depths on the order of a hundred angstroms and loads as small as a hundred milligrams.

Both the UMHT and the Kentron units were used to obtain film hardness values. Table X is a comparison of indent depths for various bulk and film materials. Data were obtained at various loads with the UMHT and scaled to 1.8 grams so that the indentations could be compared directly.

TABLE X

COMPARISON OF BULK AND FILM MICROHARDNESS VALUES

	Indentation Depth (μm) for 1.8 gm Load		
Material	Bulk	Film	Substrate
As_2S_3	0.30	0.20	ZnSe
		0.14	BaF_2
ZnSe	0.18	0.10	BaF_2
ZnS	0.15	0.07	ZnSe
ThF_4	0.53	0.11	ZnSe

Note that in all cases, the films are harder than the corresponding bulk materials (the film indentations are shallower). For all comparisons except the thorium fluoride, the indentations differ by approximately a

factor of two. This corresponds to a factor of four in the hardness numbers which are proportional to the square of the depth. Although the experiments were not extensive enough to determine the hardness behavior in detail, the behavior is at least qualitatively correct. The yield strength of polycrystalline solids is well known to increase with decreasing grain size because the dislocation motion which is responsible for macro plastic deformation is impeded by the grain boundaries. On this basis, the hardness, which is closely related to the yield strength, should be higher for these thin films (which are very fine-grained) than for the larger grain-size bulk material.

Table XI compares the indentation behavior determined by the Kentron unit (using a one gram load) of examples of the vendor-supplied films.

TABLE XI

MICROHARDNESS OF VENDOR-SUPPLIED FILMS

Film	Substrate	Supplier	Indentation Length (μm)
ThF_4	BaF_2	1	10.9
		2	10.4
		3	11.1
	ZnSe	1	8.5
		2	8.6
		3	8.5
As_2S_3	BaF_2	1	12.12
		2	12.14
		3	8.3
	ZnSe	1	11.2
		2	13.7
		3	9.1
ZnSe	BaF_2	1	4.6
		2	4.5
		3	6.9
ZnS	ZnSe	1	4.6
		2	5.4
		3	4.6

Several comments are appropriate to the table. First, the substantial variability in absorptivity of the ThF_4 films from the three suppliers are not reflected in the microhardness data. Note, however, that there is a clear effect of the substrate type upon the hardness values obtained for all thorium fluoride films. The thorium fluoride films were all on the order of 1.6 μm thick and the indentations were on the order of 0.3 μm deep, approximately a factor of five smaller than the film thickness. Clearly smaller loads will be required to detect correlations between deposition conditions and microhardness in these films.

The arsenic trisulfide films from Vendor No. 3 appear to be harder than those from the other two suppliers. In fact, however, the Vendor 3 films were also thinner than those from the other two vendors. In this case as in the thorium fluoride case, the ultramicrohardness apparatus should provide additional information. Unfortunately, time did not permit continued experimentation.

Finally, we treat qualitatively a further potential use of microhardness testing of thin films - adhesion experiments. Figure 34 contains photomicrographs of indentations of an arsenic sulfide film on zinc selenide under various loads. A light area caused by film lifting may be seen to occur at the ends of the short indentation diagonal and to increase with applied load until the film is removed from the substrate. Scanning electron micrographs of a similar case are given in Fig. 35. The film which is shown lifting in Fig. 34 was adherent enough to pass the "Scotch tape" test in paragraph 2.2.1.3. Microhardness methods may be used to produce debonding effects in films by the application of well-characterized loads. The extent to which quantitative information may be extracted from this approach must still be determined by experiments, but its applicability to films which will pass the common user-oriented pass-fail test make it attractive. Further adhesion investigations, like the direct microhardness measurements, could be carried out in environmentally-controlled chambers to study such effects as corrosion-assisted debonding of films.



a) One Gram Load

b) Three Gram Load

c) Five Gram Load

Fig. 34 Indentations in As_2S_3 Films - Nomarski Microscopy.

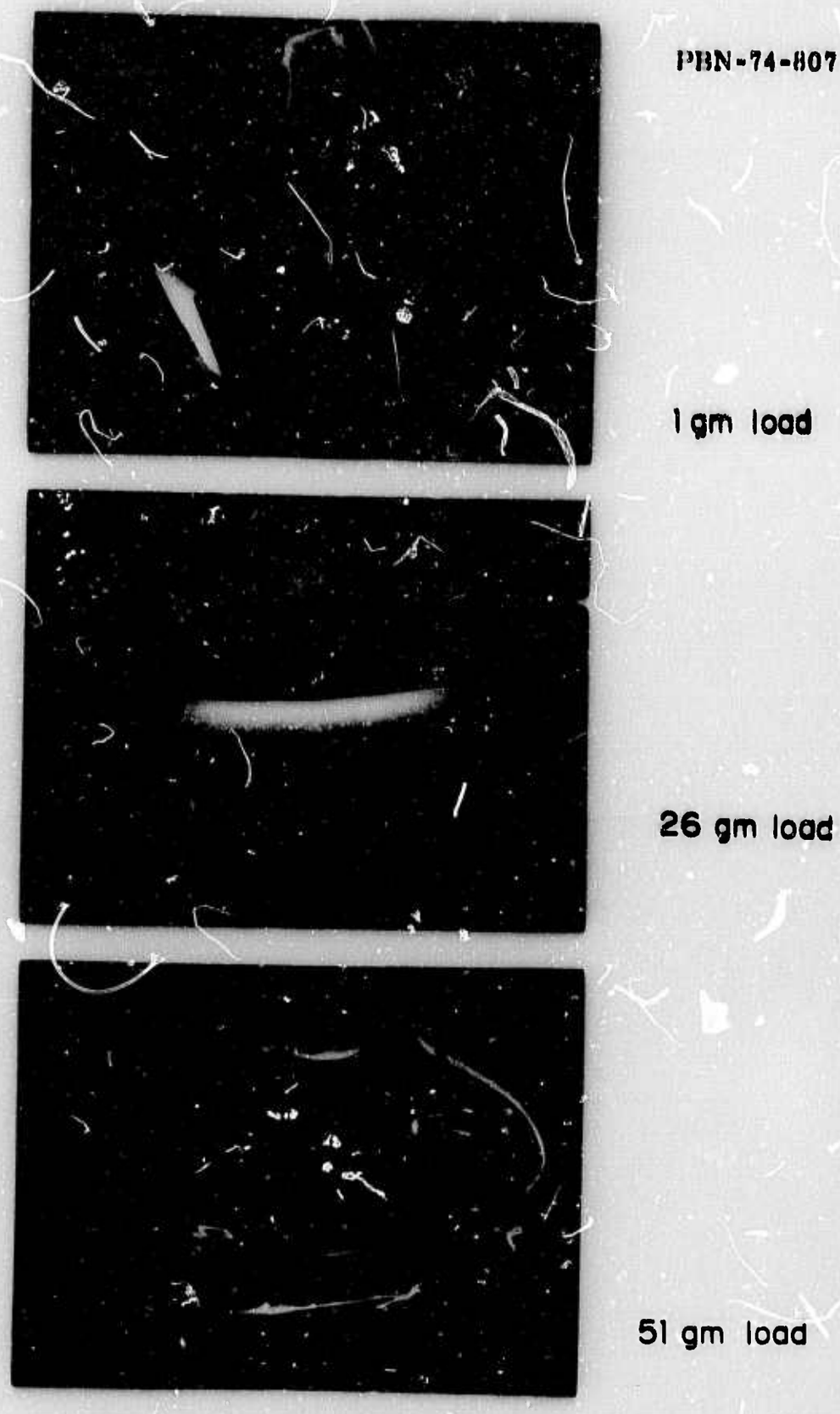


Fig. 35 Indentations in As_2S_3 Films - Scanning Electron Microscopy.

In summary, an operable ultramicrohardness apparatus has been constructed and demonstrated. Operating well above its minimum load limit, it has been shown to produce indentation behavior which is quantitatively similar to that of a commercial microhardness apparatus operating at its minimum limit. Time limitations prevented extensive experimentation with the apparatus. It was used to demonstrate the expected increase of hardness of film materials over their corresponding bulk forms. The minimum loads available on a commercial microhardness tests were shown to be large enough to produce substrate effects on 1.6 micrometer thick ThF_4 films and 1.0 micrometer As_2S_3 films. Correlation of hardness behavior with deposition conditions must be done with an ultramicrohardness apparatus. Both units were used to demonstrate that the film materials were approximately four times harder than their corresponding bulk forms. No significant variation of film hardness among the commercial vendors was determined.

Performance limitations of the existing apparatus have been defined and conceptual design of an improved version has begun. The improved apparatus will provide for single sweep indentation and environmental chamber operation.

The most promising future applications for microhardness testing of thin films, in addition to correlation of hardness and deposition conditions, are studies of environmental (particularly temperature and humidity) effects upon film hardness and film adhesion. These may be carried out by testing after or during the environmental exposure. In addition, microhardness testing information should be extendable both to the practical requirement for more quantitative film durability characterization and to more basic studies of film deformation behavior. In this last sense especially, the value of the technique extends beyond optical films to thin solid films generally.

3.0 SURFACE PREPARATION PROCEDURES

In addition to accurately-fabricated optical figures, the surfaces of high-power laser optical components must be free of field concentrating and light scattering features such as scratches and pits, as well as absorbing surface contaminant layers, embedded abrasives, and perhaps cold worked surface material. In general, the surface preparation procedures are broken into two major parts - the generation of the optical figure with as nearly defect-free surface as possible by some abrasive polishing technique, followed by a second treatment sequence which removes all harmful surface residues. This second sequence may be a simple cleaning procedure on a more complicated treatment which includes chemical polishing, annealing, or ion beam polishing.

3.1 Abrasive Polishing

Abrasive polishing of optical surfaces is commonly carried out on rotating pitch laps onto which a succession of slurries of progressively finer abrasive is fed to produce the final polished surface. Although the details of the abrasive action are not well understood, it is generally agreed that abrasive polishing of optical surfaces occurs through the action of abrasive particles which are more or less free to move on the lap surfaces. Harder pitches facilitate optical figure control, softer ones produce more nearly scratch-free surfaces. The hardness of the pitch can be selected by the optician to provide the proper balance between "free" and "bound" abrasive. Further, in many cases the abrasives used during the final polishing stages may not be substantially harder than the surface it is polishing.

While these techniques may be used effectively for single crystal and amorphous materials, they will not reliably produce scratch-free optically-figured surfaces on many polycrystalline materials. This is so because the very gentle polishing conditions which produce the most scratch-free surfaces (soft laps, very fine abrasives) polish the variously-oriented grains of a polycrystalline workpiece at difference rates and produce grain-to-grain surface relief. An example of this relief polishing is given in Fig. 36a, an interferogram of the surface of a 2-inch diameter



Lap: Politex "Supreme"
Abrasive: A-type Alumina



2.54 cm

Lap: Pitch
Abrasive: 0-0.5 μm diamond

Fig. 36 Interferograms of Polished Polycrystalline Strontium Fluoride Surfaces.

cast polycrystalline strontium fluoride window polishing on a Politex Supreme* (synthetic leather) pad using 0.3 μm alumina abrasive. The grain relief and poor optical figure are both obvious. A pitch lap would have improved the figure, but the relief polishing would have been difficult to avoid on a highly-polished surface.

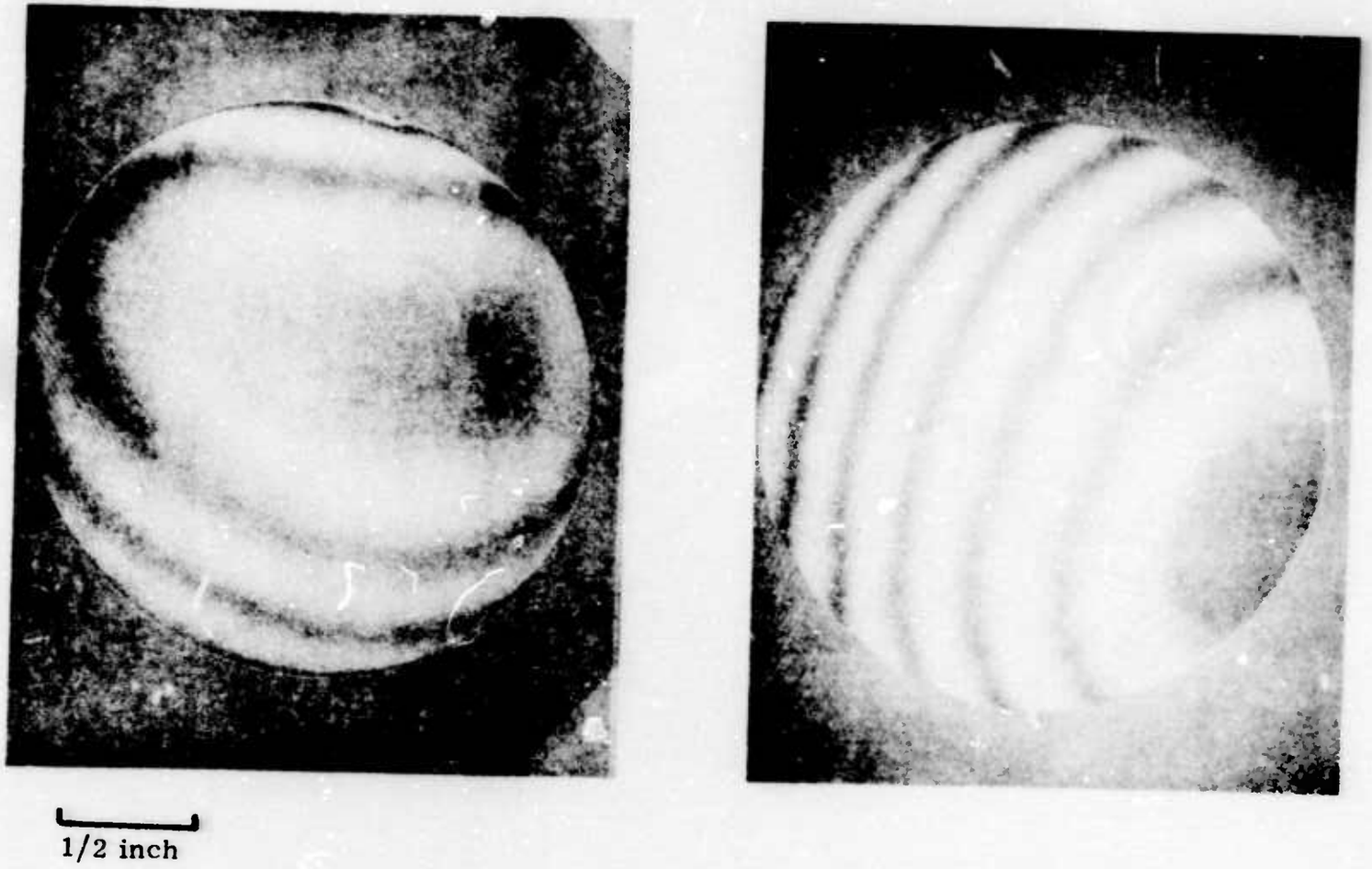
The use of diamond abrasives on pitch laps has recently been shown[18] to produce very nearly scratch-free surfaces on polycrystalline specimens of zinc selenide and calcium fluoride without producing relief polishing. The result of the diamond/pitch technique applied to the relief-polished strontium fluoride specimen of Fig. 36a is shown in Fig. 36b. Nomarski interference microscopy of the diamond-polished surface showed it to be essentially free of detectable surface scratches. No detectable relief polishing remains and the surface flatness has improved to a bit more than one half fringe at the interferometer wavelength (6328 angstroms) over the two-inch specimen. No efforts to improve the optical figure were made, but here has been no indication that any limiting optical figure for the technique has been reached.

Figure 37 demonstrates the removal of a second defect type from a strontium fluoride specimen by diamond polishing. In this case, a groove has been produced at the boundary between the large control grain and the surrounding grains. Such grooves occasionally appear during the final grinding and rough polishing steps. Once established, they are extremely difficult to remove by conventional polishing or grinding, probably because the abrasive particles cleave the workpiece at the groove edge and propagate the groove ahead of the polishing surface.

The essentials of the diamond polishing technique as developed on this and previous projects are summarized in Table XII. We believe this to be a most useful approach to the polishing of polycrystalline specimens and recommend it.

---

* Trademark, Geoscience Corp.



a) Before Polishing

b) After Polishing

Fig. 37 Grain Boundary Removal by Diamond Abrasive Polishing.

TABLE XII

SUMMARY OF DIAMOND/PITCH POLISHING TECHNIQUE

1. Preliminary Sample Preparation - This technique is the final polishing step. The preliminary steps, discussed in Ref. 18, are grinding on glass laps with alumina grinding compounds followed by polishing on pitch laps with c- and a-type alumina. The resulting surface is still scratched but not relief polished.

2. Pitch Selection - Use the hardest pitch which will not itself produce scratches in the workpiece. This facilitates optical figure control.

3. Abrasive Selection - Use loose diamond powder. The various vehicles used to produce diamond pastes all dissolve pitch. The SrF_2 surfaces discussed in this section were produced with 0-1/2 μm (nominal 1/4 micrometer) diamond. Finer (0.1 μm) abrasive is available and may produce still more perfect surfaces, but we have not used it.

4. Abrasive Application - Use water as the slurry vehicle. Ethylene glycol or triacetic glycol (triacetin) may be used on pitch in place of water on pitch for water-soluble materials. (We have not yet used them with diamonds.) The diamond slurry is brushed onto the rotating lap and forced into the lap surface by the workpiece. Once the lap surface becomes charged with diamond, it will continue to polish. Only slurry vehicle additions are necessary. Only a few minutes were required to charge the 4-inch laps used to polish the strontium fluoride windows. Diamond abrasives may contain clumps of particles which must be broken down if the abrasive is to function properly. This is especially important for polishing of soft materials.

5. Lap Resurfacing - Improperly polishing laps may be regenerated by softening their surfaces with a torch and reworking them with a clean optical flat. This technique is well known to opticians; it is mentioned here because it is especially effective for diamond-charged laps.

TABLE XII (Continued)

6. Polishing Conditions - The strontium fluoride specimens were polished at a total pressure of approximately one pound per square inch on laps rotating at approximately 40 rpm. No attempt to optimize these parameters has been made.

7. Grain Boundary Removal - The key to removal of grain boundary grooves appears to be the use of a diamond paste together with moderately hard to synthetic lap surface. In the case discussed above, the grain boundary was removed by polishing on a No. 3483-K unperforated pad* with No. 3-W-40 diamond paste.** The firm backing apparently permits the diamond to cut material away from the groove without fracturing the groove edge. The resulting surface, though free of grain boundary grooves is scratched and must be finished on pitch as described above. A reasonable optical figure may be maintained during the grain boundary groove removal by mounting the pad onto the lap with a thick pitch layer and pressing it flat.

Although the details of the material removal mechanisms are not understood, relief polishing is apparently avoided because the great hardness of the diamond permits it to cut off all grains of the polycrystalline materials with equal ease. Further, the diamond is largely fixed in the lap surface. As the polishing proceeds, it may be progressively forced into the pitch lap surface to produce the effect of progressively finer abrasives.

---

* Obtained from J.T. Morris Co., Southbridge, Mass.

** Obtained from Engis Corp, Morton Grove, Illinois

3.2 Surface Cleaning

The procedure outlined in Table XIII was adopted to clean strontium fluoride surfaces. The various steps in the process were chosen to remove both particulate matter and residues from the pitch lap.

TABLE XIII

CLEANING PROCEDURES FOR STRONTIUM FLUORIDE

1. Wash in warm, non-ammoniated detergent solution, wipe gently with cotton diaper or polyamide web material.*
2. Rinse in filtered, deionized water.
3. Rinse in filtered trichloroethylene.
4. Rinse in spray of filtered isopropanol.
5. Suspend in vapors of boiling Freon 113** until Freon condensation on surface stops dripping.
6. Remove to draft-free area and cool to room temperature.

This cleaning procedure was applied to a set of four SrF_2 specimens ranging in thickness from 1.1 to 4.5 centimeters which were polished together by the diamond technique described above. The total absorption of each specimen at 5.25 μm was determined calorimetrically at two locations. Results are summarized in Fig. 38, where a large variability of absorptivity between paired determinations on each specimen can be observed. Careful examination of the specimens revealed that they contained occasional inclusions which may have contributed to the higher of the paired values and increased the uncertainty of the measurements. These specimens were taken from a location close to the surface of the casting; such end pieces may be less perfect than the bulk of the casting.

---

* Pellon, Style 301, Pellon Corp., Lowell, MA

** Trademark, DuPont Company.

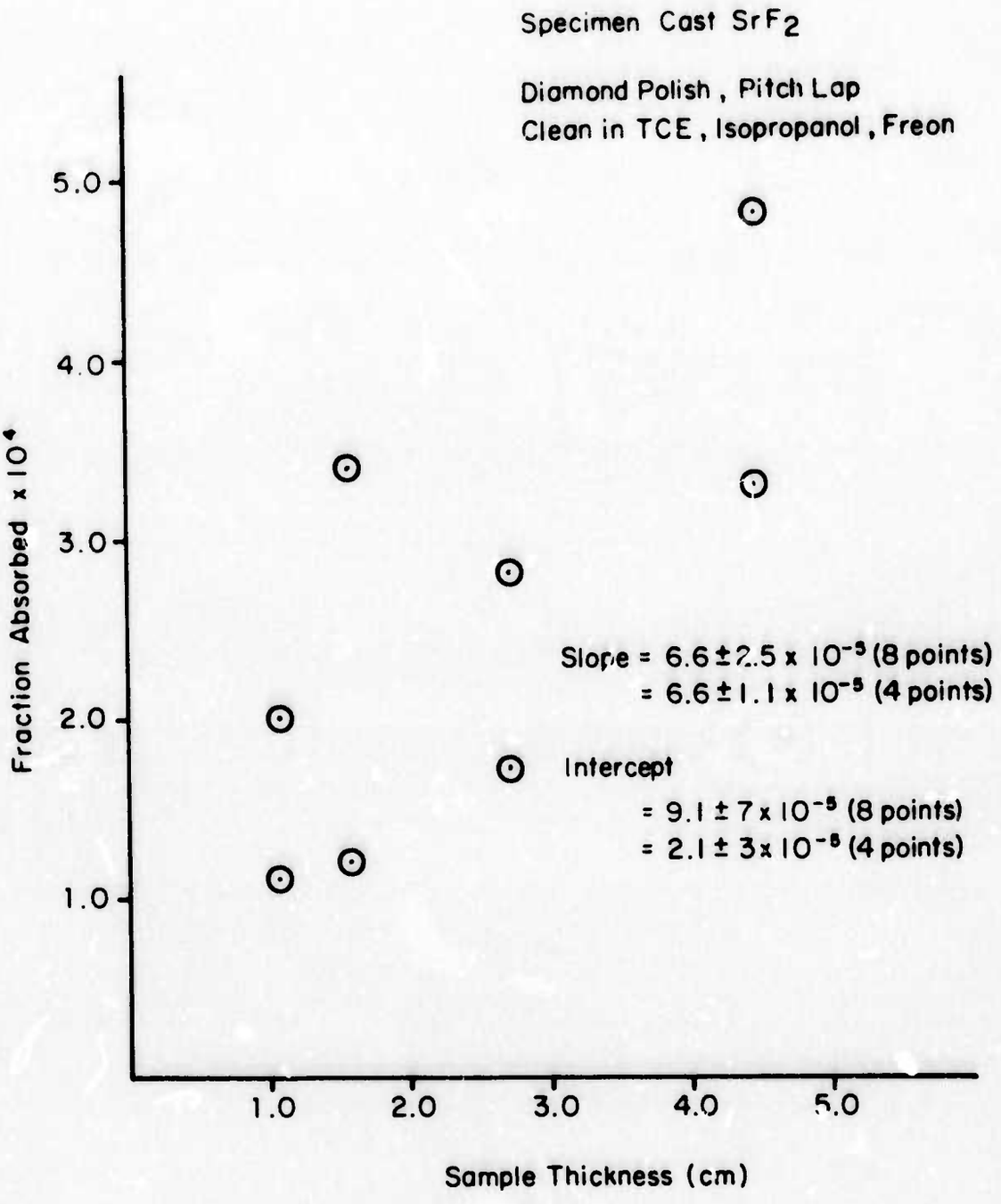


Fig. 38 Absorption vs Length, Strontium Fluoride Specimens.

If this were so, it would be reasonable to take the lower four points to represent the bulk material and calculate a surface absorptivity of approximately 1×10^{-5} per surface at 5.25 μm. Taking all eight data points increases the surface absorption only to 4.5 3.5×10^{-5}, still a low value. In both cases, the bulk value is 6.6×10^{-5} cm^{-1}. We note here that this specimen was produced (on another project at the Research Division)[19] by casting of inexpensive reagent-grade powder which had been purified prior to the casting by an uninvolved, inexpensive process.

Professor J. Harrington,[20] University of Alabama, Huntsville, has measured the absorptivity of strontium fluoride at the HF and DF chemical laser wavelengths (2.8 and 3.8 micrometers) to be $1\text{-}2 \times 10^{-3}$ for centimeter-thick pieces, an order of magnitude higher than our values which were taken at 5.25 micrometers.

We believe the difference to be caused by the presence of a contaminating surface layer which is more absorbing at 2.8 and 3.8 micrometers than at 5.25. The difficulty of obtaining a surface which is non-absorbing at the fluoride laser wavelengths is illustrated by the experiments, summarized in Fig. 39. The four traces are ATR spectra of a specimen of barium fluoride. The first was taken immediately after it was removed from its polymer shipping bag, the second after a five minute wash in trichloroethylene. Trichloroethylene was chosen as the solvent because its infrared absorption spectrum contains no bands in the 3000-2500 cm^{-1} range. Organic compounds containing C-H bonds (effectively all organic surface contaminants) contain strong absorptions at approximately 2915 and 2845 cm^{-1} due to the C-H bond stretching.

The trichloroethylene wash did not completely remove the hydrocarbon contamination so a second cleaning, a five minute immersion in boiling trichloroethylene was evaluated. Finally, the specimen was allowed to remain in the spectrometer for 24 hours following the boiling treatment and a fourth spectrum was taken.

The ATR spectra of Fig. 39 demonstrate several points. First, storage of the ATR plate in a polymer container produced a significant

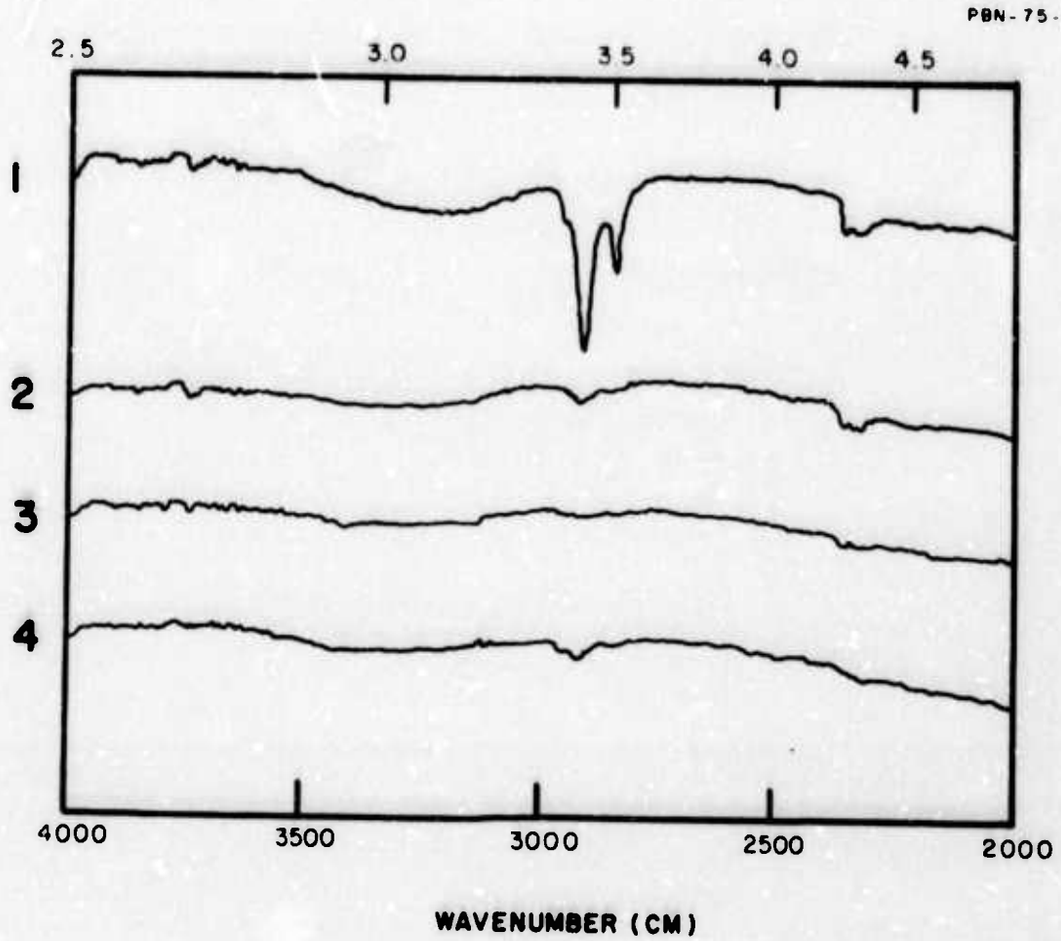


Fig. 39 Hydrocarbon Contamination of Barium Fluoride ATR Plate.

absorption both at 2915 cm^{-1} and at 2630 cm^{-1} (3.8 μm). Second, trichloroethylene cleaning cannot completely remove the contamination, although the boiling solvent nearly removes all detectable traces of it. Third, the clean surface is very easily recontaminated. The surface absorptivity of the boiled specimen increased by nearly a factor of two during the 24 hour storage in what should have been the relatively clean environment of the infrared spectrometer. The sample holder touched the specimen only at the edges and was itself cleaned in trichloroethylene prior to the experiments. The sample chamber was flushed with tank nitrogen which either contained sufficient hydrocarbon impurities or was able to desorb them from the interior of the spectrometer and redeposit them on the specimen. Finally, the experiments demonstrate the necessity of evaluating surface cleaning procedures for laser optical components at the wavelengths at which they will ultimately be used. Since these components will, in general, receive antireflection coatings, the optimized cleaning procedure must additionally produce a surface upon which an adherent coating can be deposited.

An estimate of the quantitative absorptivity of the contaminant layer was obtained by assuming the difference between the trace at 2915 cm^{-1} and at extrapolation of the curve away from the absorption peak to be the total absorption due to the contaminating hydrocarbon layer. The infrared beam is reflected twenty-two times as it transits the barium fluoride plate. At each reflection, the evanescent wave travels twice through the surface layer, which is assumed to have the same index of refraction as the strontium fluoride. The absorptions per pass, taken as the total absorption divided by forty four, are given in Table XIV. In the last column in the table, the absorption at the DF laser wavelength is estimated as being five percent of the absorptivity at 2915 cm^{-1}, the peak of the C-H bond stretching absorption. A review of infrared absorption spectra of hydrocarbon compounds indicates this to be a reasonable one.

Harrington[20] has measured total absorptions of strontium fluoride specimens at 3.8 micrometers and found them to be at least an order of magnitude higher than these surface absorption estimates, coupled with reasonable estimates for bulk absorptivity, would allow. Further, the total absorptivity of his specimens may be reduced by an amount which is several times larger than our surface absorptivity estimates by vacuum heating. We believe, therefore, that the ATR spectra should not be used to estimate surface absorptivities quantitatively although they do provide useful qualitative information.

TABLE XIV

ATR SPECTROSCOPY: HYDROCARBON CONTAMINATION OF BaF_2

Trace No.	Treatment	Absorption per Pass (fraction) At 2915 cm^{-1} (maximum)	Absorption per Pass (fraction) At 2632 cm^{-1} (3.8 μm)
1	As received	5.5×10^{-3}	2.7×10^{-4}
2	Trichloroethylene Wash	6.75×10^{-4}	3.5×10^{-5}
3	Trichloroethylene Boil	3.25×10^{-4}	1.6×10^{-5}
4	24 hour storage after boil	5.75×10^{-4}	2.9×10^{-5}

Finally, we note that the cleaning procedures of Table XIII will probably not minimize the surface absorptivity of alkaline earth fluorides at 3.8 micrometers. At the very least, some treatment with heated solvents must be included. This step will prove to be difficult to apply to large alkaline earth fluoride specimens, which are sensitive to thermal shock. In this context, we note that boiling Freon 113* appeared by ATR spectroscopy to be as effective as boiling trichloroethylene in removing hydrocarbon contamination from both barium fluoride and zinc selenide surfaces. This observation is worth noting because the Freon boils at 47° C and would be less likely to cause thermal shock problems than trichloroethylene, which boils at 87° C. The large decrease in absorption at 3.8 micrometers produced on SrF_2 by vacuum heating demonstrates that substantial surface absorptions may remain even on carefully cleaned alkaline earth fluoride specimens. Surface cleaning studies should be continued, as should calorimetric measurements at all the important laser wavelengths. Vacuum heat treatments should be pursued and should be performed in the laser calorimeter sample chamber so that atmospheric recontamination does not occur.

---

*Trademark, DuPont Co.

4.0 DIRECTIONS FOR FUTURE WORK

The tasks for this project addressed both the development of characterization techniques for thin films and the characterization of commercialiy-available examples of important film materials. Experimental work discussed in this report has identified directions for further fruitful work in both areas. Specific areas of importance are summarized below.

4.1 Optical Properties

(1) The contributors to absorptivity of optical films at important laser wavelengths should be identified by careful correlation of deposition parameters and absorption measurements. For these experiments both the depositions and absorption measurements should be carried out in the same laboratory. The goals of the experiments are the minimization of both the absolute levels of absorptivity and the deposition-to-deposition variability thereof. Results of the work should be distributed among commercial film suppliers.

(2) Evaluation of state-of-the-art examples of commercially-available films should continue. In this study, optimized substrate materials and surface preparation techniques should be used to maximize the sensitivity of the calorimetric absorption determinations and to permit study of light scattering by the films.

(3) Optical evaluation of both commercial and research films should be expanded to include light scattering. These, in turn, should be correlated with laser damage information to determine the possibility of nondestructive techniques for damage threshold prediction. In this context, the integrated optics techniques should be pursued.

(4) Optical evaluation techniques for both films and surface should be expanded to include effects of environmental exposure upon absorptivity and scattering.

(5) Optical evaluation of both films and surfaces should be expanded to include studies carried out at 2.8 and 3.8 micrometers.

This is most immediately important for the determination of techniques for producing and maintaining minimally absorbing surfaces for hydrogen and deuterium fluoride laser optical components.

(6) The theoretical and experimental treatment of thin film calorimetry should be extended to multilayer coatings. There is presently a considerable variation in film absorptivity produced by uncontrolled variations in deposition parameters among single layer films. The intentional variations of deposition parameters used by commercial suppliers to produce multilayer coatings may reasonably be expected to produce further, as yet unmeasured, variations in the properties of the coatings which will actually find use in high-energy laser optics.

4.2 Mechanical Properties

(1) The application of ultramicrohardness testing of thin films should be continued and refined. Goals of the experimental work should include:

a) Determination of environmental effects on film hardness and adhesion.

b) Separation of film durability and adhesion effects. For this work, microhardness and scratch adhesion tests might be compared.

c) Correlation of micro-testing with macroscopic film durability tests and development of new durability tests.

d) Correlation of film durability with deposition conditions.

(2) Finally, component surface finishing techniques should be optimized to produce simultaneously the lowest optical absorption (measured at the use wavelength), the maximum physical strength, and the most adherent optical coatings. This sort of coordinated information does not now exist for any material.

5.0 REFERENCES

1. Military Specifications MIL-C-675A, MIL-M-13508C.
2. T.F. Deutsch, R.I. Rudko, Contract No. DAAH01-72-C-0194, Final Technical Report (January 1973).
3. T.F. Deutsch, Contract No. DAAH01-72-C-0194, Final Technical Report (December 1973).
4. W.E.K. Gibbs, J. Butterfield, to be published in Applied Optics.
5. N.J. Harrick, Internal Reflectance Spectroscopy, Interscience, (1967).
6. R.A. Nyquist, R.O. Kagel, Infrared Spectra of Organic Compounds.
7. E. Bernal G., private communication (1975).
8. R.K. Watts, M. deWit, W.C. Holton, Applied Optics 13, 10 (1974).
9. F. Zarnske et al.,"Accurate Measurements of Some Properties of Sputtered Glass Waveguides," Perkin/Elmer Corp TuA9-1.
10. C. Weaver, J. Vac. Sci. Tech. 12, 18 (1975).
11. B.N. Chapman, J. Vac Sci. Tech. 11, 106 (1974).
12. R. Jacobsson, B. Kruse, Thin Solid Films, 15, 71 (1973).
13. J.E. Greene, J. Woodhouse, M. Pastes, Rev. Sci. Inst., 45, 74 (1974).
14. B.J. Mott, Microindentation Hardness Testing, Butterworth (1956).
15. L.S. Palatnik, N.T. Gladkikh, Industrial Lab., p. 1355 (1964).
16. S. Furuuch, H. Sakata, Japan JAP 13, 1905 (1974).
17. R.E. Hannemen, J.H. Westbrook, Phil Mag 18, 73 (1968).
18. C.B. Willingham et al., Contract No. F19628-73-C-0280, Final Report AFCRL TR-75-0225 (1975).
19. R.T. Newberg, J. Pappis, Contract No. F19628-74-C-0148.
20. J.A. Harrington, University of Alabama, Huntsville, private communication (1975).

APPENDIX A

This bibliography was gathered during the literature search of low infrared absorbing liquids for use as coolants for high-power infrared lasers. No liquids which were sufficiently transparent to act as coolants for deuterium fluoride, carbon monoxide, or carbon dioxide lasers were identified.

Infrared Absorption Spectra of Alcohols. J. Lecomte (Comptes Rendus 180, March 1925).

Change in the Infrared Absorption Spectrum of Water with Temperature. J. R. Collins (Phys. Rev. 26, Dec. 1925).

Absorption Spectra of Certain Organic Liquids in the Near Infrared. J. W. Sappenfield (Phys. Rev. 51, Jan. 1920).

Infrared Absorption of Water from 2.5-6.5 μ. E. K. Plyler and C. J. Craven (J. Chem. Phys. 2, June 1934).

Infrared Absorption Spectrum of Water Containing Deuterium. J. W. Ellis and B. W. Sorge (J. Chem. Phys. 2, Sept. 1934).

Infrared Absorption Spectrum of Heavy Water. T. Shidel (Phys. Math. Soc., Japan, Proc. 16, Oct. 1934).

Infrared Absorption of Oxygenated Water. A. Malone (N. Cimento 12, June 1935).

Absorption of Water and Alcohols between 0.70-0.95 μ. E. Ganz (Ann. d. Physik 26, June 1936).

Absorption Spectrum of Water between 2.5 and 6.5 μ. E. Ganz (Ann. d. Physik 28, March 1937).

Near Infrared Absorption Spectrum of Heavy Water. L. Kellner (Roy. Soc., Proc. 159A, April 1937).

Infrared Absorption Spectra of H_2O Liquid, Solid and in Solution. G. Bosschieter and J. Errera (Comptes Rendus 204, June 1937).

Intermolecular Association and Infrared Absorption of Water. G. Bosschieter and J. Errera (J. de Physique et le Radium 8, June 1937).

Absorption Spectrum of Water. A. Carrelli (N. Cimento 14, June 1937).

Near Infrared Absorption Band of Liquid Water at 1.79 μ. J. R. Collins (Phys. Rev. 52, July 1937).

Infrared Absorption Spectra of H_2O Liquid, Solid and in Solution in Dioxane. G. Bosschieter and J. Errera (Comptes Rendus 205, Oct. 1937).

New Infrared Absorption Band of Liquid Water at 2.52 μ. J. R. Collins (Phys. Rev. 55, March 1939).

Absorption of Water at Different Temperatures from 2.5 to 7.5 μ. J. J. Fox and A. E. Martin (Roy. Soc., Proc. A, 174, Feb. 1940).

Absorption of Light by Liquid H_2O and D_2O in the Infrared between 5 μ and 27 μ. M. Sohm (Z. Phys. 116, 1940).

The Near Infrared Absorption Spectrum of Liquid Water. J. A. Curcio and C. C. Petty (J. Opt. Soc. Amer. 41, May 1951).

Transmission of Water in the Near Infrared. L. Genzel (Optik 9, 1952).

The Molecular Spectra of Condensed Oxygen and the O_4 Molecule. A. L. Smith and H. L. Johnston (J. Chem. Phys. 20, Dec. 1952).

Infrared Absorption Spectrum of Liquid Water in the 3200 to 3600 cm^{-1} Region. S. N. Andreev and T. G. Balicheva (Dokl. Akad. Nauk SSSR 90, 1953).

Infrared Absorption of Liquid Water from 2 to 42 Microns. E. K. Plyler and N. Acquista (J. Opt. Soc. Amer. 44, June 1954).

Infrared Absorption of Liquid and Solid Hydrogen. E. J. Allin, W.F.J. Hare, and R. E. MacDonald (Phys. Rev. 98, April 1955).

Infrared Spectra of Liquid Anhydrous Hydrogen Fluoride, Liquid Sulfur Dioxide, and Hydrogen Fluoride, Sulfur Dioxide Solutions. R. H. Maybury, S. Gordon, and J. J. Katz (J. Chem. Phys. 23, July 1955).

Infrared Absorption of Liquid and Solid Hydrogen with Various Ortho-Para Ratios. W.F.J. Hare, E. J. Allin, and H. L. Welsh (Phys. Rev. 99, Sept. 1955).

Absorption Bands of CCl_4 in the Far Infrared Region. H. Yoshinaga (J. Chem. Phys. 23, Nov. 1955).

On the Structure of Absorption Bands of Liquid H_2O, D_2O, and HDO, Determined by Their Molecular Structure. M. O. Bulanin (Optika i Spektrosk 2, 1957).

Absorption Spectrum of Liquid Oxygen in the Temperature Range 77-153°K (12600-3300 A). V. I. Dianov-Klokov (Optika i Spektrosk. 4, 1958).

Absorption of Radiation in Liquid Water. E. I. Bocharov and A. S. Krutikov (Izv. Akad. Nauk SSSR 7, 1958).

The Infrared Spectrum of Liquid and Solid Hydrogen. E. J. Allin, H. P. Gush, W. F.J. Hare, and H. L. Welsh (N. Cimento Suppl. 9, 1958).

On the Origin of the Spectrum of Liquid and Compressed Oxygen (12600-3000 A). V. I. Dianov-Klokov (Optika i Spektrosk. 6, April 1959).

The Infrared Fundamental Band of Liquid and Solid Hydrogen. H. P. Gush, W. F.J. Hare, E. J. Allin and H. L. Welsh (Canad. J. Phys. 38, Feb. 1960).

Infrared Spectra of Water. R. Mecke (Current Sci. (India) 30, Feb. 1961).

Low-Frequency Infrared Absorption Spectrum of the Hydrogen Bond in Liquid Water and in Crystal Hydrates. A. E. Stanevich and N. G. Yaroslavskii (Dokl. Akad. Nauk SSSR 137, March 1961).

Absorption Cross-Sections of Water Drops for Infrared Radiation. J. J. Stephens and J. R. Gerhardt (J. Meterol. 18, Dec. 1961).

Spectrally Averaged Total Attenuation, Scattering, and Absorption Cross-Sections for Infrared Radiation. J. J. Stephens (J. Meterol. 18, Dec. 1961).

Infrared Spectra of Liquid and Solid Carbon Monoxide. G. E. Ewing (J. Chem. Phys. 37, Nov. 1962).

Near-Infrared Studies of the Structure of Water. I. Pure Water. K. Buijs and G. R. Choppin (J. Chem. Phys. 39, Oct. 1963).

The Absorption Spectra of Liquid Phase H_2O, HDO, and D_2O from 0.7 μ to 10 μ. J. G. Bayly, V. B. Kartha, and W. H. Stevens (Infrared Phys. 3, Dec. 1963).

Transmission of Infrared Radiation Through Liquid Water and Through Water Vapor Near Saturation. R. Goldstein and S. S. Penner (J. Quant. Spectrosc. Radiative Transfer 4, Mar.-Apr. 1964).

On the Spectrum and Structure of Water and Ionic Solutions. D. F. Hornig (J. Chem. Phys. 40, May 1964).

Assignment of the Near-Infrared Bands of Water and Ionic Solutions. K. Buijs and G. R. Choppin (J. Chem. Phys. 40, May 1964).

The Near-Infrared Absorption of Liquid Water at Temperatures Between 27 and 209°C. R. Goldstein and S. S. Penner (J. Quant. Spectrosc. Radiative Transfer 4, May-June 1964).

A Study of the Infrared Spectra of Liquid Oxygen and Nitrogen. M. O. Bulanin and Yu. V. Peterson (Optika i Spektrosk. 16, June 1964).

Relationship Between the Observed and True Absorption Spectra of Molecules in a Condensed Medium. IV. Intense Infrared Absorption Bands in Liquid Chloroform and Carbon Tetrachloride (740-810 cm^{-1}). V. S. Libov, N. G. Bakhshiev and O. P. Girin (Optika i Spektrosk 16, June 1964).

Near-Infrared Spectra of Water and Aqueous Solutions. H. Yamatera, B. Fitzpatrick, and G. Gordon (J. Molecular Spectrosc. 14, Nov. 1964).

A Near-Infrared Study of Hydrogen Bonding in Water and Deuterium Oxide. M. R. Thomas, H. A. Scheraga, and E. E. Schrier (J. Phys. Chem. 69, Nov. 1965).

Far Infrared Absorption in Liquid Nitrogen. N.W.B. Stone and D. Williamd (Molecular Phys. 10, Nov. 1965).

Infrared Absorption Spectrum of Liquid Boron Trifluoride. R. G. Steinhardt, G.E.S. Fetsch, and M. W. Jordan (J. Chem. Phys. 43, Dec. 1965).

Far-Infrared Spectrum of Liquid Water. D. A. Draegert, N.W.B. Stone, B. Curnutte, and D. Williams (J. Opt. Soc. Amer. 56, Jan. 1966).

Frequency Assignments in Infrared Spectrum of Water. D. Williams (Nature, 210, April 1966).

Vibrational Spectrum of Hydrazine-d_4 and a Raman Study of Hydrogen Bonding in Hydrazine. J. R. Durig, S. F. Bush and E. E. Mercer (J. Chem. Phys. 44, June 1966).

Infrared and Raman Spectra of Carbon Suboxide in Condensed Phases. W. H. Smith and G. E. Leroi (J. Chem. Phys. 45, Sept. 1966).

Near-Infrared Spectra of H_2O-D_2O Solutions. J. D. Worley and I. M. Klotz (J. Chem. Phys. 45, Oct. 1966).

Far-Infrared Spectrum of Liquid Water. J. A. Lane (J. Opt. Soc. Amer. 56, Oct. 1966).

Vibrational Spectra of $SPCl_3$, $SPCl_2F$, $SPClF_2$, and SPF_3. J. R. Durig and J. W. Clark (J. Chem. Phys. 46, April 1967).

Effects of Temperature on the Near-Infrared Absorption Spectra of Molecules in the Condensed States. I. Carbon Dioxide. W. C. Waggener, A. J. Weinberger and R. W. Stoughton (J. Phys. Chem. 71, Dec. 1967).

Observation of the Spectrum and the Amplitude Fluctuations of Light Propagating Through Nonequilibrium Liquid Helium. M. Iannuzzi (N. Cimento 55, June 1968).

The Infrared Spectrum of Liquid Tetrafluorohydrazine. D. F. Koster and F. A. Miller (Spectrochim Acta 24A, Sep. 1968).

Vibrational Dynamics in Liquid Water: A New Interpretation of the Infrared Spectrum of the Liquid. J. Schiller (J. Chem. Phys. 49, Nov. 1968).

Infrared Absorption Spectrum for Liquid Ozone. A. Barbe, P. Jouve (C.R. Acad. Sci. B 268, June 1969).

Far-Infrared Absorption in Liquid Hydrogen. M. C. Jones (J. Chem. Phys. 51, Nov. 1969).

Dispersion and Absorption of Liquid Water in the Intrared and Radio Regions of the Spectrum. V. M. Zolotarev, B. A. Mikhailov, L. I. Alperovich, and S. I. Popov (Sptika i Spectrosk. 27, Nov. 1969).

Far-Infrared Spectra of Gaseous and Liquid SF_6. A. Rosenberg and G. Birnbaum (J. Chem. Phys. 52, Jan 1970).

Infrared Spectra of Liquid H_2O and D_2O. O. D. Bonner and J. D. Curry (Infrared Phys. 10, June 1970).

The Near-Infrared Spectra of Water and Heavy Water at Temperatures between 25 and 390°. J. T. Bell, N. A. Krohn (J. Phys. Chem. 74, Oct. 1970).

Comments on 'Near-Infrared Spectra of Water and Heavy Water', by Bell and Krohn. W.A.P. Luck (J. Phys. Chem 74, Oct. 1970).

Temperature Dependence of the 1555 cm^{-1} Infrared Absorption Band in Liquid D_2O: Inflection Points. R. Oder, D.A.I. Goring (Can. J. Chem. 48, Dec. 1970).

Far-Infrared Absorption in Liquefied Gases. M. C. Jones (Report TN-390, Nat. Bur. Stand., 1970).

Lambert Absorpt on Coefficients of Water in the Infrared. C. W. Robertson, D. Williams (J. Opt. Soc. Am. 61, Oct. 1971).

Influence of the Effective Field of a Light Wave on the Observed Spectrum of Liquid Water in the 4000-0.01 cm^{-1} Range. B. A. Mikhailov (Opt. and Spektrosk. 32, Jan. 1972).

Infrared Absorption Spectra of Liquid and Crystalline Phases of Thiophene. F. Tranchant, R. Cucrin (C. R. Hebd. Sean. Acad. Sci. B. 274, March 1972).

Infrared Spectra of Liquid and Crystalline HCN and DCN. M. Pezolet, R. Savoie (Can. J. Spectrosc. 17, March 1972).

Near-Infrared Studies of the Structure of Water. III. Mixed Solvent Systems. G. R. Choppin and M. R. Violante (J. Chem. Phys. 56, June 1972).

The Correspondence of Fundamental and Combination Bands in the Infrared Spectra of Liquid H_2O and D_2O. O. D. Bonner (Infrared Phys. 12, June 1972).

The Infrared Spectrum of Water. C. W. Robertson, B. Curnutte, and D. Williams (Mol. Phys. 26, July 1973).

Thermo-optical Technique for the Measurement of Absorption Loss Spectrum in Liquids. J. Stone (Appl. Opt. 12, Aug. 1973).

A Study of the Infrared Spectra of Liquid Oxygen and Nitrogen. M. O. Bulanin and Yu. V. Peterson (Optika i Spektrosk. 16, June 1964).

Far Infrared Absorption in Liquid Nitrogen. N. W. B. Stone and D. Williams (Mol. Phys. 10, Nov. 1965).

Far Infrared Absorption in Liquefied Gases. M. C. Jones (Nat. Bur. Stand. Tech. Note 390).